THESIS

DEVELOPING TOOLS TO STUDY THE INTERACTION BETWEEN THE LIPOPEPTIDE SURFACTIN AND PHOSPHOLIPID BICELLES WITH INFRARED SPECTROSCOPY

Submitted by

Jennifer M. Blaser

Department of Chemistry

In partial fulfillment of the requirements

For the Degree of Master of Science

Colorado State University

Fort Collins, Colorado

Summer 2012

Master's Committee:

Advisor: Amber Krummel

Nancy Levinger
Matthew Kipper

ABSTRACT

DEVELOPING TOOLS TO STUDY THE INTERACTION BETWEEN THE LIPOPEPTIDE SURFACTIN AND PHOSPHOLIPID BICELLES WITH INFRARED SPECTROSCOPY

Surfactin has been shown to have concentration-dependent effects on lipid membranes with proposed mechanisms of action including ion chelation, ion channel formation, and a detergent-like effect. The concentration ranges for these behaviors have not been established, the structure of surfactin in a membrane has not been determined, and information regarding the dynamics of the surfactin-lipid interaction is limited at best. Therefore, a tunable phospholipid bicelle system was created to study the surfactin-lipid interaction as a function of surfactin concentration using infrared (IR) spectroscopy which can provide both structural and dynamic information. But first, the direct interaction between surfactin and bicelles was confirmed with dynamic light scattering (DLS) measurements that suggest surfactin exhibits detergent-like effects above a 2.0 mM concentration. For surfactin in Tris buffer, the IR spectra displayed a significant concentration-dependent shift in the amide-I band and a distinct change in the amide-I to amide-II band intensity ratio. These data indicate that surfactin experiences a conformational transition over the concentration range studied. The conformational transition may occur due to the formation of surfactin micelles and higher order aggregates upon increasing concentration. Surfactin was also studied in the presence of phospholipid bicelles. At low surfactin concentrations in the presence of bicelles, the amide-I band exhibits nearly identical spectral features to those found for higher concentrations of surfactin in Tris buffer, and the amide-I to amide-II band intensity ratios showed similar trends. The results of these studies indicate that the conformation of surfactin may be similar in micelles, higher order aggregates, and bicelles

with the bicelles limiting the conformational distribution of the surfactin molecules. Additional studies are necessary to determine surfactin's structure in these model membranes and obtain dynamic information to better understand the mechanism of the surfactin-lipid interaction.

DEDICATION

I would like to dedicate this thesis to my family. Thank you to my husband, Chris, for his unconditional love, extreme patience, and never ending support. I must also thank my parents for their support, for fostering my love of learning, and teaching me the importance of hard work. I also owe thanks to my brother for reminding me that a few hours spent playing disc golf refreshes the body and mind. I never would have made it through this process without them.

TABLE OF CONTENTS

Page No.

LIST OF FIGURES

Page No.

LIST OF SELECTED ACRONYMS AND ABBREVIATIONS

2D IR	Two-dimensional infrared spectroscopy
2D NMR	Two-dimensional nuclear magnetic resonance spectroscopy
AFM	Atomic force microscopy
Asp	Aspartate
BSA	Bovine serum albumin
CD	Circular dichroism spectroscopy
CHAPSO	3-(Cholamidopropyl)dimethylammonio-2-hydroxy-1-propane-sulfonate
CMC	Critical micelle concentration
DAGK	Diacylglycerol kinase
d-DHPC	1,2-Dihexanoyl-(d22)-sn-glycero-3-phosphocholine
d-DMPC	1,2-Dimyristoyl-(d54)-sn-glycero-3-phosphocholine
DHPC	Dihexanoylphosphatidylcholine/1,2-dihexanoyl-sn-glycero-3-phosphocholine
DLS	Dynamic light scattering
DMAP	4-(Dimethylamino)pyridine
DMPC	Dimyristoylphosphatidylcholine/1,2-dimyristoyl-sn-glycero-3-phosphocholine
DMSO	Dimethylsulfoxide
DNA	deoxyribonucleic acid
DSC	Differential scanning calorimetry
FCC	Flash column chromatography
FRET	Fluorescence resonance energy transfer
FTIR	Fourier transform infrared spectroscopy
FWHM	Full width at half maximum height

Glu	Glutamate
HPLC	High performance liquid chromatography
IR	Infrared
Leu	Leucine
MA	Myristic acid-1-^{13}C
MLV	Multilamellar vesicle
MPC	1-Myristoyl-sn-glycero-3-phosphocholine
MRSA	Methicillin-resistant *Staphylococcus aureus*
NMA	N-methylacetamide
NMM	N-methylmorpholine
NMR	Nuclear magnetic resonance spectroscopy
PBS	Phosphate buffered saline
PFT	Pore-forming toxin
POPC	1-Palmitoyl-2-oleoyl-sn-glycero-3-phosphocholine
PVDF	Polyvinylidene fluoride
R_f	Retention factor
SDS	Sodium dodecyl sulfate
SLB	Supported lipid bilayer
SLS	Static light scattering
SUV	Small unilamellar vesicle
TBCR	4-(4,6-Dimethoxy-1,3,5-triazin-2-yl)-4-methylmorpholinium tetrafluoroborate
TDC	Transition dipole coupling
TEM	Transmission electron microscopy

TLC	Thin layer chromatography
Tris	Tris(hydroxymethyl)aminomethane
Val	Valine

1 INTRODUCTION

1.1 PORE-FORMING TOXINS (PFTs)

Identified from a variety of sources including bacteria, plants, fungi, and animals, PFTs are cytotoxic proteins or peptides secreted by organisms for use in attack or defense mechanisms. PFTs allow compounds ranging in size and nature from ions to proteins to pathogenic organisms to permeate the cell membrane ultimately resulting in cell death. "Pore" in this context represents a functional term not necessarily a physical description. The PFT pores facilitate communication between two environments previously separated by the cell membrane. Pore formation occurs through a variety of mechanisms which depend on the specific amino acid sequence and secondary structure of the PFT as well as the composition of the target cell membrane.[1]

A general mechanism of pore formation can be used to describe PFT activity though the specific details involved in each step vary among the various PFTs. PFTs are initially secreted as water-soluble monomers that diffuse through aqueous environments to the target cell membranes. At the target membrane, the PFT binds to a receptor which can be the lipids that comprise the bilayer, integral membrane proteins, carbohydrates, or cholesterol. Binding to the receptor induces a conformational change in the PFT to generate a lipid-soluble structure. The lipid-soluble structure of the PFT can then insert into the membrane creating a transmembrane pore.[2-5]

PFTs respond to specific receptors on the target membrane and bind to those receptors with a high affinity. PFTs are secreted in very low concentrations, so interacting with specific receptors on a membrane increases the local PFT concentration and facilitates more efficient pore formation.[4] The factors that contribute to the biological activity of PFTs include the overall

charge of the toxin, structural nature of charge distributions, hydrophobicity, and conformation of the toxin.[5] Studies have shown that charged residues on the PFT are involved in the initial binding process indicating that electrostatic interactions may be responsible for the selectivity of some PFTs to certain membranes.[6-7] For example, antimicrobial PFTs are generally cationic, though there are exceptions, and they interact with the negatively charged lipid head groups of microbial membranes. Such PFTs will operate most efficiently at low pH conditions, which are found at the surface of negatively charged membranes. Low pH conditions are thought to protonate the peptide increasing its hydrophobic character which aids its insertion into the lipid membrane.[8] In living systems, PFTs must interact with a receptor, but under appropriate experimental conditions, they can interact with simple model membranes.[3-4] Channel formation in model membranes allows scientists to use a very simple system consisting of the toxin, a model lipid membrane, and an aqueous buffer to study specific aspects of PFT structure and pore formation.[3]

Based on their activity, PFTs can be classified into two categories: those that act directly on the cell membrane and those that act within the cytoplasm of the target cell.[4-5] PFTs that interfere with membrane function do so by disrupting the permeability barrier of the membrane to create ion-conducting pores (ion channels). The transmembrane pores allow cations such as Na^+, K^+, and Ca^{2+} to permeate the membrane while larger pores can allow compounds and microorganisms to enter the cell. The intra- and extracellular ionic imbalance as well as excess compounds in the cytoplasm cause the cell to absorb water osmotically. The rapid intake of water induces swelling followed by cell lysis as the cells burst from overcapacity.[2] Other PFTs create membrane pores to gain access to the cell's interior themselves where they interfere with the enzymatic activity of the target cell.[2, 4-5]

The cytotoxic behaviors of PFTs may be harnessed and controlled for use in biomedical applications. Many PFTs exhibit antimicrobial behavior identifying their potential use in treating antibiotic-resistant microbial infections like methicillin-resistant *Staphylococcus aureus* (MRSA) infections. An example of an antimicrobial PFT is surfactin from *Bacillus subtilis*. Surfactin is an amphipathic molecule that exhibits several biological activities due to its ability to insert into and destabilize a lipid membrane.[9] Surfactin's antiviral, antibacterial, antitumor, and biofilm formation prevention effects indentify it as a potentially powerful therapeutic agent.[9-14] The lack of information regarding surfactin's mechanism of action and its toxicity currently prevents the use of surfactin as a therapeutic agent. Medical use of antimicrobial PFTs requires research to improve the selectivity and sensitivity of antimicrobial PFTs toward microbes and not mammalian cells and tissue. In order to accomplish this goal, the PFTs' mechanism of action must be understood.[15] Function can be related to structure, so the first step in PFT research is to determine the structure of the PFT in its water-soluble and membrane-bound forms.[5]

1.1.1 CLASSIFICATION OF PFTs

PFTs can be classified according to a multitude of organizational schemes, but the common scheme categorizes PFTs according to the type of secondary structures present. The two subcategories include PFTs that form amphipathic or hydrophobic α-helices and those that form hydrophilic β-sheet structures that span a membrane as β-barrels.[1, 3-4, 8, 15] This classification scheme is independent of whether the toxin's cytotoxic behavior targets the cell membrane or the cytoplasm because both require the toxin to interact with a lipid membrane in some way.[2, 4]

Though PFTs may be classified in the same subcategory according to their α-helical or β-sheet secondary structures, the entire protein conformation, size, and mechanism of membrane insertion varies. Examples to illustrate these differences are provided in the following sections. Colicin A and gramicidin A are used to demonstrate that both possess an α-helical secondary structure, but the pores formed by these two toxins are very different in the number and arrangement of the helices. The *Staphylococcus aureus* α-hemolysin toxin is presented as an example for toxins possessing β-sheet structures.

1.1.2 α-HELICAL PFTs

PFTs with α-helical character contain α-helices in both water and lipid membranes. Examples of toxins that contain hydrophobic and amphipathic α-helices include colicins, gramicidin A, diphtheria toxin, and *Pseudomonas* exotoxin A. These toxins are secreted by different organisms, bind to different receptors, and target different organisms but have similar secondary structures.[4]

Colicins comprise several types of PFTs secreted by various strains of *Escherichia coli* that act as antibiotics against other strains of *E. coli* and closely related bacteria.[4, 8, 16] Colicin A is secreted as a monomer consisting of ten α-helices (Figure 1.1).[17-18] Three hydrophobic helices are sequestered to the center of the structure and surrounded by seven hydrophilic helices. The electrostatic interactions between the positively charged regions of the toxin and the negatively charged portion of the membrane's phospholipid head groups initiate a conformational change in the colicin A structure.[4, 19-20] The conformational change exposes the hydrophobic helices to the membrane. The hydrophobic helices insert into the membrane as a result of hydrophobic effects to create a transmembrane pore described by the umbrella (Figure 1.2) and penknife models.[21-22]

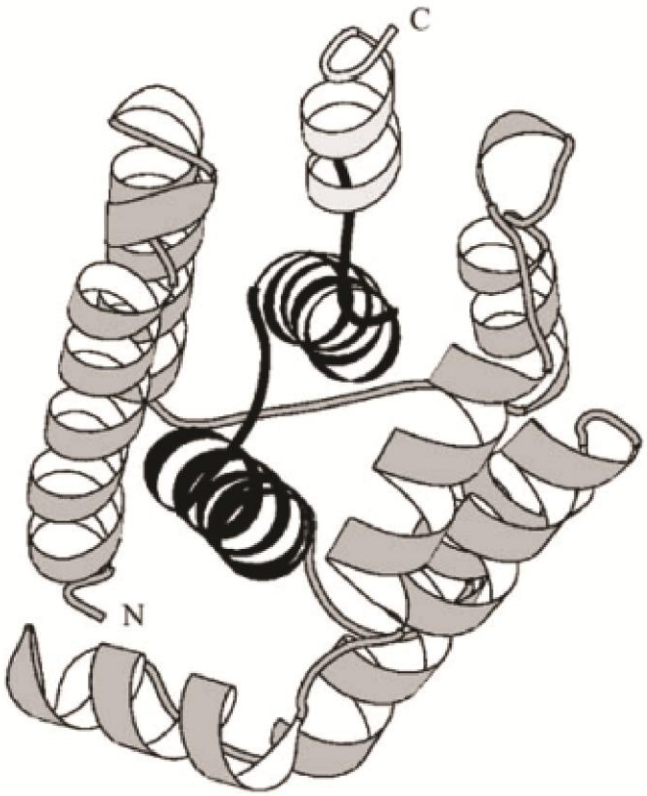

Figure 1.1: Crystal structure of colicin A. Ten α-helices arrange in three layers. The dark layer in the center is the hydrophobic region while the outer layers are hydrophilic to maintain a water-soluble structure. (Image used with permission from Parker *et al.*)[8]

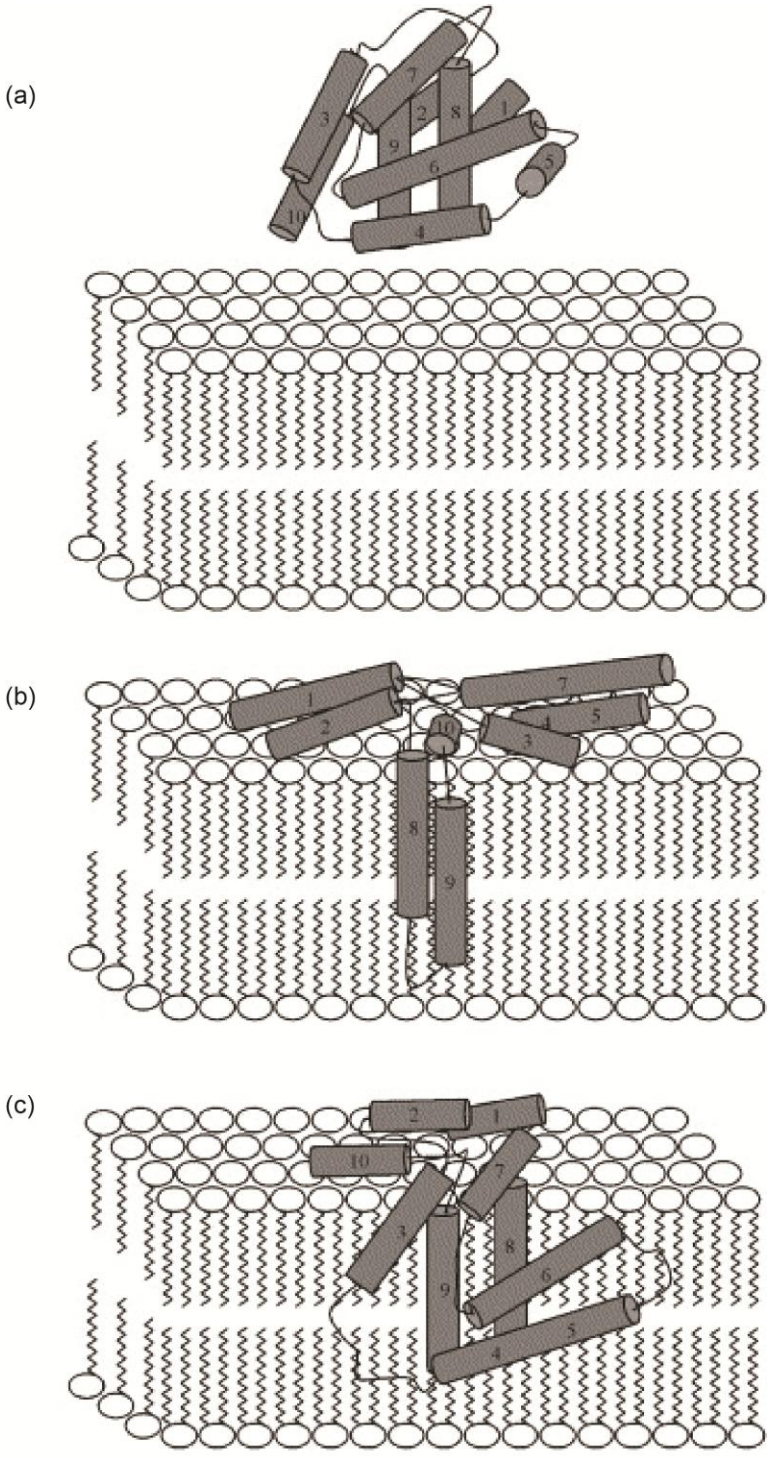

Figure 1.2: The "umbrella" model of colicin A membrane insertion. (a) Water-soluble monomer of colicin A approaching a membrane (b) Lipid-soluble umbrella conformation of the closed state channel. The penknife model describes helices 8 and 9 as tilted toward the lipid head groups in the membrane (c) Helices insert into the membrane to induce channel opening. (Image used with permission from Parker *et al.*)[8]

Gramicidin A, another α-helical PFT, is secreted by *Bacillus brevis* as a single α-helix monomer.[23] Once inserted into the membrane, gramicidin A monomers dimerize to form a transmembrane pore (Figure 1.3). The monomers stack in a head-to-head orientation to form a single α-helix that spans across the membrane. The hydrophobic amino acid side chains orient to the exterior of the helix and interact with the phospholipids of the membrane while the polar peptide backbone constitutes the core of the channel to facilitate monovalent cation transfer across the cell membrane.[15, 24-29]

Colicin A and gramicidin A are used as examples to demonstrate the similarities and differences between PFTs containing similar secondary structures. In their water-soluble form, the hydrophobic regions of the PFT's α-helices are surrounded by the hydrophilic regions. Since the hydrophilic portions comprise the exterior of the water-soluble structure, the PFT must undergo a conformational change to expose the hydrophobic portions to insert into the hydrophobic layer of the lipid membrane.[4, 8] Several studies have determined that the conformational change may be triggered by the partial unfolding of the protein at the membrane surface.[20] Conditions that can trigger the partial unfolding of the protein include pH changes, elevated temperatures, or the charge of the lipid head groups in the membrane. Once bound to the membrane, the mechanism of insertion and structure of the pore are still unknown and vary for different toxins.[4, 8]

1.1.3 β-SHEET PFTs

PFTs that do not possess large stretches of hydrophobic amino acids are categorized as β-sheet PFTs because their monomers contain large hydrophilic sections that form β-type structures.[4, 15] These characteristics are uncommon to most membrane proteins; therefore, it is

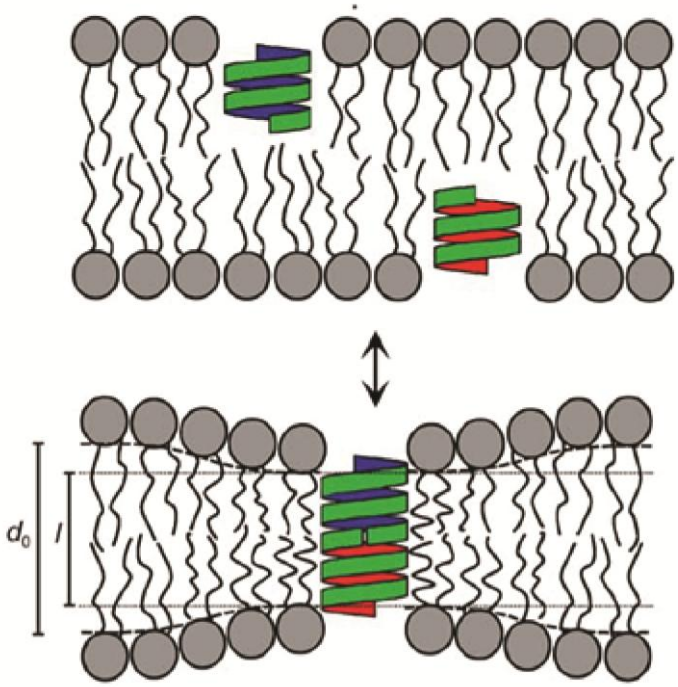

Figure 1.3: Gramicidin A transmembrane pore. Gramicidin A dimerizes two α-helices in a head-to-head orientation to create a transmembrane pore which allows small, monovalent cations to pass into the cell. (Image used with permission from Andersen *et al*.)[30]

hypothesized that the PFT monomers must self-assemble to generate a hydrophobic region allowing the toxin to interact with the membrane. Each monomer in the assembly contributes to the amphipathic character of the complex creating a hydrophobic exterior and a hydrophilic interior, a structure necessary for membrane insertion. Typically, these β-sheet monomer structures assemble via hydrogen bonding to create a structure called a β-barrel. The β-barrel structure forms a physical pore thereby disrupting the natural membrane permeability of the target cell.[4]

An example of a β-sheet PFT is the α-hemolysin peptide secreted by *Staphylococcus aureus*. This particular PFT is a known pathogen to humans, and due to its prevalence in nosocomial (incurred as a result of being hospitalized) MRSA infections, it receives a fair amount of research attention.[8] The α-hemolysin PFT is secreted from *S. aureus* as water soluble monomer with three domains: the cap, rim, and pre-stem domains (Figure 1.4a). The monomers bind to a receptor on target cell membranes and oligomerize to form a heptameric structure with the pre-stem domains oriented toward the center. After oligomerization, the monomers undergo a conformational change to extend the pre-stem hairpin (Figure 1.4b). The hairpins then insert into the membrane to generate a transmembrane pore.[8, 31-32] The heptameric complex generates a β-barrel pore in the membrane, a structure that was solved by Song *et al*. and depicted in Figure 1.5.[4, 31-32] Although the general mechanism of pore formation is known, the exact steps and interactions involved in oligomerization and hairpin insertion have yet to be determined.[4]

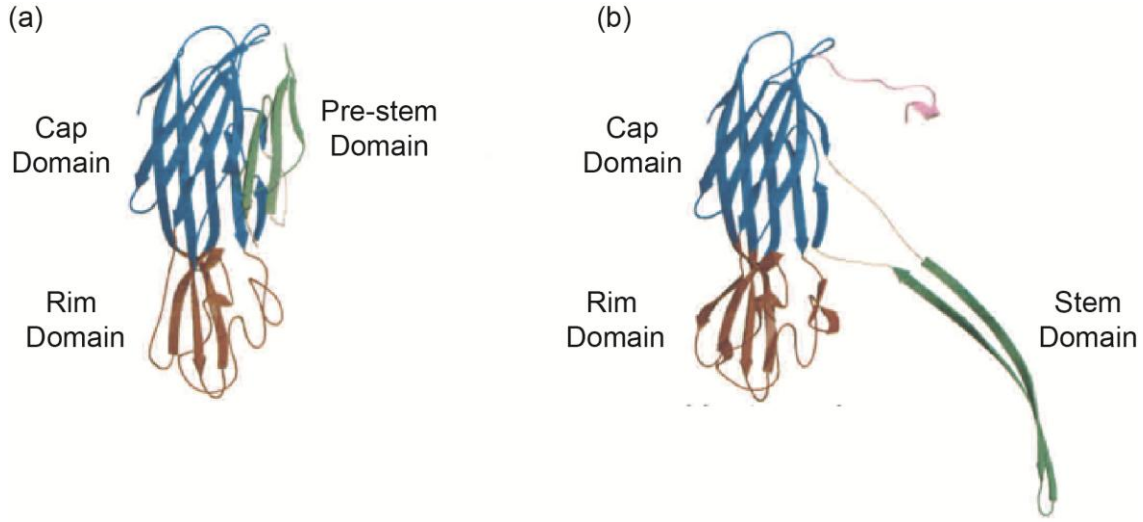

Figure 1.4: Monomer structures of α-hemolysin. (a) The structure of the water-soluble α-hemolysin monomer. (b) The structure of the α-hemolysin monomer when it is in the heptameric pore complex. (Image used with permission from Kawate and Gouaux.)[32]

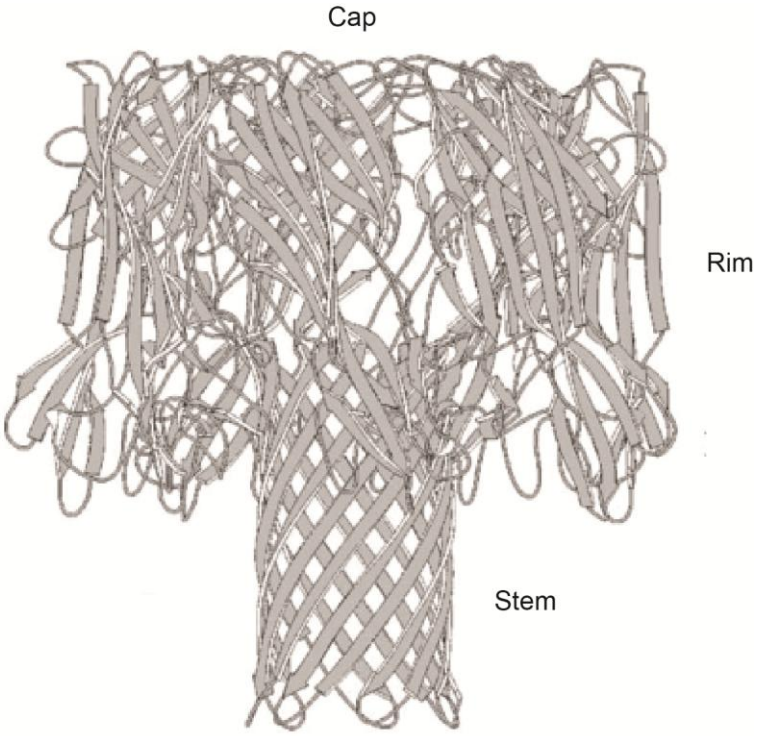

Figure 1.5: The β-barrel structure of the heptameric α-hemolysin pore. (Image used with permission from Parker *et al.*)[8]

1.1.4 SUMMARY OF PFTs

PFTs are proteins and peptides secreted by organisms for a variety of purposes. Some PFTs target mammalian cells to cause disease while others have antimicrobial characteristics that could eventually be used in pharmaceutical applications. Determining the mode of pore formation can provide information about how to control the function of the PFT. Scientists can utilize the knowledge of PFT mechanisms to exploit them in pharmaceutical settings as antibiotics or to chemically interfere with their action as a method of disease treatment.

PFTs have developed a successful mechanism of action. They are secreted as water-soluble monomers enabling their transport from the host cell to the target membrane. At the target membrane, PFTs change conformation to a lipid-soluble form to insert into the cell membrane in order to exhibit their cytotoxic behavior. PFTs have been classified into two broad subgroups: those that form α-helices and those that form β structures.

The α-helical PFTs have distinct hydrophilic and hydrophobic regions that interact with a lipid membrane to create a transmembrane pore. Both the water-soluble state and the transmembrane state are α-helical in structure. It was shown through two examples that while PFTs may belong to the same subcategory, their total three dimensional structures, sizes, and method of pore formation vary. Colicin A pores are formed from a protein consisting of ten α-helices of which only a few span the membrane. The hydrophobic helices form a pore as described by the umbrella and penknife models. Gramicidin A forms transmembrane pores through the dimerization of single α-helices in a head-to-head orientation forming a narrow channel selective to monovalent cations.

PFTs in the subgroup of β-structures do not have monomers with significant hydrophobic regions capable of directly interacting with a membrane; however, self-assembly of β-sheet

monomers creates distinct hydrophobic regions allowing a membrane pore to form. The water-soluble structures of the monomers do not generally resemble their structure after pore formation since a conformational change is induced upon interaction with the target membrane. Once the target membrane triggers the conformational change, a β-barrel transmembrane pore is formed as demonstrated for α-hemolysin.

PFT structures and mechanisms show great diversity. In order to understand the function of a PFT, its structure must be determined in both aqueous environments and in lipid membranes. In some cases, as with surfactin, the water-soluble structure is already known; however, the lipid-soluble structure and mechanism of action have yet to be determined. Until this information is discovered, surfactin's unknown toxicity to mammalian tissues will prevent its use in medical applications. To elucidate details regarding surfactin's or any PFT's mechanism, scientists need to develop tools to study not only the structure of the molecules in an aqueous buffer and membranes, but also the dynamics of the interaction between the toxin and phospholipid membranes. Understanding the structure-function relationship will allow scientists to control the use of PFTs in a variety of applications, most notably pharmaceutics.

1.2 BICELLES AS MODEL MEMBRANES

Biological membranes define a boundary between two volumes. For example, the cell membrane is a phospholipid membrane that creates a permeability barrier separating the contents of the cell from the surrounding aqueous medium.[33-34] The cell membrane serves as a barrier but it must also allow controlled communication between the separated volumes for proper cell function. The organization of the membrane's components must be dynamic to facilitate important cellular processes such as conformational changes, signaling, trafficking, and

recognition of other cells.[33] Biological membranes play a fundamental role in almost all biological processes, and scientists strive to understand this role. But the composition of biological membranes is complex necessitating the use of model membranes to study select features. Studying selected membrane features enables scientists to characterize the role of those features in the function of biological membranes.[33, 35] Employing model membranes is especially useful in studies of PFTs to study lipid-peptide interactions.

Bicelles, a type of model membrane, present a morphology suitable for investigating peptide-membrane interactions. Bicelles contain two components, a long chain phospholipid and a detergent or short chain phospholipid, which form disk shaped aggregates.[35-36] The long chain phospholipids self-assemble to form a bilayered disk with their hydrophilic head groups interacting with the aqueous solvent. The rim of the bilayered phospholipid disk is stabilized by the detergent or short chain phospholipid to maintain the discrete hydrophilic and hydrophobic regions of the model membrane (Figure 1.6).[37-38] The disk structure of a bicelle has been confirmed by deuterium NMR,[38] dynamic light scattering (DLS),[39] and electron microscopy experiments.[39-40]

Bicelles were originally developed by Sanders *et al.* for NMR studies of membrane protein structures. When bicelles are formed with a long chain to short chain phospholipid/detergent ratios greater than 2.5, they spontaneously orient in an applied magnetic field.[36-37, 41-43] The ability of bicelles to orient in a magnetic field proves their utility for structure determination of proteins via solid-state NMR experiments. The bicelles orient the proteins and eliminate powder patterns that frequently complicate solid-state NMR spectra.[36, 41] As the lipid ratio is reduced, bicelles lose their ability to orient in a magnetic field resulting in small aggregates that possess a fast tumbling time. The fast tumbling time of the smaller

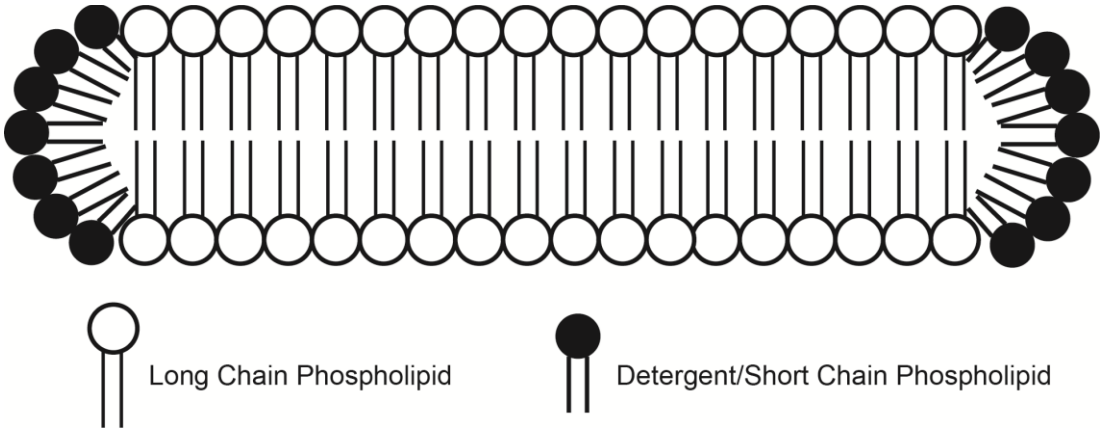

Figure 1.6: Cross section of a phospholipid bicelle.

aggregates serves useful for high resolution solution-state NMR experiments to determine membrane protein structures.[38] The bicelle systems most commonly used in NMR studies are composed of dimyristoylphosphatidylcholine (DMPC) and either dihexanoylphosphatidylcholine (DHPC) or the bile salt derivative 3-(cholamidopropyl)dimethylammonio-2-hydroxy-1-propane-sulfonate (CHAPSO) as the stabilizing short chain phospholipid or detergent, respectively.[37-38]

CHAPSO and DHPC were originally chosen because they are mild detergents with zwitterionic head groups. The zwitterionic character of the head groups for CHAPSO, DHPC, and DMPC provide a chemically inert membrane in which membrane proteins can be studied.[37] DMPC also makes an appropriate component of model membranes since phosphocholines are a dominant type of lipid found in eukaryotic membranes.[34] It must be noted that the composition of bicelles can be tuned by varying the lipid composition in order to control charge characteristics and thickness of the bicelles. Creating a tunable bicelle system allows for various membrane proteins to be studied since proteins may preferentially interact with certain lipids based on factors like head group charge, the saturation of the tails, and the length of the tails.[37] Incorporating different lipids of similar acyl tail length into a bicelle with different head group charges can help alter the charge characteristics of the model membrane while altering the length of the acyl tails determines the thickness of the bicelle.[35, 41]

The size of a bicelle is controlled by the ratio of long chain lipid to short chain lipid (q value) and the total lipid concentration (c_L).[35, 39] The core of the bicelle is composed of a disk shaped bilayer formed by the long chain lipids devoid of the short chain lipid/detergent effectively mimicking a section of a natural biological membrane. The short chain lipid/detergent only serves to cap the rim of the disk to maintain the hydrophobic interior of the membrane. Since the head groups are identical for bicelles formed from DMPC and DHPC, the

size of these bicelles is directly related to the q value which as supported by electron microscopy images.[41, 44] Raising the q value increases the size of the bicelles because the greater amount of long chain lipid present form larger bilayered disks capped off by the limited amount of short chain lipid/detergent present in solution.[39] Above q values of six, no discrete disks are formed because there is not enough short chain phospholipid/detergent. The long chain phospholipid creates a bilayer sheet with scattered pores whose rims are capped by the short chain phospholipid/detergent. An equation relating the radius of the bicelle to the q value was provided by Vold and Prosser in 1996. The equation shows that for a DMPC/DHPC bicelle with a q value of three, the radius of the disk is approximately 20 nm.[38] The c_L value controls the aggregation of bicelles since a fraction of the short chain lipid/detergent in solution remains as monomers while the rest are incorporated into the bicelle structure.[45]

Bicelles are formed by hydrating the individual lipids in a phosphate buffer solution followed by mixing them in the appropriate molar ratios to obtain the desired q value. Upon cycles of sonication and freezing of the lipid mixture, bicelles form spontaneously in the solution. The transformation of the white cloudy solution to a colorless, transparent gel indicates the formation of the bicelles.[42]

Bicelles are not compartmentalized and are optically transparent enhancing their appeal for use in membrane protein studies via optical techniques. Bicelle preparation is simple and yields relatively monodisperse samples. The method of bicelle synthesis also proves easier to achieve homogeneous mixing of the lipids than what is found when preparing vesicles. Bicelles have a lower detergent content than micelles that are used as model membranes in NMR studies of protein structures. Detergents have been shown to potentially perturb the structure of proteins which means that the structures determined of membrane proteins in a micellar system may not

be accurate. The packing of the detergents in a micelle do not accurately mimic the bilayer arrangement of lipids in a biological membrane.[37, 46-47] Biochemical studies concerning the catalytic activity of diacylglycerol kinase (DAGK) in bicelles were conducted to determine if a membrane protein is still functional in a bicelle system. The results found that DAGK was still active in bicelles but its activity was dependent upon the composition of the bicelles. This study showed that bicelles are useful model membranes in structural studies of membrane proteins but that the composition of the bicelle may need to be tailored to the needs of the membrane protein. Tailoring the bicelle composition includes controlling the charge of the lipid head groups, the saturation of the acyl tails, and the length of the acyl tails.[48]

Bicelles are emerging as the model membrane of choice for structural studies because they can be oriented in an applied magnetic field for NMR experiments. The synthesis procedure is simple, easily modified to control composition, and yields a monodisperse distribution of bicelles. Bicelles are bilayered and contain smaller amounts of detergent thus more accurately mimicking a cell membrane.

1.3 SURFACTIN

1.3.1 DISCOVERY AND STRUCTURE

Surfactin was discovered in 1968 by Arima *et al.* when studying the culture broth of *Bacillus subtilis*.[49] The name surfactin arose from its impressive surfactant activity. One year later, Kakinuma *et al.* elucidated surfactin's amino acid sequence as Glu1-Leu2-Leu3-Val4-Asp5-Leu6-Leu7. Using mass spectrometry techniques, they also determined that the amino acid moiety was cyclic and closed to a lactone ring by a β-hydroxy fatty acid with 10-15 carbons (Figure 1.7).[50-51] The three dimensional structure of surfactin was revealed through 2D NMR

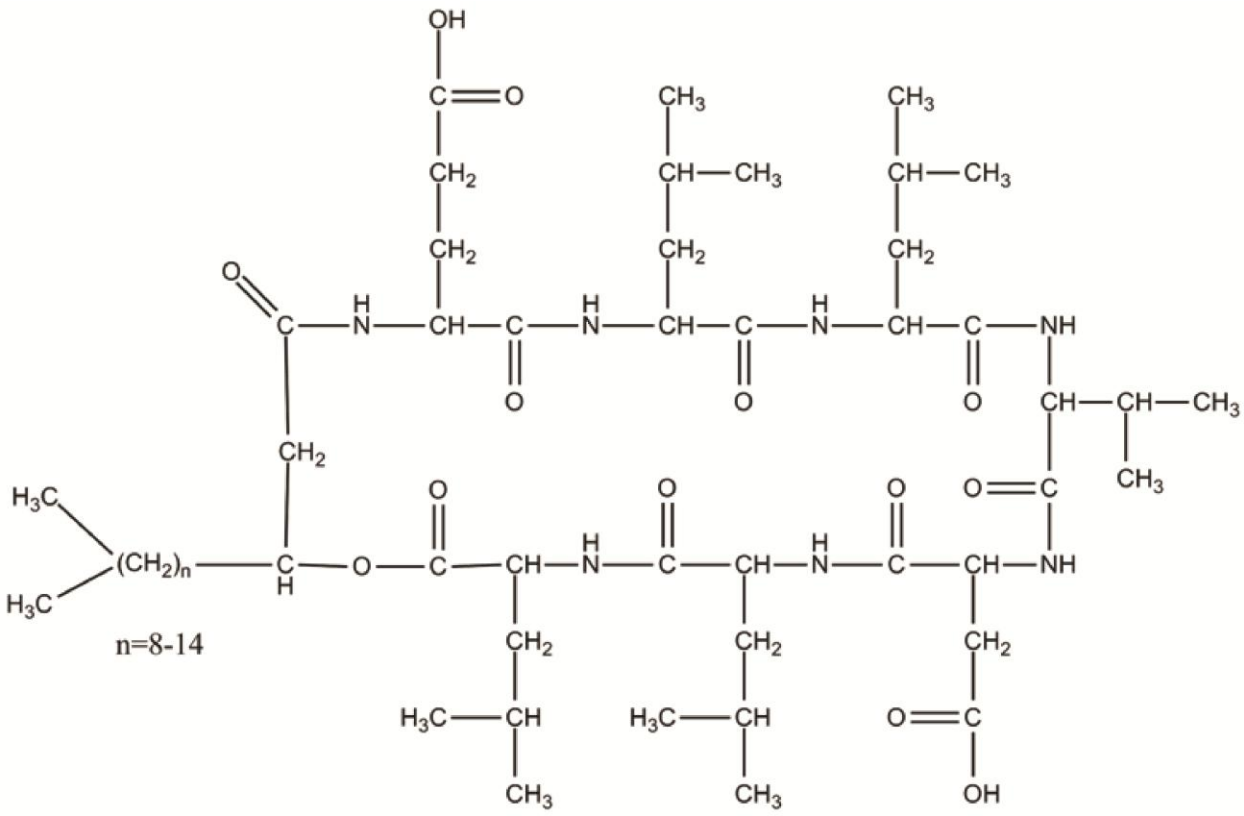

Figure 1.7: Chemical structure of surfactin.

and modeling experiments conducted by Bonmatin *et al*.[52] Their proposed "horse-saddle" topology of surfactin in dimethylsulfoxide (DMSO) is often called a β-sheet structure (Figure 1.8) and has been credited as the structural basis for all of surfactin's physiological properties. The three-dimensional structure generated from the NMR data they obtained indicates the presence of a β-turn involving the Leu2-Leu3-Val4-Asp5 residues stabilized by a hydrogen bond between the Leu2 carbonyl group and Asp5 amide group.[53] Surfactin's compact topology is a direct result of cyclization requirements, its chiral sequence, and favorable intramolecular interactions; however, when surfactin is completely ionized, its conformation is less compact due to electrostatic repulsions between the deprotonated carboxylic acid side chains of the aspartate (Asp) and glutamate (Glu) residues. The amino acid sequence contributes to the molecule's amphipathic structure which is primarily responsible for its biological activities.[52-54]

Ishigami *et al*. demonstrated that the three-dimensional structure of surfactin is stable in the aqueous phase and at an air/water interface using circular dichroism (CD) spectroscopy.[55] The saddle topology places the acidic glutamate and aspartate residues in the same vicinity at the top of the molecule. The intramolecular bridge formed by the acidic aspartate and glutamate residues forms an anionic "claw" at the top of the molecule while the neutral amino acids and the fatty acid tail constitute the rest of the molecule.[53, 56-57] The anionic "claw" at the top of the molecule generates a minor hydrophilic domain while the remainder of the molecule constitutes a major hydrophobic domain creating an amphipathic molecule (Figure 1.9). The acyl tail may extend freely in solution but is capable of strong intermolecular hydrophobic interactions involved in micellization. The hydrophobic domain also provides a way for surfactin to interact with the hydrophobic acyl tails in a phospholipid membrane. Peptides must have hydrophobic regions to insert into a lipid membrane and hydrophilic portions to be stable in aqueous

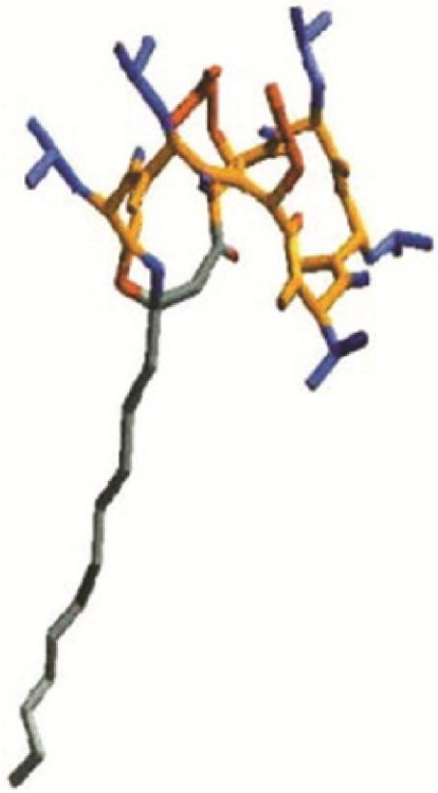

Figure 1.8: The "horse-saddle" topology of surfactin with the acyl tail freely extended. (Image used with permission from Nicolas.)[58]

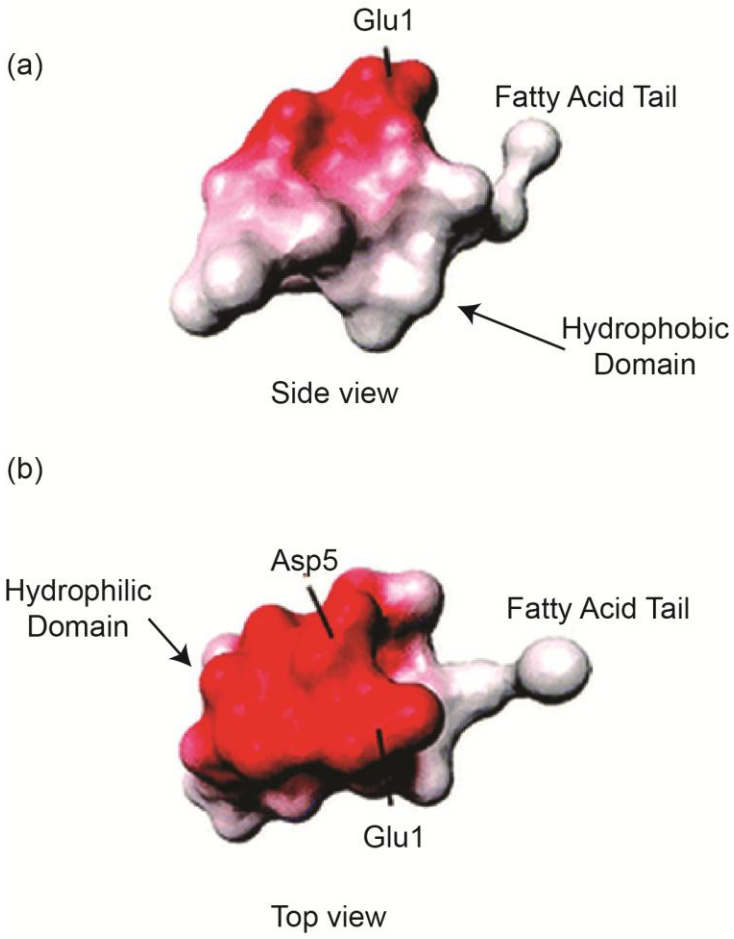

Figure 1.9: Surfactin has an amphipathic three-dimensional structure. The minor hydrophilic domain for surfactin is demonstrated in red and the major hydrophobic portion is white. (a) A side view and (b) the top view of surfactin. (Image used with permission from Tsan *et al.*)[57]

solutions, characteristics that demonstrate the solubility and biological activities of surfactin depend on its amphipathic structure.[54]

To elucidate the role of the carboxylic acid side chains of the aspartate and glutamate residues in surfactin's three-dimensional structure, Ferré *et al*. conducted Fourier transform infrared (FTIR) spectroscopy studies on surfactin and its mono- and di-methylester derivatives. In these samples, surfactin had either one or both of its carboxylic acids methylated to form esters. They were able to identify component bands in the FTIR spectra of surfactin and its derivatives.[59] Vass *et al*. conducted comparative FTIR and CD studies of surfactin and its diester in different solvents and in the presence of calcium ions. Spectral differences between surfactin and its ester derivatives indicate structural distortion of the peptide backbone when the carboxylic acid groups are methylated. These results emphasize the importance of the carboxylic groups of the aspartate and glutamate residues in stabilizing the conformation of the peptide backbone.[59-60]

Shen *et al*. researched surfactin's structure at interfaces noting that this information is necessary in order to eventually determine its mechanism of action. Neutron reflectometry studies showed surfactin adopts a ball-like structure in an aqueous solution. They describe this as a hydrophobic nanoparticle that only maintains solubility in water by its negative charge, a behavior that differs from conventional surfactants. They propose that these characteristics are responsible for surfactin's impressive surface activity at lower concentrations than observed with other surfactants.[61]

Shen *et al.* also used their neutron reflection data to determine the surface area surfactin occupies at an air/water interface. Ishigami *et al*., Maget-Dana and Ptak, and Gallet *et al.* all used surface tension and surface pressure-area curves to calculate the same parameter. The

surface area calculated for surfactin ranged from 89 to 147 $Å^2$. The range in the obtained data can be accounted for by the varying experimental conditions.[55, 61-63] The lower range was determined for surfactin in lower pH conditions where surfactin may have been completely protonated. The data presented by Shen *et al.* and Gallet *et al.* were in agreement producing surface area values at the higher end of the range. They studied ionized surfactin while the others studied a more stable film of neutral surfactin. The larger values obtained by Shen *et al.* and Gallet *et al.* make sense because ionized surfactin molecules experience electrostatic repulsions thereby increasing the surface area occupied.[61, 63] Shen *et al.* suggest the acyl tail is folded back on the peptide moiety and in contact with the leucine residues to form a compact, ball-like structure as shown in Figure 1.10.[61, 63]

1.3.2 ROLE IN BACTERIA

Surfactin is synthesized by several strains of *Bacillus subtilis* when nutrients in the culture media are low. The bacteria produce surfactin under these conditions to help the colony grow and/or move to an area with more nutrients. It has been suggested that surfactin is responsible for increasing the surface area of water-insoluble growth substrates resulting in an increased bioavailability of the nutrients.[64-66] Kinsinger *et al*. have shown that surfactin may be involved in the surface motility of the bacteria while Ahimou *et al*. studied the role of surfactin on bacterial surface hydrophobicity.[64, 67]

The studies carried out by Kinsinger *et al*. concerning the effect of surfactin on bacterial surface motility showed that the growth of *B. subtilis* on agarose plates displayed obvious dendritic qualities. The dendritic growth pattern and colony development was enhanced in the presence of potassium ions. Potassium's role in increasing surfactin production may be due to a

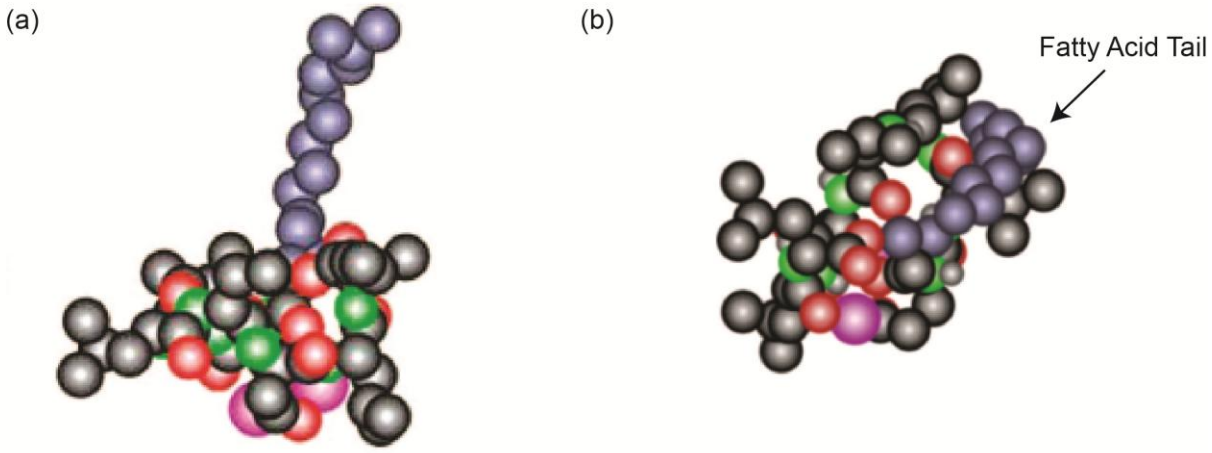

Figure 1.10: Structure of surfactin at an interface. Blue represents the carbons of the fatty acid tail, black represents carbons in the peptide moiety, red is oxygen, green is nitrogen, and the magenta represents the deprotonated carboxylic acid residues. (a) Orientation of surfactin at an interface with the peptide moiety parallel to the interface and the fatty acid tail extended normal to the plane of the interface. (b) Orientation of surfactin at an interface which better matches neutron scattering results. Here, the fatty acid tail is folded back on the peptide moiety and in contact with the leucine residues on one side of the molecule. (Image used with permission from Shen *et al.*)[61]

high-affinity potassium ion transporter in the bacteria or it could induce the expression of potassium-dependent genes involved in controlling colonization.[64]

Kinsinger *et al*. determined surfactin played a significant role in bacterial surface motility. Secretion of surfactin by *B. subtilis* appeared to decrease the surface tension of the surrounding fluid easing the movement of flagellated and non-flagellated bacteria as they travelled across the growth medium. This result indicates that the surface motility of *B. subtilis* relies more on the production of surfactin to use in a sliding motility than it does on the presence of flagella for swarming motility. With the removal or alteration of the gene responsible for surfactin expression, surfactin was not produced and biofilm growth was inhibited.[64]

In combination with surface motility, the surface hydrophobicity of bacteria plays a large role in the adhesion of bacterial cells to a surface during biofilm formation and colonization. Ahimou *et al*. utilized water contact angle and hydrophobic interaction chromatography experiments to study surfactin's effect on the surface hydrophobicity of several *B. subtilis* strains. The studies found that the different strains of the bacteria varied in surface hydrophobicity. Interestingly, surfactin reversed the natural hydrophobicity of the bacteria. The amphipathic surfactin molecules orient toward and adsorb to the bacterial cell in a manner dependent of the surface character of the cell. The hydrophobic portions of surfactin will adsorb to a hydrophobic cell membrane with the hydrophilic moiety exposed to the surrounding environment and vice versa.[67] Modification to surface hydrophobicity helps the bacterial cells adhere to a surface during biofilm formation, but it has been shown that surfactin interferes with the adhesion of other bacteria to inhibit their biofilm formation. Surfactin's inhibition of bacterial biofilm formation could be a useful tool in treating nosocomial infections that result from antibiotic-resistant biofilms.[14, 67]

1.3.3 APPLICATIONS AND BIOLOGICAL ACTIVITIES

The use of PFTs in a variety of applications also stems from the broad spectrum of activities and molecular structures exhibited by these molecules which can be exploited for use in specific applications. PFTs can also be biosurfactants which are advantageous in several applications due to their ability to act at extreme pH values and temperatures while presenting decreased toxicity in comparison to synthetic surfactants.[68-69] Biosurfactant PFTs are characterized by the combination of a fatty acid with a peptide moeity which was demonstrated for surfactin in Section 1.3.1. The peptide moiety can contain rare and modified amino acids that are not used in ribosomal protein synthesis; therefore, the biosurfactant PFTs are produced as mixtures of closely related compounds with slight variations in their amino acid composition and/or lipid portion.[69]

As a biosurfactant PFT secreted by *B. subtilis*, surfactin displays powerful surface activities which have been studied through a variety of methods. Razafindralambo *et al*. conducted studies on a homologous series of surfactins with tail lengths varying from 13 to 16 carbon atoms. Dynamic surface tension measurements yielded results showing that surfactin occupied the same surface area at an interface regardless of tail length. From these results, they proposed that the peptide moiety of surfactin occupied space at the interface while the acyl tails extended perpendicular to the plane of the interface.[70] Additional studies were performed to look at surfactin's foaming properties. Surfactin was found to produce greater volumes and more stable foams than those produced by other conventional surfactants such as sodium dodecyl sulfate (SDS) and bovine serum albumin (BSA). These results demonstrate the superior surface activity of surfactin in comparison to other biosurfactants.[71]

In addition to its surface activity, surfactin has also been shown to interact with biological systems resulting in a variety of biochemical and physiological activities. Surfactin has been shown to have antiviral,[10] anti-inflammatory,[72] antibacterial,[12] and antitumor effects.[13, 73] Each of these activities requires the interaction of surfactin with cellular membranes, and each of these activities makes surfactin's potential use in biomedical applications apparent.[56] Using a biosurfactant PFT as a therapeutic agent may prove beneficial, especially against drug resistant infections which may be unable to develop a resistance to these molecules.[54]

Surfactin plays a crucial role in the surface colonization of pathogens. As previously mentioned, surfactin aids the swarming motility and biofilm formation processes for *B. subtilis* but inhibits these process for the colonization of a surface by other bacteria.[14, 64, 67] Nosocomial infections, which are frequently associated with biofilm formation on biomaterials, are more likely to occur when their motility and biofilm formation abilities are encouraged.[74] The most important feature of infections caused by bacterial biofilms is their high resistance to antibiotics thereby complicating treatment options.[75] It has been demonstrated that surfactin, as well as other biosurfactants, inhibit the ability of bacteria to adhere to a surface preventing biofilm formation.[14] The prevention of biofilm formation can be an important first step in preventing the occurrence of nosocomial infections; therefore, the use of surfactin as a therapeutic agent is gaining research interest.

Studies have shown surfactin to be active against several strains of viruses including Semliki forest virus, herpes simplex virus, and vesicular stomatitis virus among others.[56] Vollenbroich *et al*. performed experiments to study surfactin's effect on various viruses by comparing surfactin's effect on enveloped and non-enveloped viruses. Their data showed that surfactin only inactivated enveloped viruses providing evidence to support the explanation that

the antiviral effects of surfactin are primarily due to the physicochemical interactions between surfactin and the lipid membrane surrounding the virus.[10] Kracht *et al*. completed additional studies concerning surfactin's antiviral behavior in which they determined that one important factor associated with surfactin's ability to inactivate a virus is the length of its fatty acid tail. As the length of surfactin's acyl tail increases, the hydrophobic character of the molecule increases in addition to its ability to inhibit viral activity. They proposed that surfactin incorporates itself in the lipid bilayer surrounding the viral proteins responsible for viral adhesion and penetration. Once incorporated into the viral envelope, surfactin exhibits PFT qualities by inducing the complete disintegration of the membrane successfully inactivating the virus.[11]

In addition to antiviral effects, surfactin has been shown to demonstrate antitumor capabilities. Kameda *et al*. have reported that surfactin exhibits antitumor activity against Ehrlich's ascite carcinoma cells.[13] Recent studies completed by Kim *et al*. have shown that surfactin strongly blocks cell proliferation of a cell line of human colon carcinoma. They proposed that the growth inhibition caused by surfactin occurred because surfactin initiated a sustained increase in intracellular Ca^{2+} concentrations and arrested the cell cycle which resulted in apoptosis.[73] Cao *et al.* studied surfactin's antitumor effect on human breast cancer MCF-7 cells, and the results confirmed the method of growth inhibition proposed by Kim *et al*.[73, 76]

Another important biological activity exhibited by surfactin is its ability to inhibit fibrin clot formation. Surfactin prevents platelet aggregation which inhibits any fibrin clot formation.[77] Kim *et al*. followed up these discoveries by determining that the thrombolytic activity of surfactin is not the result of a detergent effect but rather a result of surfactin's role in downstream signaling pathways. Surfactin enhances the production of plasminogen, an enzyme involved in breaking down the clots.[78]

Surfactin demonstrates several biological activities that could be utilized in therapeutics. However, surfactin also exhibits hemolytic activities presenting a possibility of toxicity to mammalian tissues.[79] Until the mechanism of surfactin's PFT activities are elucidated and its toxicity further researched, surfactin cannot be employed as a therapeutic agent. This information can be gathered from techniques that acquire structural and dynamic information about the surfactin-lipid interaction.

1.3.4 SURFACTIN IN SOLUTION

Amphipathic molecules, like surfactin, tend to form micelles in an aqueous solution. Micelles are the simplest form of amphipathic assemblies and are a direct consequence of the hydrophobic effect. The length scale dependence of hydrophobic effects has been used to model the formation of micelles by Maibaum *et al*. They explain that the free energy required to solvate a small hydrophobic particle scales linearly with the volume of the particle, but the energy required to solvate large hydrophobic particles scales linearly to the surface area of those particles. The hydrophobic driving force for micellization is the result of the energy difference between solvating small particles and solvating larger assemblies.[80]

Han *et al*. investigated thermodynamic parameters associated with the micellization of surfactin. They measured the enthalpy of an aqueous solution as a function of surfactin concentration and found micellization was an endothermic process. Micellization is spontaneous and the enthalpic contribution to the free energy is positive; therefore, surfactin micellization must be driven by entropy.[81] Dehydration of surfactin's hydrophobic tails disrupts the surrounding solvent cage resulting in an increased mobility of the tails. Disruption of the solvent cage and increased mobility of the hydrophobic tails increase entropy. Micellization also

involves disrupting hydrogen bonds between surfactin's peptide moiety and water which is an endothermic process that also increases entropy. From this information, it can be seen that micellization of surfactin is an entropy driven process.[82]

Several studies have been conducted to measure the critical micelle concentration (CMC) of surfactin. Zou *et al*. used isothermal titration calorimetry to measure the CMC of surfactin to be 15.4 μM in a phosphate buffered saline (PBS) at pH 7.4. This measured CMC value is significantly lower than that measured for other ionic surfactants indicating surfactin's strong ability to self-assemble.[83] Ishigami *et al*. determined the CMC of surfactin to be 9.4 μM in a 0.1 M sodium bicarbonate solution using surface tension measurements.[55] Han *et al*. used microcalorimetry to calculate surfactin's CMC to be 38 μM in a PBS buffer at pH 7.4.[81] As demonstrated by Li *et al*., the presence of inorganic cations decreases the CMC of surfactin, but the magnitude of CMC reduction was dependent upon the type of cation. Divalent cations produced a greater change since they completely neutralize the double negative charge on the surfactin molecules.[84] These studies demonstrate that surfactin's CMC is strongly influenced by the experimental conditions.

In addition to measuring surfactin's CMC, some groups calculated the aggregation number for surfactin micelles. The aggregation number varied from 11 to 173 which are lower values than seen for conventional surfactants like SDS which have aggregation numbers in excess of 200.[61, 83, 85] The small aggregation number in surfactin micelles is the result of strong hydrophobic interactions between the fatty acid tails balanced with the electrostatic repulsion between the anionic surfactin head groups. The steric hindrance introduced by surfactin's bulky head groups also limits the packing of surfactin molecules resulting in a high surface curvature

of the micelles, a characteristic consistent with what has been demonstrated for other surfactants possessing bulky head groups.[83, 86-87]

Additional studies involving DLS measurements,[81, 86] static light scattering (SLS) measurements,[55] isothermal titration calorimetry,[55, 81] and transmission electron microscopy (TEM)[81, 85] were carried out to determine the shape and size of surfactin micelles. The results demonstrated that surfactin formed micelles ranging in shape (spherical, ellipsoidal, and/or cylindrical) and size depending on the experimental conditions.[55, 81, 85-86] These studies all indicate that the experimental conditions employed have a large impact on surfactin's CMC, aggregation number, and micelle shape. Micellization of surfactin requires a balance between two competing factors: electrostatic repulsions between ionic head groups and the favorable aggregation process to remove the hydrocarbon tails from the aqueous solvent.[84] Reducing pH or adding a salt to the system screens the electrostatic repulsion between surfactin molecules in favor of micellization reducing the CMC and forming smaller micelles.[84-85, 88-90]

Several groups investigated the shape of surfactin micelles in an attempt to uncover more information about the micellization process. Knoblich *et al*. studied surfactin micelles as a function of pH. Cryo-TEM micrographs obtained for surfactin in a 5 mM Tris buffer showed that at normal pH surfactin formed globular and ellipsoidal micelles which transformed to globular and cylindrical micelles as the pH was increased. At all pH values, when salts were added to the system, the micelles were small and spherical.[85] Ishigami *et al*. provided data from several experiments for surfactin in 0.1 M sodium bicarbonate at pH 8.7 which indicates the formation of large rod-shaped micelles.[55] Han *et al.* also obtained cryo-TEM micrographs of surfactin in a pH 7.4 phosphate buffer. The images showed surfactin micelles were present as small spheres and larger aggregates. They proposed that the larger aggregates were formed

through intermicelle hydrogen bonds.[81] These experiments illustrate that surfactin easily forms micelles, and the morphology and size of those micelles depend on the experimental conditions such as pH and salt concentration.

The morphology of the surfactin micelles were the motivation behind some studies, but some groups investigated further into surfactin micellization in an attempt to determine the structure of a surfactin molecule in a micelle. Molecular dynamics simulations carried out by Nicolas demonstrate that surfactin exhibits structural variability dependent upon environmental conditions such as the nature of the solvent and salt concentrations. These results also show that crowded environments cause surfactin molecules to adopt a conformation in which the hydrophobic residues and the hydrophilic medium minimally interact. The resulting structures are stabilized by van der Waals forces and some intermolecular hydrogen bonding involving the carboxylic acid side chains of the aspartate and glutamate residues.[58]

CD data obtained by several groups consistently predict the conformation of surfactin in micelles. The data suggest surfactin exhibits a β-turn at low concentrations and transforms to a β-sheet conformation at higher concentrations.[55, 81, 88, 91] The β-turn structure has been proposed to be formed through intramolecular hydrogen bonding whereas the β-sheet structure may depend on intermolecular hydrogen bonding.[53, 81, 83] The CD experiments performed by Osman *et al*. were corroborated with data from NMR and X-ray diffraction structures to identify the β-structures present in surfactin. Their interpretation of the results differs slightly from that presented in the other experiments.[88, 92] Osman *et al.* point out that CD experiments alone cannot identify β-turns in cyclic peptides. They explain that the changes observed in the CD spectra indicating a conformational change in the surfactin molecules is the result of aggregational behavior. Their pH dependent experiments indicate that surfactin adopts a β-sheet conformation

at a biological pH suggesting that the biologically active form of surfactin is the β-sheet structure. The addition of calcium ions enhanced the β-sheet structures found in surfactin micelles providing additional evidence for this being the biologically active conformation of surfactin.[88, 92]

1.3.5 INTERACTIONS WITH LIPID MEMBRANES

Microorganisms have been shown to produce a wide range of biosurfactants. Biosurfactant PFTs receive attention due to their potential applications in biomedical industries. The broad spectrum of structures and surface activities exhibited by these molecules prove useful for these applications. Several biosurfactant PFTs do not have well defined mechanisms, but studies have clearly shown that surface- and membrane-active properties play a significant role in their behavior. Surfactin is one such example of these biosurfactant PFTs and has previously been shown to exhibit a variety of biological activities proving its worth as a potential therapeutic agent. However, while surfactin's structure and interaction with lipid membranes have been studied, its mechanism of action remains unknown. Until surfactin's mechanism is elucidated providing a full understanding of its function and potential toxicity to mammalian tissues, it cannot be used as a therapeutic agent. This means an analysis concerning surfactin's physicochemical parameters, molecular structures, dynamics, and identification of targets are necessary to provide information regarding its mechanism.[56, 68-69]

Surfactin's effect on cellular membranes is a direct result of altering the membrane's integrity.[9] The basis of membrane integrity disruption is based on the fact that surfactin can directly interact with the phospholipids of a membrane. Surfactin penetrates a membrane via hydrophobic interactions between its fatty acid tail and the acyl tails of the membrane

phospholipids. Incorporation of surfactin into a membrane alters the organization of the lipid tails and the thickness of the membrane.[91] Carrillo *et al*. have used FTIR spectroscopy to show that the interaction of surfactin with a phospholipid membrane results in dehydration of the lipids' polar head groups. The local dehydration and perturbations to the packing of lipid tails induced by the incorporation of surfactin in the membrane compromise the stability of the membrane.[93] Maget-Dana *et al*. conducted CD experiments that suggest interacting with a lipid membrane may also induce a conformational change in the surfactin molecules which appeared to further facilitate the interaction.[91]

One way to study interactions between surfactin and lipid membranes is to evaluate surfactin's ability to penetrate membranes of varying compositions.[94-95] Bouffioux *et al.* and Eeman *et al*. used atomic force microscopy (AFM) and surface pressure isothermal calorimetry to study the interaction between cyclic and linear surfactin analogues and phospholipid monolayers as a function of the lipids' tail length and head group charge.[96-97] Maget-Dana and Ptak performed similar experiments by measuring the surface pressure of the lipid monolayers in the presence of surfactin isoforms.[91] All groups found that increasing the lipid tail length reduced surfactin's depth of penetrations into the monolayer. The presence of negative lipid head groups creates electrostatic repulsion to reduce surfactin's ability to penetrate the monolayer; however, they found that the addition of salts to the system screened the electrostatic repulsions allowing for deeper penetration of surfactin into the monolayer.[91, 96-97] Comparing the activity of cyclic and linear surfactin proved that both analogues were surface active but only the cyclic analog was able to penetrate a lipid membrane.[96, 98]

The results from these studies indicate that surfactin's penetration into a lipid membrane is primarily governed by hydrophobic interactions.[91, 96-98] Results from differential scanning

calorimetry (DSC) measurements and X-ray diffraction studies demonstrated that surfactin appears to preferentially interact with membranes composed of lipids possessing acyl tails similar in length to surfactin's fatty acid tail.[99] The presence of calcium resulted in deeper penetration of surfactin into the lipid membrane supporting the idea that surfactin forms 1:1 complexes with the divalent cation which possibly induces a conformational change.[88, 91, 99] Eeman *et al*. also suggest that negatively charged lipids promote immiscibility of surfactin into the lipid membrane thus favoring surfactin self-assembly for insertion. Self-assembly is a key step in pore-forming activities of other antimicrobial peptides. Therefore, self-assembly could be involved in surfactin's membrane selectivity by explaining that surfactin could exhibit pore-forming activities for membranes possessing high anionic lipid content such as those of bacterial cells and some cancer cells.[96] The increased biological activity of cyclic surfactin could be due to the three-dimensional structure which generates the necessary amphiphilic nature of the molecule.[52-53, 96, 98]

The thermodynamics of the surfactin-lipid interaction has also been studied. Razafindralambo *et al.* used isothermal titration calorimetry to gather information about thermodynamic parameters during the process of surfactin binding to lipid vesicles. Their study compared surfactin analogues with varying ionic charge and fatty acid chain length. Surfactin spontaneously interacted with the vesicles through endothermic binding interactions indicating an entropy driven process.[100-101] The calculated binding constants show that a cyclic surfactin structure and an increase in surfactin's fatty acid tail length are favorable for the binding affinity to vesicles. Increasing negative charge on surfactin's peptide moiety reduced the measured binding affinity. Their data suggests that the binding of surfactin to lipid membranes is a balance between hydrophobic interactions and electrostatic repulsions.[100]

The amphipathic nature of surfactin's structure provides the ability to interact with lipid bilayers to exhibit behaviors similar to pore-forming toxins. Three mechanisms have been proposed to describe the nature of the interaction between surfactin and lipid membranes: ion chelation, ion channel formation, and detergent-like effects.[56] Various experiments involving monolayer and bilayer model membranes have shown that surfactin's mechanism is concentration dependent. At low and intermediate concentrations, it has been proposed that surfactin undergoes a conformational change during ion chelation and membrane insertion to transport the cation across the membrane and/or creates ion channels in the membrane.[54, 99, 102] At high concentrations, the detergent effect dominates surfactin's mode of action thereby completely solubilizing the lipid membrane.[54, 103]

Surfactin has the ability to complex with cations and this chelating interaction may be a mechanism in which surfactin transfers cations across a lipid membrane. Conductivity titration and two-phase distribution experiments allowed Thimon *et al*. to study surfactin's ability to transport cations across an interface and determine surfactin's affinity for various cations. The titration data showed surfactin formed a 1:1 complex with divalent cations confirming the presence of two negative charges arising from the deprotonated aspartate and glutamate carboxylic acid groups (Figure 1.11). The two-phase distribution experiments demonstrated that surfactin dissolved in organic solvent could effectively extract cations from the aqueous phase at the interface and transport the chelated cations to the organic phase.[104] Spectral changes in CD experiments comparing surfactin alone and in the presence of calcium ions were indicative of a conformational change induced by cation chelation.[91] Taken together, the data from these experiments provide evidence for the cation chelation mechanism describing cation transport across a membrane, a process supported by computer simulations performed by Deleu *et al*.[104-105]

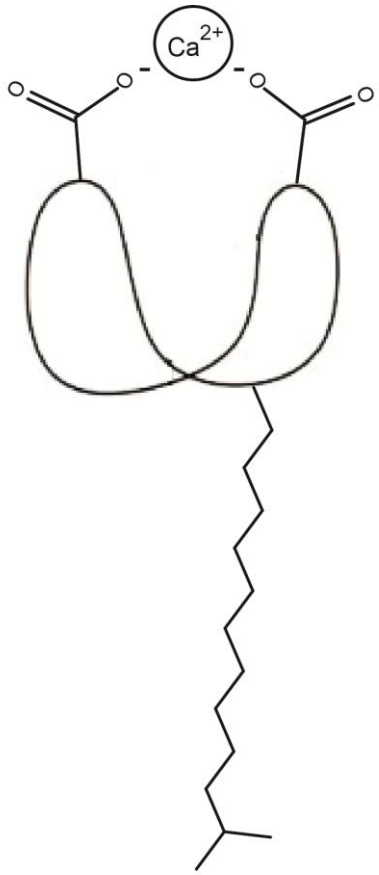

Figure 1.11: Surfactin chelates cations. Surfactin's acidic residues form an anionic "claw" at the top of the molecule. This claw is capable of chelating ions. This interaction could induce a conformational change in surfactin which subsequently transports the cation across a membrane. (This image is not drawn to scale.)

Surfactin more efficiently binds to and transfers divalent cations. Thimon *et al.* explain that this occurs because surfactin exhibits two negative charges in its fully ionized form, a property that exists at pH values greater than its pK_a value of 5.8.[55, 104] The two anionic residues are completely neutralized by a divalent cation.[89, 104] Further studies have shown that surfactin can discriminate between the binding of monovalent and divalent cations as well as the binding of calcium and magnesium ions. The preferential binding of Ca^{2+} over Mg^{2+} indicates the ionic radius of a calcium ion is better fitted to the "claw" formed by surfactin's acidic residues.[84, 88-89]

The second proposed mechanism for surfactin's biological activities is the formation of an ion channel in the target membrane. Sheppard *et al*. used conductivity measurements to study surfactin's ability to allow cations to permeate a supported lipid bilayer (SLB). Surfactin induced current steps indicative of conductive pores present in the membrane. Additional data demonstrated that the surfactin-induced pores were selective to cations. Incorporating surfactin into the lipid bilayer prior to the introduction of cations instead of concurrently showed no evidence of a pore. From this result, Sheppard *et al.* proposed that cations in the aqueous solvent facilitated the association of surfactin into dimers or larger oligomers prior to insertion and stabilization in the membrane and/or association into complexes once in the membrane (Figure 1.12).[102] The results of vesicle leakage measurements obtained by Carrillo *et al.* support these findings by identifying the minimal unit required to induce vesicle content leakage as a dimer.[93] Results of vesicle leakage experiments carried out by Heerklotz and Seelig further support the formation of ion conducting channels. Their data suggest the channel is formed by surfactin's disruption of the membrane to form a channel whose rim is capped by surfactin molecules. The surfactin molecules are described to insert into the membrane with their acyl

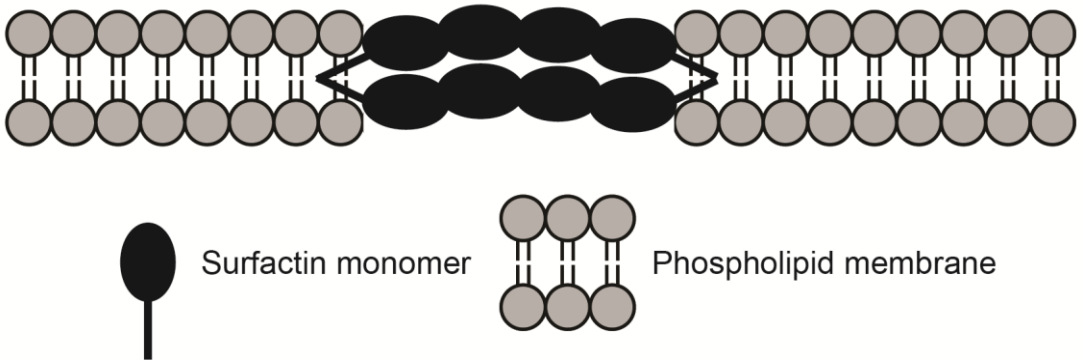

Figure 1.12: Surfactin creates ion channels in a lipid membrane. This schematic provides a cross sectional view of a surfactin channel in a lipid membrane.

tails interacting with the phospholipid tails and their hydrophilic portions tilted to line the interior of the channel. The surfactin-capped rim maintains the hydrophobic interior of the membrane. These findings are consistent with the data suggestive of surfactin-rich domains present in phosphatidylcholine membranes discovered by Grau *et al*.[99, 103] Molecular modeling conducted by Nicolas provides further evidence for this mechanism of action by showing that surfactin's peptide ring exhibits flexibility and a tendency to self-associate into clusters at a water-hexane interface.[58]

Surfactin has been shown to demonstrate "detergent-like" actions on lipid membranes.[106] The behavior has been described as detergent-like because the mechanism of membrane permeabilization is unspecific but usually results in the formation of mixed micelles.[107-109] A schematic of a potential mechanism is provided in Figure 1.13. Detergents act on membranes by increasing the surface curvature. The increased curvature destabilizes the membrane by disordering the acyl tails of the phospholipids, decreasing membrane thickness, and decreasing the lateral packing density of the lipid head groups. The detergent-like behavior of surfactin is temperature dependent exhibiting increased activity at lower temperatures. Heerklotz and Seelig explain the occurrence of this phenomenon is due to the tighter packing and higher organization of lipid tails at lower temperatures increasing the membrane's sensitivity to surfactin's disruptive effects.[101]

Surfactin's detergent-like effects have been studied on a variety of phospholipid vesicle systems. Liu *et al*. used DLS to find that surfactin reduced the size of phosphatidylcholine vesicles, and TEM images confirmed the presence of mixed micelles formed from surfactin and lipid constituents.[109] NMR, DLS, and TEM experiments carried out by Buchoux *et al*. revealed information about the morphology changes of multilamellar vesicles (MLVs) formed from

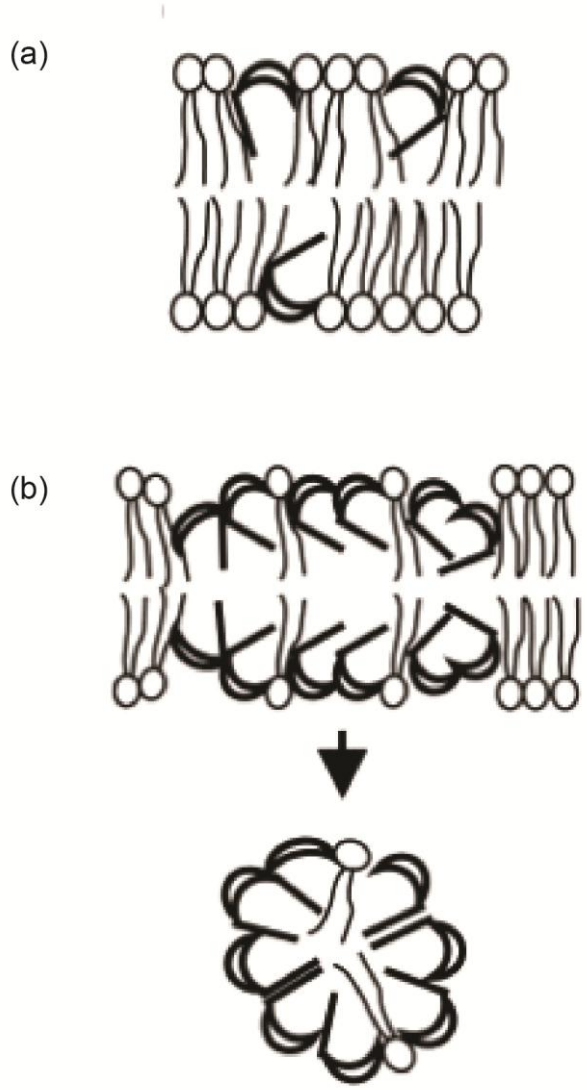

Figure 1.13: Surfactin's detergent-like mechanism. (a) At low concentrations, surfactin penetrates the lipid membrane. (b) At higher concentrations, surfactin solubilizes the membrane to form mixed micelles. (Image used with permission from Deleu *et al.*)[105]

negatively charged phospholipids after treatment with low doses of surfactin. Surfactin induced the transformation of the MLVs to small unilamellar vesicles (SUVs). Buchoux *et al*. proposed the mechanism by which the MLVs were turned into SUVs was due to repulsive electrostatic interactions between the surfactin and lipid head groups. Hydrophobic interactions initiate surfactin's membrane insertion. Once embedded in the membrane, electrostatic repulsions between the anionic surfactin and lipid head groups increase membrane curvature and destabilize the membrane. The modified membrane morphology allows for leakage of the vesicle's contents, and by extrapolation, a cell's contents.[110]

By studying the leakage of fluorescent dyes from phospholipid vesicles, researchers have been able to identify additional features involved in surfactin's PFT activities. DLS, TEM, and vesicle content leakage experiments conducted by Carrillo *et al*. indicate that surfactin, above a surfactin to lipid ratio of 0.92, will completely solubilize a membrane. The vesicle leakage was found to depend on the surfactin concentration further supporting the idea that surfactin is capable of altering membrane permeability allowing leakage of the vesicle's internal contents.[93] The experimental results obtained by Carrillo *et al.* support the idea that surfactin destabilizes a membrane by introducing positive curvature to the membrane inducing stress in the bilayer. FTIR studies looking at the carbonyl stretching of POPC vesicles showed a blue shift in the peak indicating a dehydration of the phospholipid head groups when surfactin was present in the membrane. The FTIR results also showed perturbations to the lipid acyl tail packing. Both pieces of information provide evidence that surfactin compromises bilayer stability.[93]

It is known that detergents induce positive curvature in a membrane thereby increasing the lateral pressure in the lipid head group region of a membrane while also disordering the acyl chains. These alterations reduce membrane thickness and mechanical stability. Heerklotz,

Wieprecht, and Seelig used deuterium NMR to complete a comparative study between surfactin's detergent effect and the effect of known detergents on phospholipid vesicles. The experimental results demonstrated that surfactin's ability to destabilize a membrane does not appear to cause extreme disordering of the acyl tails as observed with known detergents. It does appear that surfactin tilts the acyl tails thereby reorganizing the lipid head groups which provides an indication of the depth of surfactin's membrane penetration.[106]

While surfactin's behavior can still be considered detergent-like, there are key differences between the effects surfactin and detergents have on a membrane. Surfactin induces tilting of the lipid acyl tails while detergents disorder acyl tails. The volume occupied by surfactin takes on an inverted cone shape, like most detergents, and is a shape that would induce further membrane curvature and destabilization. It was also found that unlike detergent head groups that remain near the lipid head groups, surfactin's peptide moiety is capable of inserting into the hydrophobic interface of the lipid membrane demonstrating a deeper penetration of surfactin into the membrane. The deeper penetration experienced by surfactin and its double negative charge requires the anionic residues to interact with the aqueous environment preventing the molecule from flipping to the inner leaflet. This results in membrane destabilization at lower concentrations since the surfactin molecules cannot flip to the inner leaflet to minimize the curvature strain induced upon their insertion.[106] The computer simulation data presented by Deleu *et al*. notes the insertion of a single surfactin molecule does not significantly perturb a membrane, but it is the first step to membrane solubilization.[105]

1.3.6 SURFACTIN SUMMARY

Surfactin, a biosurfactant produced by *B. subtilis* forms a "horse-saddle" topology in which the acidic residues form a minor hydrophilic domain at the top of the molecule. The remaining neutral residues and the fatty acid tail constitute the rest of the molecule and form a major hydrophobic domain. This amphipathic structure is responsible for its biological activities. Surfactin plays a role in the surface motility and hydrophobicity of *B. subtilis* enabling biofilm formation though it inhibits biofilm formation for other bacteria. Other biological activities displayed by surfactin include antibacterial, antiviral, and antitumor effects. These biological activities identify surfactin as a potential therapeutic agent. In order to use surfactin in biomedical applications, its mechanism of membrane insertion must be determined. Three types of membrane interactions have been proposed: ion chelation, ion channel formation, and membrane destabilization through detergent-like effects. Studies have determined the structure of surfactin in buffer and lipid membranes, but no dynamic information has been presented.

1.4 PROJECT GOALS

To obtain a complete description of surfactin's PFT mechanism, we must combine structural and dynamic information. IR spectroscopies provide both structural and dynamic information for protein-lipid systems. While IR spectroscopies cannot probe structural information with a comparable resolution to NMR and X-ray diffraction techniques, it can probe faster time scales allowing for the investigation of processes such as protein folding which can occur over nanoseconds to milliseconds and changes to the protein's local structure and environment as a result of fluctuating hydrogen bond networks which occur on the sub-

picosecond time scale.[111] IR spectroscopies provide structural information through the location of spectral peaks and relative peak intensities. The peak locations correspond to the vibrational frequency of the observed oscillator. In peptides, the carbonyls of the backbone are coupled. Coupling results in peak splitting and distribution of the peak intensities. The degree of coupling depends on the orientation and distance between the coupled oscillators. Conformational changes in the peptide modify the coupling resulting in peak shifts and redistribution of relative intensities in the IR spectrum. In contrast, the peak widths provide information regarding the system's vibrational dynamics. These characteristics are discussed in more detail in Chapter 2.

Since IR spectroscopies can provide both structural and dynamic information necessary to determine surfactin's mechanism of action, tools such as appropriate model membranes must be developed that allow the desired information to be extracted from IR spectra. I have developed a tunable bicelle system to study the surfactin-lipid interaction. DLS measurements effectively proved the direct interaction between surfactin and bicelles in a method that appears consistent with a detergent-like mechanism. The direct interaction of surfactin and the bicelles demonstrates that these bicelles can be utilized in IR spectroscopies to obtain necessary structural and dynamic information concerning surfactin's mechanism of pore-forming activities in biological systems. Bicelle composition can be varied to include different phospholipids, deuterated lipids, and selective ^{13}C labeling of the phospholipid esters. Utilizing these tools with linear IR spectroscopy measurements, peak shifts and changes in relative intensities in the spectra for a range of surfactin concentrations in a buffer were observed. The observed trends indicate that surfactin undergoes a conformational change upon micellization. Spectral data also suggests the interaction with bicelles may induce the same conformational change in surfactin but at lower surfactin concentrations. The use of the tunable bicelle system allows for different

parameters of the spectral data to be analyzed. Isotope labeling shifts peak locations to isolate desired peaks so information concerning peak location, width, and intensity can be extracted from the IR spectrum. Surfactin interacts with all of the bicelle systems created, but each system alters the IR spectrum to elucidate different information.

While this information provides a glimpse into the interaction between surfactin and bicelles, further studies must be conducted to obtain more detailed structural information and dynamic information about the interaction between surfactin and bicelles. The full potential of the tunable bicelle system was not fully recognized in these studies; however, they will prove invaluable in future studies involving multidimensional IR spectroscopies which are more sensitive to three-dimensional protein structures and can provide more accurate and detailed information about the system's vibrational dynamics. Data collected from multidimensional IR spectroscopies can be fit with models and recreated via computer simulations to provide necessary parameters to elucidate surfactin's structure in a membrane. Peak locations, intensities, and the presence of cross-peaks will provide structural information while the lineshapes will provide dynamic information. Once the structural and dynamic information is obtained for surfactin's interaction with a bicelle, a more detailed mechanism for surfactin's biological activities can be determined. Understanding surfactin's mechanism of action allows for a safer and controlled use of surfactin in biomedical applications for the prevention of life-threatening infections and the treatment of various diseases.

1.5 REFERENCES

1. Gilbert, R. J. C., Pore-Forming Toxins. *Cell. Mol. Life Sci.* **2002,** *59* (5), 832-844.

2. Aroian, R.; van der Goot, F. G., Pore-Forming Toxins and Cellular Non-Immune Defenses (CNIDs). *Curr. Opin. Microbiol.* **2007,** *10* (1), 57-61.

3. Gouaux, E., Channel-Forming Toxins: Tales of Transformation. *Curr. Opin. Struct. Biol.* **1997,** *7* (4), 566-73.

4. Lesieur, C.; Vecsey-Semjen, B.; Abrami, L.; Fivaz, M.; Gisou van der Goot, F., Membrane Insertion: The Strategies of Toxins (Review). *Mol. Membr. Biol.* **1997,** *14* (2), 45-64.

5. Zhao, H. X., Structural and Charge Requirements for Antimicrobial Peptide Insertion into Biological and Model Membranes. In *Cellular and Molecular Mechanisms of Toxin Action: Pore-Forming Peptides and Proteins*, Taylor and Francis: New York, 2003.

6. Gonzalez-Manas, J. M.; Lakey, J. H.; Pattus, F., Interaction of the Colicin-A Pore-Forming Domain with Negatively Charged Phospholipids. *Eur. J. Biochem.* **1993,** *211* (3), 625-633.

7. Lakey, J. H.; Parker, M. W.; Gonzalez-Manas, J. M.; Duche, D.; Vriend, G.; Baty, D.; Pattus, F., The Role of Electrostatic Charge in the Membrane Insertion of Colicin A: Calculation and Mutation. *Eur. J. Biochem.* **1994,** *220* (1), 155-163.

8. Parker, M. W.; Feil, S. C., Pore-Forming Protein Toxins: From Structure to Function. *Prog. Biophys. Mol. Bio.* **2005,** *88* (1), 91-142.

9. Bernheimer, A. W.; Avigad, L. S., Nature and Properties of a Cytolytic Agent Produced by *Bacillus subtilis*. *J. Gen. Microbiol.* **1970,** *61*, 361-369.

10. Vollenbroich, D.; Ozel, M.; Vater, J.; Kamp, R. M.; Pauli, G., Mechanism of Inactivation of Enveloped Viruses by the Biosurfactant Surfactin from *Bacillus subtilis*. *Biologicals* **1997,** *25* (3), 289-297.

11. Kracht, M.; Rokos, H.; Ozel, M.; Kowall, M.; Pauli, G.; Vater, J., Antiviral and Hemolytic Activities of Surfactin Isoforms and Their Methyl Ester Derivatives. *J. Antibiot.* **1999,** *52* (7), 613-619.

12. Thimon, L.; Peypoux, F.; Maget-Dana, R.; Roux, B.; Michel, G., Interactions of Bioactive Lipopeptides, Iturin-A and Surfactin from *Bacillus subtilis*. *Biotechnol. Appl. Bioc.* **1992,** *16* (2), 144-151.

13. Kameda, Y.; Ouhira, S.; Matsui, K.; Kanatomo, S.; Hase, T.; Atsusaka, T., Antitumor Activity of Bacillus natto 5. Isolation and Characterization of Surfactin in Culture Medium of Bacillus natto Kmd 2311. *Chem. Pharm. Bull.* **1974,** *22* (4), 938-944.

14. Mireles, J. R.; Toguchi, A.; Harshey, R. M., *Salmonella enterica* Serovar Typhimurium Swarming Mutants with Altered Biofilm-Forming Abilities: Surfactin Inhibits Biofilm Formation. *J. Bacteriol.* **2001,** *183* (20), 5848-5854.

15. Epand, R. M.; Vogel, H. J., Diversity of Antimicrobial Peptides and Their Mechanisms of Action. *BBA-Biomembranes* **1999,** *1462* (1-2), 11-28.

16. Lakey, J. H.; Vandergoot, F. G.; Pattus, F., All in the Family: The Toxic Activity of Pore-Forming Colicins. *Toxicology* **1994,** *87* (1-3), 85-108.

17. Parker, M. W.; Pattus, F.; Tucker, A. D.; Tsernoglou, D., Structure of the Membrane-Pore-Forming Fragment of Colicin A. *Nature* **1989,** *337* (6202), 93-96.

18. Parker, M. W.; Postma, J. P. M.; Pattus, F.; Tucker, A. D.; Tsernoglou, D., Refined Structure of the Pore-Forming Domain of Colicin A at 2.4 Angstrom Resolution. *J. Mol. Biol.* **1992,** *224* (3), 639-657.

19. Vetter, I. R.; Pattus, M. W.; Tsernoglou, D., Insights into Membrane Insertion Based on Studies of Colicins. In *Protein Toxin Structure*, Parker, M. W., Ed. Springer: Germany, 1990.

20. Parker, M. W.; Tucker, A. D.; Tsernoglou, D.; Pattus, F., Insights into Membrane Insertion Based on Studies of Colicins. *Trends Biochem. Sci.* **1990,** *15*, 126-129.

21. Duche, D.; Parker, M. W.; Gonzalez-Manas, J. M.; Pattus, F.; Baty, D., Uncoupled Steps of the Colicin A Pore Formation Demonstrated by Disulfide Bond Engineering. *J. Biol. Chem.* **1994,** *269* (9), 6332-6339.

22. Lakey, J. H.; Duche, D.; Gonzalez-Manas, J. M.; Baty, D.; Pattus, F., Fluorescence Energy Transfer Distance Measurements: The Hydrophobic Helical Hairpin of Colicin A in the Membrane Bound State. *J. Mol. Biol.* **1993,** *230* (3), 1055-1067.

23. Ketchem, R. R.; Hu, W.; Cross, T. A., High-Resolution Conformation of Gramicidin A in a Lipid Bilayer by Solid-State NMR. *Science* **1993,** *261* (5127), 1457-1460.

24. Wallace, B. A., Structure of Gramicidin A. *Biophys. J.* **1986,** *49* (1), 295-306.

25. Allen, T. W.; Andersen, O. S.; Roux, B., Structure of Gramicidin A in a Lipid Bilayer Environment Determined Using Molecular Dynamics Simulations and Solid-State NMR Data. *J. Am. Chem. Soc.* **2003,** *125* (32), 9868-9877.

26. Hladky, S. B.; Urban, B. W.; Haydon, D. A., Ion Movements in the Gramicidin Pore. In *Ion Permeation Through Membrane Channels*, Stevens, C.; Tsien, R. W., Eds. Raven Press: New York, 1979.

27. Bamberg, E.; Apell, H. J.; Alpes, H., Structure of Gramicidin A Channel - Discrimination between $\pi_{L,D}$ and β Helix by Electrical Measurements with Lipid Bilayer Membranes. *P. Natl. Acad. Sci. USA* **1977,** *74* (6), 2402-2406.

28. Urry, D. W.; Goodall, M. C.; Glickson, J. D.; Mayers, D. F., The Gramicidin A Transmembrane Channel: Characteristics of Head-to-Head Dimerized $\pi_{(L,D)}$ Helices. *Proc. Natl. Acad. Sci. U S A* **1971,** *68* (8), 1907-11.

29. Andersen, O. S., Gramicidin Channels. *Annu. Rev. Physiol.* **1984,** *46*, 531-548.

30. Andersen, O. S.; Koeppe, R. E.; Roux, B., Gramicidin Channels. *IEEE T. Nanobiosci.* **2005,** *4* (1), 10-20.

31. Song, L. Z.; Hobaugh, M. R.; Shustak, C.; Cheley, S.; Bayley, H.; Gouaux, J. E., Structure of Staphylococcal α-hemolysin, a Heptameric Transmembrane Pore. *Science* **1996,** *274* (5294), 1859-1866.

32. Kawate, T.; Gouaux, E., Arresting and Releasing Staphylococcal β-hemolysin at Intermediate Stages of Pore Formation by Engineered Disulfide Bonds. *Protein Sci.* **2003,** *12* (5), 997-1006.

33. Chan, Y. H. M.; Boxer, S. G., Model Membrane Systems and Their Applications. *Curr. Opin. Chem. Biol.* **2007,** *11* (6), 581-587.

34. Cullis, P. R.; Fenske, D. B.; Hope, M. J., Physical Properties and Functional Roles of Lipids in Membranes. In *Biochemistry of Lipids, Lipoproteins, and Membranes*, Vance, D. E.; Vance, J. E., Eds. Elsevier Science B.V.: California, 1996.

35. Whiles, J. A.; Deems, R.; Vold, R. R.; Dennis, E. A., Bicelles in Structure-Function Studies of Membrane-Associated Proteins. *Bioorg. Chem.* **2002,** *30* (6), 431-442.

36. Arora, A.; Tamm, L. K., Biophysical Approaches to Membrane Protein Structure Determination. *Curr. Opin. Struc. Biol.* **2001,** *11* (5), 540-547.

37. Sanders, C. R.; Prosser, R. S., Bicelles: A Model Membrane System for All Seasons? *Struct. Fold. Des.* **1998,** *6* (10), 1227-1234.

38. Vold, R. R.; Prosser, R. S., Magnetically Oriented Phospholipid Bilayered Micelles for Structural Studies of Polypeptides. Does the Ideal Bicelle Exist? *J. Magn. Reson. Ser. B* **1996,** *113* (3), 267-271.

39. Glover, K. J.; Whiles, J. A.; Wu, G. H.; Yu, N. J.; Deems, R.; Struppe, J. O.; Stark, R. E.; Komives, E. A.; Vold, R. R., Structural Evaluation of Phospholipid Bicelles for Solution-State Studies of Membrane-Associated Biomolecules. *Biophys. J.* **2001,** *81* (4), 2163-2171.

40. Rodriguez, G.; Soria, G.; Coll, E.; Rubio, L.; Barbosa-Barros, L.; Lopez-Iglesias, C.; Planas, A. M.; Estelrich, J.; de la Maza, A.; Lopez, O., Bicosomes: Bicelles in Dilute Systems. *Biophys. J.* **2010,** *99* (2), 480-488.

41. Marcotte, I.; Auger, M., Bicelles as Model Membranes for Solid- and Solution-State NMR Studies of Membrane Peptides and Proteins. *Concept. Magn. Reson. A* **2005,** *24* (1), 17-37.

42. Ottiger, M.; Bax, A., Characterization of Magnetically Oriented Phospholipid Micelles for Measurement of Dipolar Couplings in Macromolecules. *J. Biomol. NMR.* **1998,** *12* (3), 361-372.

43. Sanders, C. R.; Schwonek, J. P., Characterization of Magnetically Orientable Bilayers in Mixtures of Dihexanoylphosphatidylcholine and Dimyristoylphosphatidylcholine by Solid-State NMR. *Biochemistry-US* **1992,** *31* (37), 8898-8905.

44. Arnold, A.; Labrot, T.; Oda, R.; Dufourc, E. J., Cation Modulation of Bicelle Size and Magnetic Alignment as Revealed by Solid-State NMR and Electron Microscopy. *Biophys. J.* **2002,** *83* (5), 2667-2680.

45. Struppe, J.; Vold, R. R., Dilute Bicellar Solutions for Structural NMR Work. *J. Magn. Reson.* **1998,** *135* (2), 541-546.

46. Keller, S. L.; Bezrukov, S. M.; Gruner, S. M.; Tate, M. W.; Vodyanoy, I.; Parsegian, V. A., Probability of Alamethicin Conductance States Varies with Nonlamellar Tendency of Bilayer Phospholipids. *Biophys. J.* **1993,** *65* (1), 23-27.

47. Matsuzaki, K.; Sugishita, K.; Ishibe, N.; Ueha, M.; Nakata, S.; Miyajima, K.; Epand, R. M., Relationship of Membrane Curvature to the Formation of Pores by Magainin 2. *Biochemistry-US* **1998,** *37* (34), 11856-11863.

48. Czerski, L.; Sanders, C. R., Functionality of a Membrane Protein in Bicelles. *Anal. Biochem.* **2000,** *284* (2), 327-333.

49. Arima, K.; Kakinuma, A.; Tamura, G., Surfactin a Crystalline Peptidelipid Surfactant Produced by *Bacillus subtilis:* Isolation Characterization and Its Inhibition of Fibrin Clot Formation. *Biochem. Bioph. Res. Co.* **1968,** *31* (3), 488-494.

50. Kakinuma, A.; Hori, M.; Isono, M.; Tamura, G.; Arima, K., Determination of Amino Acid Sequence in Surfactin, a Crystalline Peptidelipid Surfactant Produced by *Bacillus subtilis*. *Agr. Biol. Chem. Tokyo* **1969,** *33* (6), 971.

51. Kakinuma, A.; Ouchida, A.; Shima, T.; Sugino, H.; Isono, M.; Tamura, G.; Arima, K., Confirmation of the Structure of Surfactin by Mass Spectrometry. *Agr. Biol. Chem.* **1969,** *33* (11), 1669-1671.

52. Bonmatin, J. M.; Genest, M.; Labbe, H.; Ptak, M., Solution Three-Dimensional Structure of Surfactin: A Cyclic Lipopeptide Studied by ^{1}H NMR, Distance Geometry, and Molecular Dynamics. *Biopolymers* **1994,** *34*, 975-986.

53. Bonmatin, J. M.; Genest, M.; Petit, M. C.; Gincel, E.; Simorre, J. P.; Cornet, B.; Gallet, X.; Caille, A.; Labbe, H.; Vovelle, F.; Ptak, M., Progress in Multidimensional NMR Investigations of Peptide and Protein 3D Structures in Solution: From Structure to Functional Aspects. *Biochimie.* **1992,** *74* (9-10), 825-836.

54. Peypoux, F.; Bonmatin, J. M.; Wallach, J., Recent Trends in the Biochemistry of Surfactin. *Appl. Microbiol. Biot.* **1999,** *51* (5), 553-563.

55. Ishigami, Y.; Osman, M.; Nakahara, H.; Sano, Y.; Ishiguro, R.; Matsumoto, M., Significance of β-Sheet Formation for Micellization and Surface Adsorption of Surfactin. *Colloid Surface B* **1995,** *4* (6), 341-348.

56. Seydlova, G.; Svobodova, J., Review of Surfactin Chemical Properties and the Potential Biomedical Applications. *Cent. Eur. J. Med.* **2008,** *3* (2), 123-133.

57. Tsan, P.; Volpon, L.; Besson, F.; Lancelin, J. M., Structure and Dynamics of Surfactin Studied by NMR in Micellar Media. *J. Am. Chem. Soc.* **2007,** *129* (7), 1968-1977.

58. Nicolas, J. P., Molecular Dynamics Simulation of Surfactin Molecules at the Water-Hexane Interface. *Biophys. J.* **2003,** *85* (3), 1377-1391.

59. Ferre, G.; Besson, F.; Buchet, R., Conformational Studies of the Cyclic L,D-lipopeptide Surfactin by Fourier Transform Infrared Spectroscopy. *Spectrochim. Acta A* **1997,** *53* (4), 623-635.

60. Vass, E.; Besson, F.; Majer, Z.; Volpon, L.; Hollosi, M., Ca^{2+}-Induced Changes of Surfactin Conformation: A FTIR and Circular Dichroism Study. *Biochem. Bioph. Res. Co.* **2001,** *282* (1), 361-367.

61. Shen, H. H.; Thomas, R. K.; Chen, C. Y.; Darton, R. C.; Baker, S. C.; Penfold, J., Aggregation of the Naturally Occurring Lipopeptide, Surfactin, at Interfaces and in Solution: An Unusual Type of Surfactant? *Langmuir* **2009,** *25* (7), 4211-4218.

62. Maget-Dana, R.; Ptak, M., Interfacial Properties of Surfactin. *J. Colloid. Interf. Sci.* **1992,** *153* (1), 285-291.

63. Gallet, X.; Deleu, M.; Razafindralambo, H.; Jacques, P.; Thonart, P.; Paquot, M.; Brasseur, R., Computer Simulation of Surfactin Conformation at a Hydrophobic/Hydrophilic Interface. *Langmuir* **1999,** *15* (7), 2409-2413.

64. Kinsinger, R. F.; Shirk, M. C.; Fall, R., Rapid Surface Motility in *Bacillus subtilis* is Dependent on Extracellular Surfactin and Potassium Ion. *J. Bacteriol.* **2003,** *185* (18), 5627-5631.

65. Julkowska, D.; Obuchowski, M.; Holland, I. B.; Seror, S. J., Comparative Analysis of the Development of Swarming Communities of *Bacillus subtilis* 168 and a Natural Wild Type: Critical Effects of Surfactin and the Composition of the Medium. *J. Bacteriol.* **2005,** *187* (1), 65-76.

66. Rosenberg, E.; Ron, E. Z., High- and Low-Molecular Mass Microbial Surfactants. *Appl. Microbiol. Biot.* **1999,** *52* (2), 154-162.

67. Ahimou, F.; Jacques, P.; Deleu, M., Surfactin and Iturin A Effects on *Bacillus subtilis* Surface Hydrophobicity. *Enzyme Microb. Tech.* **2000,** *27* (10), 749-754.

68. Singh, P.; Cameotra, S. S., Potential Applications of Microbial Surfactants in Biomedical Sciences. *Trends Biotechnol.* **2004,** *22* (3), 142-146.

69. Vater, J., Lipopeptides, An Attractive Class of Microbial Surfactants. *Progress in Colloid & Polymer Science* **1986,** *72*, 12-18.

70. Razafindralambo, H.; Thonart, P.; Paquot, M., Dynamic and Equilibrium Surface Tensions of Surfactin Aqueous Solutions. *J. Surfactants Deterg.* **2004,** *7* (1), 41-46.

71. Razafindralambo, H.; Paquot, M.; Baniel, A.; Popineau, Y.; Hbid, C.; Jacques, P.; Thonart, P., Foaming Properties of Surfactin, a Lipopeptide Biosurfactant from *Bacillus subtilis*. *J. Am. Oil Chem. Soc.* **1996,** *73* (1), 149-151.

72. Hwang, M. H.; Lim, J. H.; Yun, H. I.; Rhee, M. H.; Cho, J. Y.; Hsu, W.; Park, S. C., Surfactin C Inhibits the Lipopolysaccharide-Induced Transcription of Interleukin-1β and Inducible Nitric Oxide Synthase and Nitric Oxide Production in Murine RAW 264.7 Cells. *Biotechnol. Lett.* **2005,** *27* (20), 1605-1608.

73. Kim, S. Y.; Kim, J. Y.; Kim, S. H.; Bae, H. J.; Yi, H.; Yoon, S. H.; Koo, B. S.; Kwon, M.; Cho, J. Y.; Lee, C. E.; Hong, S., Surfactin from *Bacillus subtilis* Displays Anti-Proliferative Effect via Apoptosis Induction, Cell Cycle Arrest and Survival Signaling Suppression. *Febs. Lett.* **2007,** *581* (5), 865-871.

74. Rodrigues, L.; Banat, I. M.; Teixeira, J.; Oliveira, R., Biosurfactants: Potential Applications in Medicine. *J. Antimicrob. Chemoth.* **2006,** *57* (4), 609-618.

75. Morikawa, M., Beneficial Biofilm Formation by Industrial Bacteria *Bacillus subtilis* and Related Species. *J. Biosci. Bioeng.* **2006,** *101* (1), 1-8.

76. Cao, X. H.; Wang, A. H.; Jiao, R. Z.; Wang, C. L.; Mao, D. Z.; Yan, L.; Zeng, B., Surfactin Induces Apoptosis and G_2/M Arrest in Human Breast Cancer MCF-7 Cells Through Cell Cycle Factor Regulation. *Cell. Biochem. Biophys.* **2009,** *55* (3), 163-171.

77. Lim, J. H.; Park, B. K.; Kim, M. S.; Hwang, M. H.; Rhee, M. H.; Park, S. C.; Yun, H. I., The Anti-Thrombotic Activity of Surfactins. *JPN J Vet. Sci.* **2005,** *6* (4), 53-5.

78. Kim, S. D.; Park, S. K.; Cho, J. Y.; Park, H. J.; Lim, J. H.; Yun, H. I.; Park, S. C.; Lee, K. Y.; Kim, S. K.; Rhee, M. H., Surfactin C Inhibits Platelet Aggregation. *J. Pharm. Pharmacol.* **2006,** *58* (6), 867-870.

79. Dehghan-Noudeh, G.; Housaindokht, M.; Bazzaz, B. S. F., Isolation, Characterization, and Investigation of Surface and Hemolytic Activities of a Lipopeptide Biosurfactant Produced by *Bacillus subtilis* ATCC 6633. *J. Microbiol.* **2005,** *43* (3), 272-276.

80. Maibaum, L.; Dinner, A. R.; Chandler, D., Micelle Formation and the Hydrophobic Effect. *J. Phys. Chem. B* **2004,** *108* (21), 6778-6781.

81. Han, Y. C.; Huang, X.; Cao, M. W.; Wang, Y. L., Micellization of Surfactin and Its Effect on the Aggregate Conformation of Amyloid β(1-40). *J. Phys. Chem. B* **2008,** *112* (47), 15195-15201.

82. Dai, S.; Tam, K. C., Isothermal Titration Calorimetric Studies of Alkyl Phenol Ethoxylate Surfactants in Aqueous Solutions. *Colloid Surface A* **2003,** *229* (1-3), 157-168.

83. Zou, A. H.; Liu, J.; Garamus, V. M.; Yang, Y.; Willumeit, R.; Mu, B. Z., Micellization Activity of the Natural Lipopeptide [Glu_1, Asp_5] Surfactin-C15 in Aqueous Solution. *J. Phys. Chem. B* **2010,** *114* (8), 2712-2718.

84. Li, Y.; Zou, A. H.; Ye, R. Q.; Mu, B. Z., Counterion-Induced Changes to the Micellization of Surfactin-C_{16} Aqueous Solution. *J. Phys. Chem. B* **2009,** *113* (46), 15272-15277.

85. Knoblich, A.; Matsumoto, M.; Ishiguro, R.; Murata, K.; Fujiyoshi, Y.; Ishigami, Y.; Osman, M., Electron Cryo-Microscopic Studies on Micellar Shape and Size of Surfactin, an Anionic Lipopeptide. *Colloid Surface B* **1995,** *5* (1-2), 43-48.

86. Dejugnat, C.; Diat, O.; Zemb, T., Surfactin Self-Assembles into Direct and Reverse Aggregates in Equilibrium and Performs Selective Metal Cation Extraction. *Chem. Phys. Chem.* **2011,** *12* (11), 2138-2144.

87. Auzely-Velty, R.; Djedaini-Pilard, F.; Desert, S.; Perly, B.; Zemb, T., Micellization of Hydrophobically Modified Cyclodextrins: 1. Micellar Structure. *Langmuir* **2000,** *16* (8), 3727-3734.

88. Osman, M.; Hoiland, H.; Holmsen, H.; Ishigami, Y., Tuning Micelles of a Bioactive Heptapeptide Biosurfactant via Extrinsically Induced Conformational Transition of Surfactin Assembly. *J. Pept. Sci.* **1998,** *4* (7), 449-458.

89. Thimon, L.; Peypoux, F.; Michel, G., Interactions of Surfactin, a Biosurfactant from *Bacillus subtilis*, with Inorganic Cations. *Biotechnol. Lett.* **1992,** *14* (8), 713-718.

90. Li, Y.; Ye, R. Q.; Mu, B. Z., Influence of Sodium Ions on Micelles of Surfactin-C_{16} in Solution. *J. Surfactants Deterg.* **2009,** *12* (1), 31-36.

91. Maget-Dana, R.; Ptak, M., Interactions of Surfactin with Model Membranes. *Biophys. J.* **1995,** *68*, 1937-1943.

92. Osman, M.; Ishigami, Y.; Ishikawa, K.; Ishizuka, Y.; Holmsen, H., Dynamic Transition of α-Helix to β-Sheet Structure in Linear Surfactin Correlating to Critical Micelle Concentration. *Biotechnol. Lett.* **1994,** *16* (9), 913-918.

93. Carrillo, C.; Teruel, J. A.; Aranda, F. J.; Ortiz, A., Molecular Mechanism of Membrane Permeabilization by the Peptide Antibiotic Surfactin. *BBA-Biomembranes* **2003,** *1611* (1-2), 91-97.

94. Bonmatin, J. M.; Laprevote, O.; Peypoux, F., Diversity Among Microbial Cyclic Lipopeptides: Iturins and Surfactins. Activity-Structure Relationships to Design New Bioactive Agents. *Comb. Chem. High. T. Scr.* **2003,** *6* (6), 541-556.

95. Kowall, M.; Vater, J.; Kluge, B.; Stein, T.; Franke, P.; Ziessow, D., Separation and Characterization of Surfactin Isoforms Produced by *Bacillus subtilis* OKB 105. *J. Colloid Interf. Sci.* **1998,** *204* (1), 1-8.

96. Eeman, M.; Berquand, A.; Dufrene, Y. F.; Paquot, M.; Dufour, S.; Deleu, M., Penetration of Surfactin into Phospholipid Monolayers: Nanoscale Interfacial Organization. *Langmuir* **2006,** *22* (26), 11337-11345.

97. Bouffioux, O.; Berquand, A.; Eeman, M.; Paquot, M.; Dufrene, Y. F.; Brasseur, R.; Deleu, M., Molecular Organization of Surfactin-Phospholipid Monolayers: Effect of Phospholipid Chain Length and Polar Head. *BBA-Biomembranes* **2007,** *1768* (7), 1758-1768.

98. Dufour, S.; Deleu, M.; Nott, K.; Wathelet, B.; Thonart, P.; Paquot, M., Hemolytic Activity of New Linear Surfactin Analogs in Relation to Their Physicochemical Properties. *BBA-Gen. Subjects* **2005,** *1726* (1), 87-95.

99. Grau, A.; Fernandez, J. C. G.; Peypoux, F.; Ortiz, A., A Study on the Interactions of Surfactin with Phospholipid Vesicles. *BBA-Biomembranes* **1999,** *1418* (2), 307-319.

100. Razafindralambo, H.; Dufour, S.; Paquot, M.; Deleu, M., Thermodynamic Studies of the Binding Interactions of Surfactin Analogues to Lipid Vesicles Application of Isothermal Titration Calorimetry. *J. Therm. Anal. Calorim.* **2009,** *95* (3), 817-821.

101. Heerklotz, H.; Seelig, J., Detergent-Like Action of the Antibiotic Peptide Surfactin on Lipid Membranes. *Biophys. J.* **2001,** *81* (3), 1547-1554.

102. Sheppard, J. D.; Jumarie, C.; Cooper, D. G.; Laprade, R., Ionic Channels Induced by Surfactin in Planar Lipid Bilayer Membranes. *Biochim. Biophys. Acta* **1991,** *1064* (1), 13-23.

103. Heerklotz, H.; Seelig, J., Leakage and Lysis of Lipid Membranes Induced by the Lipopeptide Surfactin. *Eur. Biophys. J. Biophy.* **2007,** *36* (4-5), 305-314.

104. Thimon, L.; Peypoux, F.; Wallach, J.; Michel, G., Ionophorous and Sequestering Properties of Surfactin, a Biosurfactant from *Bacillus subtilis*. *Colloid Surface B* **1993,** *1* (1), 57-62.

105. Deleu, M.; Bouffioux, O.; Razafindralambo, H.; Paquot, M.; Hbid, C.; Thonart, P.; Jacques, P.; Brasseur, R., Interaction of Surfactin with Membranes: A Computational Approach. *Langmuir* **2003,** *19* (8), 3377-3385.

106. Heerklotz, H.; Wieprecht, T.; Seelig, J., Membrane Perturbation by the Lipopeptide Surfactin and Detergents as Studied by Deuterium NMR. *J. Phys. Chem. B* **2004,** *108* (15), 4909-4915.

107. Kell, H.; Holzwarth, J. F.; Boettcher, C.; Heenan, R. K.; Vater, J., Physicochemical Studies of the Interaction of the Lipoheptapeptide Surfactin with Lipid Bilayers of L-α-dimyristoyl phosphatidylcholine. *Biophys. Chem.* **2007,** *128* (2-3), 114-124.

108. Boettcher, C.; Kell, H.; Holzwarth, J. F.; Vater, J., Flexible Loops of Thread-Like Micelles are Formed Upon Interaction of L-α-dimyristoylphosphatidylcholine with the Biosurfactant Surfactin as Revealed by Cryo-Electron Tomography. *Biophys. Chem.* **2010,** *149* (1-2), 22-27.

109. Liu, J.; Zou, A. H.; Mu, B. Z., Surfactin Effect on the Physicochemical Property of PC Liposome. *Colloid Surface A* **2010,** *361* (1-3), 90-95.

110. Buchoux, S.; Lai-Kee-Him, J.; Garnier, M.; Tsan, P.; Besson, F.; Brisson, A.; Dufourc, E. J., Surfactin-Triggered Small Vesicle Formation of Negatively Charged Membranes: A Novel Membrane-Lysis Mechanism. *Biophys. J.* **2008,** *95* (8), 3840-3849.

111. Hunt, N. T., 2D-IR Spectroscopy: Ultrafast Insights into Biomolecule Structure and Function. *Chem. Soc. Rev.* **2009,** *38* (7), 1837-1848.

2 OPTICAL METHODS TO STUDY THE SURFACTIN-BICELLE INTERACTION

2.1 SAMPLE PREPARATION

2.1.1 SURFACTIN

A 30 mM Tris buffer was prepared by dissolving Tris(hydroxymethyl)aminomethane (Fisher Scientific, Pittsburgh, PA) in deuterium oxide (D_2O; Cambridge Isotope Laboratories, Andover, MA) and adjusting to pD 8.5 with deuterium chloride (Fisher Scientific).[1-2] Surfactin from *Bacillus subtilis* (Sigma Aldrich, St. Louis, MO) was used without further purification to prepare a 9 mM stock solution by dissolving the appropriate amount of surfactin in Tris buffer. The surfactin stock solution was sonicated for at least 10 minutes to ensure complete dissolution and homogeneity of the solution. Aliquots of the surfactin stock solution were placed into Eppendorf tubes and diluted with Tris buffer to generate samples with final surfactin concentrations ranging from 0.5 mM to 4.5 mM. The final Tris buffer concentration was still 30 mM. Samples were stored at -20°C while not in use.

2.1.2 BICELLES

A 100 mM phosphate buffer was prepared in D_2O and pD adjusted to 6.6 with deuterium chloride. A 15 mM sodium azide (NaN_3; Fisher Scientific) solution was prepared in D_2O. The phosphate buffer and azide solution were combined and diluted with D_2O to yield a final buffer solution with phosphate buffer and azide concentrations of 10 mM and 0.15 mM, respectively.[3]

DMPC (1,2-dimyristoyl-sn-glycero-3-phosphocholine; Bachem, Torrance, CA) and DHPC (1,2-dihexanoyl-sn-glycero-3-phosphocholine; Avanti Polar Lipids, Alabaster, AL) were used without further purification. Individual lipid suspensions were prepared to a concentration of 15% (w/v) by suspending the appropriate mass of each lipid in the buffer solution. The

suspensions were sonicated for approximately 15 minutes and then allowed to sit at room temperature over night to allow for complete hydration.

Bicelles are prepared and classified with a given q value which defines the molar ratio of the long chain lipid (DMPC) to the short chain lipid (DHPC) and is related to the disk's radius as discussed in Section 1.2.[4-5] In these experiments, bicelles with a q value of three were prepared by mixing the DMPC and DHPC suspensions in a 3:1 molar ratio, respectively. A q value of 3 was chosen because this ratio forms a bicelle with a radius of approximately 20 nm allowing sufficient room for the insertion of a small peptide like surfactin.[5] The sample was sonicated until the milky white solution transformed into a clear gel indicating the formation of bicelles. At room temperature, bicelles with q values larger than 3 form a clear gel. As the q value decreases, the viscosity of the bicelle solution also decreases. Placing the bicelles on ice reduces the viscosity to a more liquid consistency.

Deuterated bicelle samples were prepared in the same manner as the non-deuterated bicelles just described using d-DMPC and d-DHPC (1,2-dimyristoyl-(d54)-sn-glycero-3-phosphocholine and 1,2-dihexanoyl-(d22)-sn-glycero-3-phosphocholine, respectively; Avanti Polar Lipids). Deuterated bicelles were prepared to create a model membrane environment for surfactin that would not contain any lipid signal in the C-H stretching region of the linear IR spectrum corresponding to the acyl tails. By deuterating the acyl tails, the reduced mass of the oscillator is increased and the frequency of the stretching vibration is reduced. This corresponds to an 800 cm^{-1} red shift in the FTIR signal for the lipids' acyl tails. Shifting the lipid acyl tail peaks to a different frequency range allows for the isolation of the peptide acyl stretching peaks in the linear IR spectrum.

Bicelles were stored at -20°C. While in use, samples containing bicelles were kept on ice until needed.

2.1.3 SURFACTIN IN BICELLES

Equal 30 µL aliquots of the bicelle solution were added to Eppendorf tubes. Appropriate aliquots of the surfactin stock solution were added to the bicelle solution. Tris buffer was then added to dilute each sample to a constant final volume of 70 µL. The final bicelle concentration was 6.4% (w/v). Final concentrations of surfactin ranged from 0.5 mM to 4.5 mM. Samples were stored at -20°C and kept on ice while in use to lower the viscosity for ease of use.

2.2 DYNAMIC LIGHT SCATTERING (DLS)

2.2.1 SAMPLE PREPARATION AND DATA ANALYSIS

Samples of surfactin in a bicelle solution were studied with DLS in order to prove that surfactin does interact directly with the bicelles by monitoring changes in the bicelle size as a function of surfactin concentration. Disposable polystyrene semi-micro cuvettes (Fisher Scientific) were cleaned with a mild soap solution and thoroughly rinsed with Millipore water. The cuvettes were then rinsed three times with Tris buffer. Three drops of Tris buffer were pushed through Millex syringe filters (Millipore; Burlington, MA) to wet the filter and remove dust from the filter tip. The filters had a 4 mm diameter, 0.45 µm pore size, and a low protein binding PVDF (polyvinylidene fluoride) membrane. Approximately 800 µl of sample was taken up by syringe. Three drops of sample were pushed through the filter into a waste beaker to remove residual buffer and to avoid altering the sample concentration. The remainder of the sample was filtered directly into the cuvette. The cuvette was sealed with parafilm to prevent any dust from contaminating the filtered sample.

DLS measurements were taken with a DynaPro Titan DLS spectrophotometer (Wyatt Technology, Santa Barbara, CA) at 22°C and a 90° detection angle. Samples were allowed to thermally equilibrate in the instrument for five minutes prior to data collection. Three trials were performed for each sample. Each trial consisted of 20 five-second acquisitions. Results are an average of the extracted data for at least 43 acquisitions per sample. Data were analyzed using the Dynamics 6.12.0.3 software. The size distribution was determined by the percent intensity of the scattered light. The data were fit following the regularization fit method accounting for polydispersity in the sample. Data were analyzed for the average size of particles in solution and the distribution of sizes reported as the polydispersity. Results from the analysis were compiled and plotted in Matlab.

2.2.2 DLS BACKGROUND

Particles suspended in solution undergo Brownian motion. When light impinges on a sample of suspended particles in solution, those particles will scatter the light if their polarizability differs from the surrounding solvent. Light impinging on a sample induces an oscillating polarization of the electrons in the particle. The oscillating polarization of electrons in the particles acts as a secondary light source to scatter the incident light.[6] If the polarizabilities of the particles and the solvent are similar, both would emit the same scattered signal. The intensity of the scattered light from the suspended particles is determined by factors including the particle's size, shape, and interactions with other particles.[6-7]

Since there are multiple particles scattering the incident light at any given time, the scattered light will undergo interference. The interference of the scattered light produces an intensity profile. The intensity profile fluctuates with time as the scattering particles diffuse in

the solution. By measuring the time-dependence of the average scattered intensity fluctuations, the particles' translational diffusion through solution can be determined. The translational diffusion of a particle through solution can then be mathematically related to its size.[7]

The DLS instrument consists of a light source, sample compartment, detector, correlator, and computer. The light source is a laser which provides the incident light that is scattered by the sample. The wavelength of the laser is chosen to be in a range where the sample does not absorb otherwise scattering would be undetectable. The laser's power must also be monitored to ensure that the solution is not heated to avoid thermally-induced, non-Brownian motions. The sample compartment contains optics that direct the scattered light to the detector which is oriented at a specific angle relative to the incident beam. The detector converts the intensity of scattered light hitting it to an electric signal which is sent to the correlator and computer.[7]

The correlator takes the electrical signal from the detector and generates an autocorrelation function. The autocorrelation function describes the relationship, or correlation, between two intensity measurements as a function of time. The correlation function, G(τ), is described by the equation:

$$G(\tau) = \left\langle I\left(t\right) \cdot I\left(t+\tau\right) \right\rangle \tag{2.1}$$

where *I(t)* is the intensity of scattered light at some time, *t*, and *I(t+τ)* is the scattered intensity at some time, τ, later. The value of τ is determined by the time difference of the instrument's correlator.[6-7]

The correlation function is an exponential decay that must be fit with a model to describe the distribution of particle sizes in the sample. For a monodisperse sample, the model is described by:

$$G(\tau) = A\left[1 + Be^{-2\Gamma\tau}\right] \tag{2.2}$$

given that A is the baseline of the correlation function and B is the y-intercept. The decay rate of the correlation function is given by Γ. For a polydisperse sample, the model changes to:

$$G(\tau) = A\left[1 + Bg_1(\tau)^2\right] \tag{2.3}$$

In this equation, $g_1(\tau)$ is the sum of all exponential decays for each size of particle present in the sample. The fluctuations in scattered intensity are related with $G(\tau)$ and the decay rate of this function is measured and used to calculate the translational diffusion coefficient (D_T).[6-7]

The decay rate, Γ, of the correlation function is used to calculate D_T (in m^2s^{-1}) for the particles from the equation:

$$\Gamma = D_T q^2 \tag{2.4}$$

The variable q (in m^{-1}) is the magnitude of the scattering vector and its value depends on the refractive index of the solvent ($n(\lambda)$), the wavelength of incident light (λ), and the detection angle (θ) of the instrument according to:

$$q = \frac{4\pi n(\lambda)}{\lambda}\sin\frac{\theta}{2} \tag{2.5}$$

Once the translational diffusion coefficient for the particles has been determined, it is used in the Stokes-Einstein equation to calculate the hydrodynamic radius (R_H) of the particles in the sample. The hydrodynamic radius provides the radius of a sphere that would produce the same measured D_T under the given experimental conditions.[6-7]

$$R_H = \frac{k_B T}{6\pi\eta D_T} \tag{2.6}$$

T is the absolute temperature of the sample, k_B is Boltzmann's constant, and η is the viscosity of the solvent. Other mathematical models are used to fit the correlation function to estimate the size distribution of the sample and report a polydispersity value.[6-7] Since DLS is a method to

determine particle size, it can easily be used to monitor chemical interactions that result in changes to the particle size distribution of the sample. For example, a direct surfactin-bicelle interaction should result in a measured alteration of the bicelles' average hydrodynamic radius.

In summary, DLS is sensitive to the size and size distribution of particles suspended in solution. The technique was used to monitor the measured hydrodynamic radius of bicelles as a function of the surfactin concentration. Any alteration in the size of the bicelles can be attributed to surfactin and indicates a direct surfactin-bicelle interaction. If the surfactin directly interacts with the bicelles, the bicelles can be used as a suitable model membrane system for IR studies used to study conformational aspects of the surfactin-lipid interaction.

2.3 FOURIER TRANSFORM INFRARED SPECTROSCOPY (FTIR)

2.3.1 SAMPLE PREPARATION AND DATA ANALYSIS

A 10 µL aliquot of each sample was placed in a sample cell between two calcium fluoride (CaF_2) plates separated by a 50 µm Teflon spacer to set the path length. Nitrogen gas was used to purge the sample compartment for 10 minutes prior to data collection for each sample to eliminate interference from water vapor. Spectra for all samples were collected for a 400-4000 cm^{-1} spectral window at 4 cm^{-1} resolution on a Nicolet 6700 FTIR spectrometer (Thermo Fisher Scientific, Madison, WI) equipped with OMNIC software. The collected spectra were manually plotted and analyzed in Matlab. The spectra presented in the results are the average of 128 scans. The carbonyl (1500-1800 cm^{-1}) and acyl (2820-3020 cm^{-1}) regions were the foci of these experiments. Background subtractions and baseline corrections were performed manually using custom Matlab programs. Center frequencies, linewidths, and intensities were extracted from the spectra by fitting the data with Gaussian lineshapes in a minimization routine

performed in Matlab. The extracted data was used to generate plots of the concentration dependence of the carbonyl vibrational frequency and intensity ratios.

2.3.2 IR BACKGROUND

The vibrational motion of atomic stretching can be thought of as a mechanical model where two masses are connected by a spring. When the positions of the masses are disturbed, the entire assembly begins to vibrate. This vibrational motion is an example of a simple harmonic motion. The displaced masses are accelerated back towards their equilibrium positions by a restoring force, *F*, proportional to the displacement of each mass. The restoring force is described by Hooke's law:

$$F = -ky \tag{2.7}$$

where *k* is the force constant of the spring and *y* is the displacement of each mass. Since *F* is a negative quantity, it is called a restoring force because it will act to return the mass to its equilibrium position.[8]

The potential energy associated with the system is assigned a value of zero when at equilibrium. Any displacement of the masses will change the potential energy by an amount proportional to the amount of work required to cause the displacement. For a simple harmonic oscillation, this potential energy is described by a parabola. The parabola demonstrates that the potential energy is at a maximum when the system has reached its maximum compression and expansion.[8]

The oscillating motion of each mass about its equilibrium position is a vibration. Using Newton's second law of motion and substituting in the expression for acceleration that describes the position as a function of time, one can obtain the differential equation that describes the

periodic motion of each mass. The solution to the differential equation is the cosine function. The periodicity of the cosine function can be used to determine the frequency of the oscillation. The frequency of the oscillation when considering both masses on the spring is given by:

$$\nu_m = \frac{1}{2\pi}\sqrt{\frac{k}{\mu}} \tag{2.8}$$

where k is the force constant and μ is the reduced mass of the system. This equation points out that the vibrational frequency depends on the strength of the spring and the reduced mass of the system. The equation also demonstrates that the vibrational frequency is independent of the amount of energy put into the system; the energy only changes the amplitude of the displacement and not the frequency of the oscillation.[8]

However, this classical mechanics description of the vibration does not describe systems with atomic dimensions and a quantum mechanical description is necessary. The vibrational frequency of a molecular oscillation depends on the strength of the bond and the reduced mass of the oscillator. Molecular energy levels are quantized which is not part of the classical description of vibrations. Since molecular vibrational energy levels are quantized, absorbed radiation must match the difference in energy levels exactly to facilitate a transition.[8]

Molecular vibrations are not harmonic oscillations like the two masses connected by a spring. As the two atoms approach one another, Coulombic interactions repel the atoms acting in the same direction as the restoring force. This causes the potential energy to quickly rise as the atoms approach one another. As the atoms move away from one another, the potential decreases. Therefore, the potential energy curve is no longer a parabola. This also results in the unequal spacing of the vibrational energy levels. The difference between levels decreases between higher vibrational energy states.[8]

Infrared spectroscopy measures the frequencies of vibrations present in a molecular species. At room temperature, molecules are in their ground vibrational state which has a nonzero energy meaning that the bonds still vibrate. As a molecular bond vibrates, its distribution of charges fluctuates generating a transition dipole moment. The dipole can then interact with the electric field of IR light impinging on the sample. If the energy of the IR light matches the energy difference between vibrational energy states in the molecule, the IR light is absorbed and vibrationally excites the molecule.[8]

IR selection rules state that a molecular vibration will only be IR active if the atomic displacement results in a net change of its dipole moment meaning that it must have a transition dipole. A dipole moment is the static description of the distribution of charges in a molecule. A transition dipole moment describes how the charge distribution, or the dipole moment, oscillates as the bond vibrates. The second selection rule says that a quantum of energy can only move one vibrational energy level at a time ($\Delta v = \pm 1$).[8-9]

Molecular bonds can vibrate in two different ways: stretching or bending. Stretching motions change the interatomic distance along the axis of the bond between two atoms while bending motions change the angle between two bonds. The number of vibrational motions available to a nonlinear molecule with N atoms is given by 3N-6. An IR spectrum contains peaks corresponding to the vibrational motions occurring in the molecule and their relative frequencies. An IR spectrum will not necessarily contain 3N-6 peaks. Molecular oscillations with degenerate energies will vibrate at the same frequency resulting in peaks that cannot be resolved so as to appear as a single peak. Other molecular vibrations give rise to weak intensities undetectable in the spectrum.[8]

The peaks that do arise in an IR spectrum have locations that depend on the vibrational frequency of the given motion. The intensity of the peak is determined by the path length of the sample cell and the concentration of the sample in accordance with Beer's law. A longer path length and higher concentration provide more oscillators in the beam path contributing to the measured signal. The strength of the oscillator also contributes to the peak intensity with stronger oscillators producing a more intense signal. The shape of the peak is determined by contributions from homogeneous and inhomogeneous broadening.[9] Details of these parameters will be discussed in the following text.

Atoms are composed of positive and negative charges. The distribution of these charges in a molecule defines bond lengths between atoms and the bond strength. The charge distribution in the molecule gives rise to a potential energy that is associated with that molecule. When molecules are close together, their potentials can interact and alter the electronic structure of the molecules. These types of perturbations to a molecule's electronic structure can modify its vibrational frequency. The modification of the potential due to inter- or intramolecular interactions is depicted in Figure 2.1. When potentials interact and affect vibrations, they are said to be vibrationally coupled. Coupling can be electrostatic or electrodynamic in nature. Electrostatic coupling occurs through space and electrodynamic coupling occurs through bonds. An example of electrodynamic coupling is mechanical coupling.[8-9]

Figure 2.1 demonstrates the effect of intermolecular interactions between a carbonyl and the surrounding water molecules on the carbonyl vibration. The solid line in Figure 2.1a demonstrates the potential energy of the carbonyl bond at equilibrium. When water pushes on the carbonyl bond through electronic repulsion forces as depicted in the top panel of Figure 2.1b, the electron density between the carbon and oxygen of the carbonyl is increased. The increased

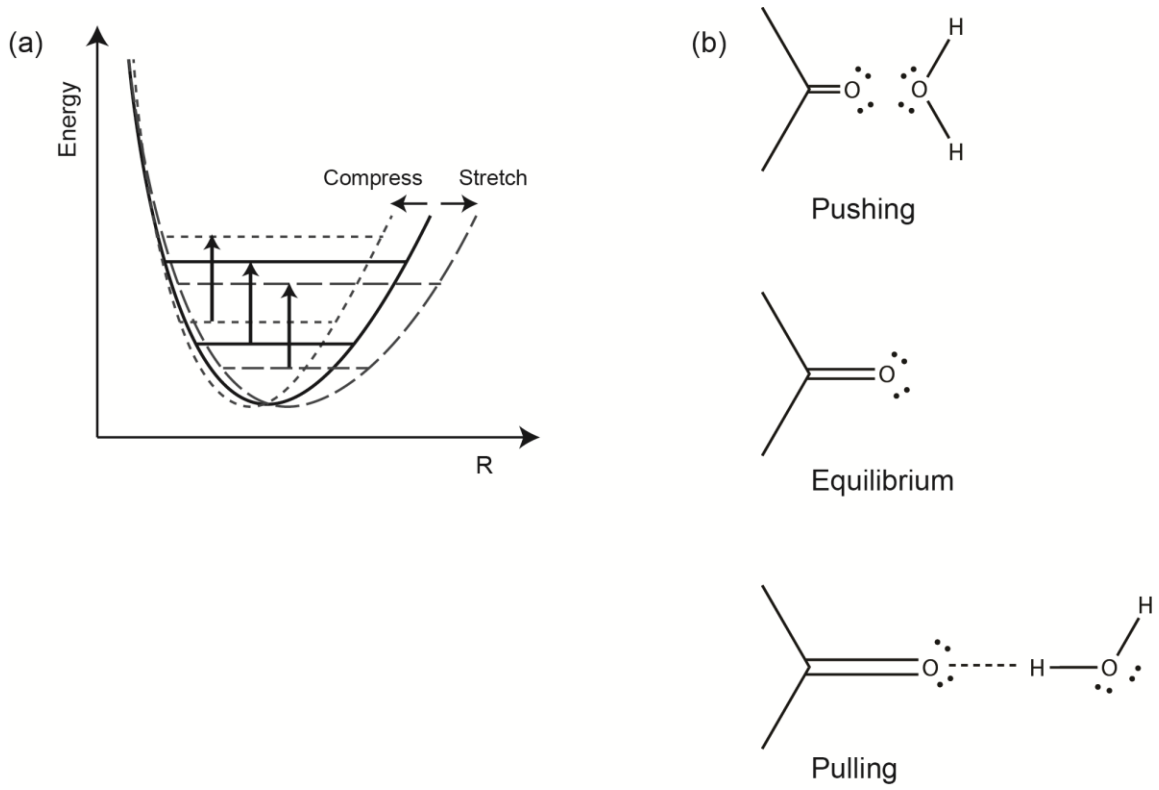

Figure 2.1: The effect of intermolecular interactions on a molecule's vibrational potential. (a) The potential energy of a molecular bond where R describes the atomic displacement. Dashed lines illustrate modifications to the potential energy as the molecular bond is pushed and pulled by interactions with another oscillator. (b) Molecular level representation of how intermolecular interactions can compress and stretch a bond to alter its potential energy. These interactions alter the value of k and/or μ for the bond thereby altering the vibrational frequency of the oscillator. A carbonyl bond in water is used as an example for this figure.

electron density increases the bond strength (*k*) and an increase in the vibrational energy levels as demonstrated by the small dashed lines in Figure 2.1a. These modifications to the carbonyl oscillator result in a higher vibrational frequency. When water pulls on the carbonyl through hydrogen bonding as depicted in Figure 2.1b, the bond strength is reduced due to the redistribution of electron density. The reduced mass of the oscillator is also modified through hydrogen bonding. The result of hydrogen bonding is to reduce the vibrational energy levels as demonstrated by the large dashed lines in Figure 2.1a. The modifications to the oscillator as the result of hydrogen bonding result in a lower vibrational frequency.

The peaks in IR spectra are representative of normal modes. Normal modes describe the fundamental frequencies of the molecule when each atom vibrates with the same frequency and phase. This means that the atoms reach their point of maximum displacement and pass through their equilibrium positions at the same time. Local modes describe localized vibrations in a molecule such as carbonyl stretches.[10-11] The linear combination of local modes gives rise to the normal mode which accounts for all of the possible atomic displacements. Therefore, the normal mode describes how the entire molecule is vibrating. The different peaks formed by the normal modes provide information about which atoms are being displaced. Since each local mode contributes to the normal mode, the intensity and frequency of each local mode will be present in the IR spectrum.[9, 12-13]

In the IR spectra of peptides and proteins, the carbonyl region is the area most commonly studied due to its ability to report on structure. This spectral region contains intense peaks for the amide normal modes of the peptide backbone. The amide-I mode is an intense band in proteins and consists of the local modes of the C=O and C-N stretching in the linkages between

amino acid residues in the peptide's backbone. The nature of the amide-I normal mode provides sensitivity to the three dimensional structure of the peptide.[9, 12-14]

The amide-I local modes of a peptide are electrostatically coupled and are often modeled using the simplest electrostatic model of coupling——the transition dipole coupling (TDC) model. This model describes the magnitude of vibrational coupling (β) of the amide-I transition dipoles between the amino acid residues. The equation for β contains terms that describe the angular and distance dependence of coupling. TDC only describes the electrostatic coupling between transition dipoles. The TDC model breaks down when the oscillators are within 2.5 Å of one another, and it does not account for any contributions from mechanical coupling. The TDC model treats the atoms involved in vibrations as point charges. If oscillators are closer than 2.5 Å, they can no longer be considered point charges and a more sophisticated model must be employed. When residues are separated by more than 2.5 Å but less than what would result in the absence of coupling and mechanical coupling is negligible, TDC is adequate to describe coupling between amide-I local modes.[9, 12-14]

The coupling between oscillators contributes to the peak location and intensity in an IR spectrum.[9, 12-13] The coupling provides insight to the peptide's structure since the amide-I modes of the peptide backbone are known to be coupled. Therefore, as the structure of a peptide changes, the relative orientation and distance between amide-I local modes along the backbone vary resulting in modifications to the amount of coupling. Changes in coupling result in the shifting of the amide-I peak location and changes in the peak intensity.

Coupling causes peak splitting as demonstrated in Figure 2.2. When two degenerate oscillators are not coupled, absorbed energy vibrationally excites both oscillators, but the vibration of one has no effect on the vibration of the other. For the carbonyls of the amide-I

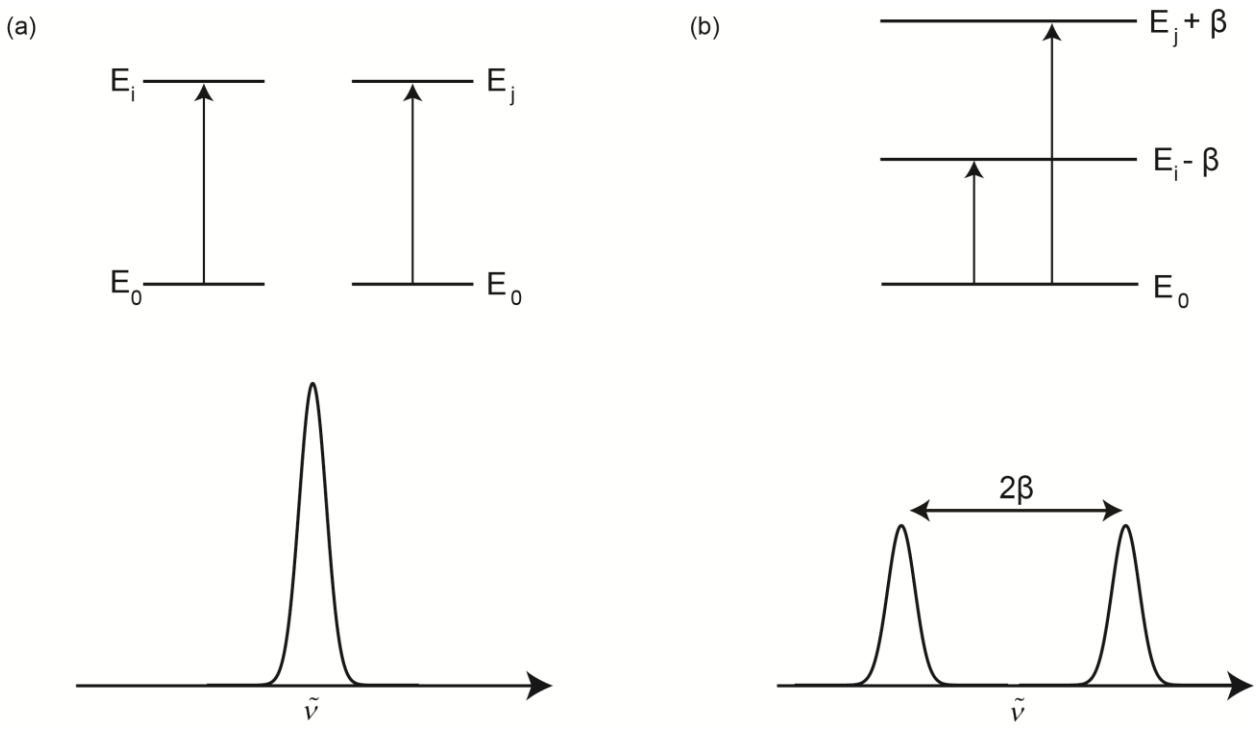

Figure 2.2: Coupling causes peak splitting. (a) Uncoupled, degenerate oscillators i and j. Since the oscillator energies are degenerate, there is only one peak in the IR spectrum. (b) Oscillators i and j are coupled resulting in the splitting of energy levels.

mode, the vibrational energy is localized on the individual oscillators as determined through previous work with N-methylacetamide (NMA) and computer modeling.[15] Since the oscillators are degenerate, only one peak is present in the IR spectrum corresponding to the vibrational frequency of the oscillators' motion. When the oscillators are coupled, the vibrational motion of one oscillator perturbs the vibrational motion of the other. The energy is delocalized over both oscillators. The oscillators can either vibrate in a symmetric or antisymmetric manner to reach either the E_i-β or the E_j+β energy levels giving rise to two peaks in the IR spectrum.[14]

The magnitude of coupling contributes to the peak locations and their relative intensities in an IR spectrum. The influence of coupling on spectral features is a direct result of diagonalizing the Hamiltonian. As the coupling between two oscillators is altered, the location of the peaks and their relative intensities will be modified accordingly. The intensity of the peak scales as the square of the transition dipole strength for the normal mode but not for the local modes.[9, 14]

Peak locations and intensities provide some insight into peptide secondary structure but no information about the peptide's environment. Each amide-I local mode vibrates with a fundamental frequency that can be perturbed by its environment. As the local environment of the oscillator changes, the vibrational frequency will fluctuate. If these fluctuations are fast, the lineshape of the peak is Lorentzian. This type of lineshape is indicative of homogeneous broadening. If the frequency fluctuations are slow compared to the vibrational lifetime, the lineshape reflects only the distribution of vibrational frequencies due to variances in local environment. This lineshape is Gaussian. Gaussian lineshapes are indicative of inhomogeneous broadening. Both lineshapes provide information regarding the samples' environment. The distribution of frequencies provides the structural information while the overall lineshape

provides information about vibrational dynamics. Lorentzian shapes identify a fast solvent while a Gaussian lineshape describes a slow moving environment. All real samples have contributions from both homogeneous and inhomogeneous broadening which cannot be distinguished using IR spectroscopy; however, changes in the amide-I lineshapes can provide information about the distribution of amide-I local mode frequencies.[16]

IR spectroscopy can provide useful information about the secondary structure of peptides due to the coupling of the amide-I modes in the peptide backbone. Secondary structural information regarding peptides in both aqueous buffers and model membranes can be extracted from IR spectra. The presence of spectral peak shifts and changes in the relative intensities can indicate conformational changes to the peptide's secondary structure. The peak widths can be analyzed to comment on the relative distribution of frequencies present in the sample providing some information regarding the system's vibrational dynamics. The IR spectra of the peptide in solution and interacting with a lipid membrane can be studied to identify any structural changes induced by the peptide-lipid interaction. While the cause of these changes cannot be known unambiguously, they provide an indication of a change in structure and/or environment. The exact structure and environment can then be studied through a variety of other techniques including two dimensional infrared spectroscopy and computer modeling.

Samples of surfactin in Tris buffer and DMPC/DHPC bicelles were prepared for FTIR studies concerning the structure of surfactin in solution and in a membrane. The system was controlled with techniques such as deuteration of lipid tails to control the location of the acyl peaks present in the spectrum and isotope labeling of the ester linkages in the lipids to control its peak location in the carbonyl region. Data were collected for surfactin in buffer and bicelles at

various concentrations and analyzed with a focus on peak locations and relative intensities in order to note any structural changes that may have occurred.

2.4 RESULTS AND DISCUSSION: SURFACTIN DIRECTLY INTERACTS WITH BICELLES AND UNDERGOES CONCENTRATION-DEPENDENT CONFORMATIONAL CHANGES

A tunable bicelle system was created to serve as a model membrane to study the surfactin-lipid interaction. The bicelle composition can be varied to include different phospholipids, deuterated lipids, and ^{13}C-labeled phospholipids. Each bicelle system employed can isolate select spectral features to study various parameters in the surfactin-bicelle interaction. Surfactin interacts with all of the bicelle systems created, but each system produces a different IR spectrum. The spectral features can be used to report on the surfactin-bicelle interaction. For example, isotope-labeling the phospholipid ester carbonyls red shifts the signal. If all phospholipid esters in the bicelle samples were labeled with ^{13}C, the entire bicelle signal would be red shifted approximately 30 cm^{-1} separating it from the signal arising from surfactin's aspartate and glutamate carboxylic acid side chains and the ester of the lactone ring allowing different aspects of the surfactin-bicelle interaction to be probed. Labeling DMPC with ^{13}C will be discussed in more detail in the next chapter. Isotope-labeling and DLS techniques can also be utilized to prove the direct interaction of surfactin with the tunable bicelle system.

In order to confirm direct interaction between surfactin and bicelles, dynamic light scattering (DLS) measurements were performed. The hydrodynamic radii of the scattering bodies were extracted from the DLS data. Figure 2.3 shows the evolution of the hydrodynamic radius of bicelles as surfactin is added to the system. The initial data point was acquired for a sample containing bicelles in the absence of surfactin and shows that the initial hydrodynamic

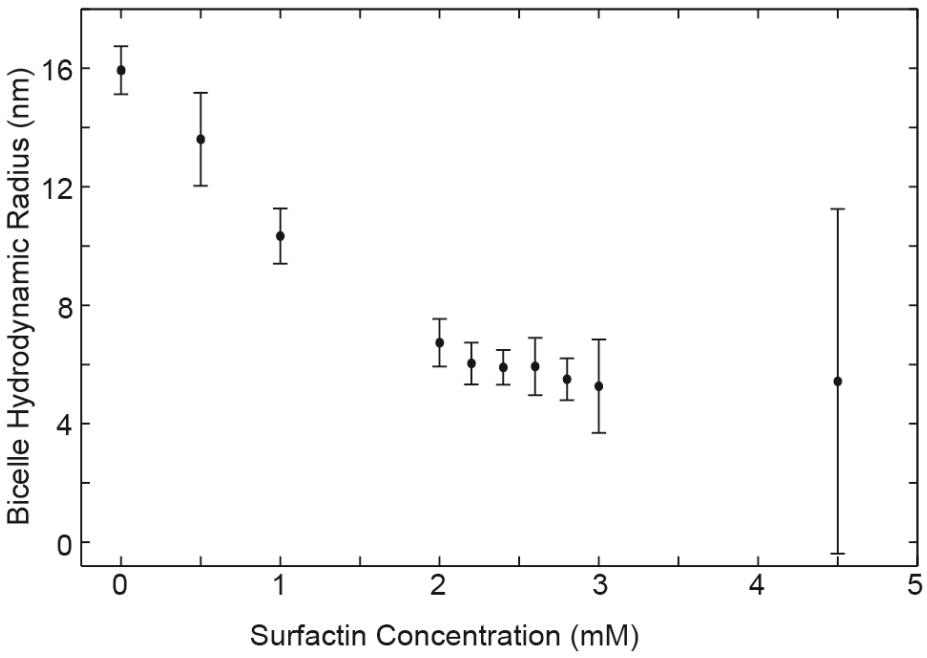

Figure 2.3: Bicelle hydrodynamic radius as a function of surfactin concentration. The hydrodynamic radius of the bicelles extracted from DLS measurements is plotted as a function of surfactin concentration present in the sample. The bars indicate the full width at half maximum of the hydrodynamic radii distribution extracted from the correlation functions.

radius of the bicelle is 15.9 ± 0.8 nm. This result is consistent with bicelles formed with a q value equal to three used in this study.[5] The hydrodynamic radius of the bicelles decreases with increasing amounts of surfactin and plateaus around 5 nm for samples containing surfactin concentrations above 2.0 mM. In addition, the width of the distribution remains constant until the surfactin concentration is above 2.0 mM. Beyond a surfactin concentration of 2.0 mM, the mean hydrodynamic radius is nearly constant, but the width of the distribution increases dramatically.

When no surfactin is present, the solution consists of monodisperse bicelles. Upon the addition of surfactin, the average hydrodynamic radius of the bicelles decreases. The observed change to the size of the bicelles in the presence of surfactin indicates a direct interaction between the two species in solution. The inflection point seen in the data at a surfactin concentration around 2.0 mM may indicate the limit between surfactin's PFT mechanisms. Below a concentration of 2.0 mM, surfactin may be acting via the cation chelation and/or ion channel formation mechanisms discussed in Chapter 1. Above this concentration, the dramatic increase in the size distribution of the scattering bodies suggests that surfactin is operating in a detergent-like manner producing mixed micelles consisting of surfactin and phospholipids.[17-21] The change in particle size measured by DLS confirms that surfactin is interacting directly with the bicelles over the entire concentration range studied; therefore, the bicelles are suitable model membranes to study the surfactin-lipid interaction via other methods.

IR spectroscopies are capable of providing both structural and dynamic information that is necessary to determine and understand the driving mechanism for surfactin's biological activities. Surfactin's interaction with a lipid membrane is still poorly understood. Utilizing linear IR spectroscopy to study a surfactin-lipid interaction could prove useful information

regarding surfactin's structure and vibrational dynamics. However, to obtain a more complete picture of what happens during the surfactin-lipid interaction, tools must be developed to isolate select spectral features to probe specific parameters. These tools have been developed and are presented as the tunable bicelle system discussed here.

In order to probe the conformational transitions of surfactin in aqueous and lipid environments, I monitored the amide-I and amide-II bands in the linear IR absorption spectrum of surfactin as a function of its concentration. The linear IR spectra of surfactin display three peaks in the carbonyl region: a small peak centered at 1731 cm^{-1}, the amide-I band centered around 1640 cm^{-1}, and the amide-II band centered around 1570 cm^{-1}. The peak centered at 1731 cm^{-1} corresponds to the carboxylic acid side chains of the aspartate and glutamate residues as well as the ester of the lactone ring. As mentioned in Section 2.3.2, the amide-I band arises mostly from the C=O stretching of the peptide backbone with some C-N stretching. This mode is sensitive to structural changes due to coupling among the local amide-I modes. The amide-II band comes from the N-H bending and some C-N stretching in the peptide backbone.[9, 12-14]

Representative spectra of surfactin in Tris buffer at high and low surfactin concentrations are provided in Figure 2.4a and b, respectively. Over the entire surfactin concentration range studied, the 1731 cm^{-1} peak and the amide-II band locations remained constant. In contrast, the amide-I band center frequency experienced a significant blue shift upon increasing surfactin concentration. At a surfactin concentration of 0.5 mM, the amide-I band is centered at 1634 cm^{-1} with a full width at half maximum (FWHM) linewidth of 60 cm^{-1}. At 9.0 mM surfactin concentrations, the amide-I band is centered at 1643 cm^{-1} with a FWHM linewidth equal to 50 cm^{-1}. It is obvious from this information that surfactin's amide-I band shifts to higher frequencies and narrows as the surfactin concentration is increased. The FWHM linewidth of the

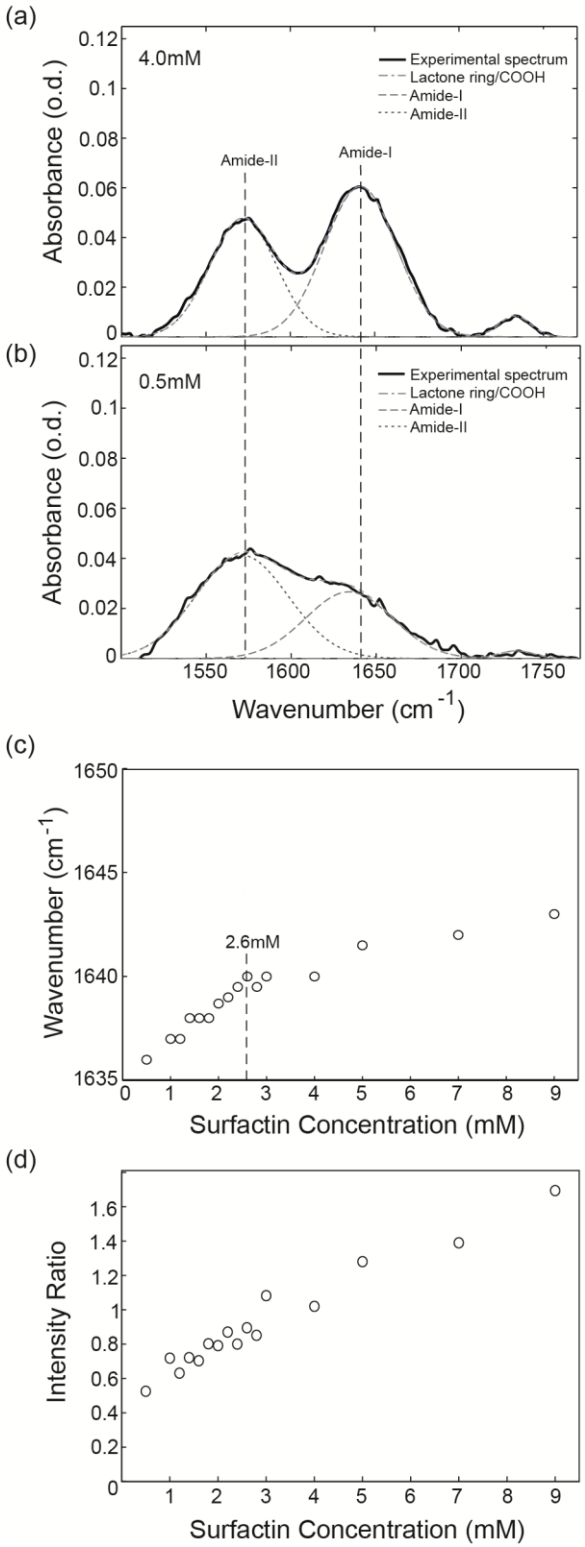

Figure 2.4: FTIR spectra of surfactin in Tris buffer. (a) 4.5 mM and (b) 0.5mM. (c) The amide-I band center frequency plotted as a function of surfactin concentration. (d) The amide-I to amide-II intensity ratio plotted as a function of surfactin concentration.

amide-II band is 64 cm^{-1} at low surfactin concentrations and narrows to 47 cm^{-1} at higher surfactin concentrations in Tris buffer.

The center frequency of the amide-I band determined for each sample of surfactin in Tris buffer is plotted as a function of surfactin concentration in Figure 2.4c. A 9 cm^{-1} shift of the amide-I band is observed. It should also be noted that there is an inflection point in this data at a surfactin concentration of 2.6 mM. Above a 2.6 mM surfactin concentration, the amide-I band center frequency shift only constitutes 2 cm^{-1} of the total 9 cm^{-1} shift observed. Moreover, when comparing the intensity of the amide-I band to the amide-II band, we observe an increase in the ratio of the intensities as the surfactin concentration in Tris buffer increases. The intensity ratio of the amide-I band to the amide-II band is plotted as a function of surfactin concentration in Figure 2.4d.

In order to begin to delineate lipid-induced surfactin behaviors, linear IR absorption experiments were performed on surfactin in the presence of bicelles. The bicelle concentration in each sample was held constant while varying the surfactin concentration from 0.5 mM to 4.5 mM. A representative IR absorption spectrum of surfactin in the presence of bicelles is shown in Figure 2.5a. In this spectrum, the peak centered at 1731 cm^{-1} is more prominent than that seen in the linear IR spectra of surfactin in Tris buffer. This peak still contains information regarding the carboxylic acid side chains and lactone ring of surfactin, but it also contains the signal of the carbonyl stretch associated with the carbonyl esters present on the phospholipid head group. The bicelle's signal overwhelms the signal that arises from the carboxylic acid side chains and carbonyl ester in the lactone ring of surfactin. The peaks centered at 1640 cm^{-1} and 1570 cm^{-1} still report only on surfactin's amide-I and amide-II bands, respectively. As was observed with the samples of surfactin in Tris buffer, the peak at 1731 cm^{-1} and the amide-II

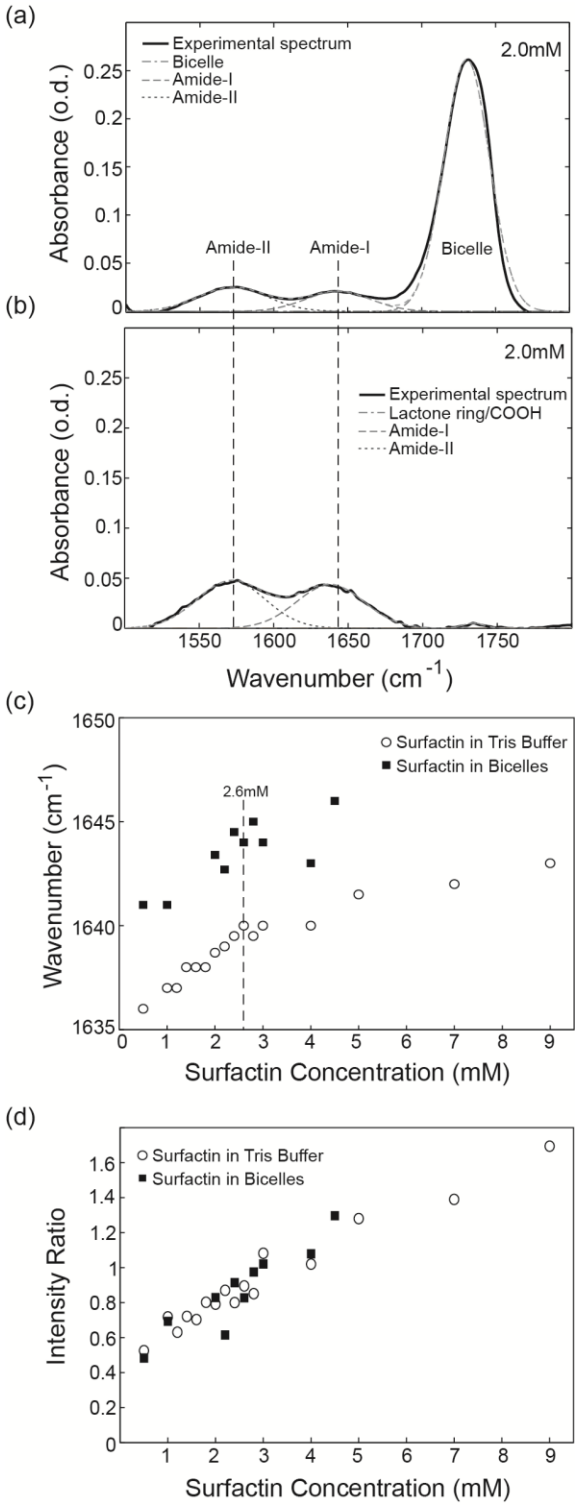

Figure 2.5: FTIR spectrum of surfactin in the presence of bicelles (a) 2.0 mM surfactin in the presence of bicelles. (b) 2.0 mM surfactin in Tris buffer. The surfactin concentration is the same in (a) and (b) to allow for direct comparison between the spectra. (c) The amide-I band center frequency plotted as a function of surfactin concentration. (d) The amide-I to amide-II band intensity ratio plotted as a function of surfactin concentration.

band locations remained constant over the surfactin concentration range studied. At a surfactin concentration of 0.5 mM in the presence of bicelles, the amide-I band location is centered at 1641 cm^{-1} with a FWHM linewidth of 52 cm^{-1}. A 5 cm^{-1} blue shift of the amide-I band center frequency to 1646 cm^{-1} occurs when the surfactin concentration is increased to 4.5 mM. The FWHM linewidth also experiences significant narrowing to 32.3 cm^{-1} at the 4.5 mM surfactin concentration. For comparison, the linear IR absorption spectra for 2.0 mM surfactin in the presence of bicelles and in Tris buffer are presented in Figure 2.5a and b, respectively. These plots emphasize the spectral differences induced by the surfactin-lipid interaction.

The amide-I band location is plotted as a function of surfactin concentration for both surfactin in the presence of bicelles and in Tris buffer (Figure 2.5c). The samples containing bicelles exhibit higher wavenumbers for the amide-I band locations than what was observed for surfactin in Tris buffer; however, the lowest concentrations of surfactin in bicelles appear to have similar spectral features as surfactin at its highest concentration in Tris buffer. The intensity ratio of the amide-I to amide-II bands increases as the surfactin concentration is increased (Figure 2.5d).

Frequency shifts in linear IR absorption spectra can arise from changes in the environment surrounding the oscillator and changes to the coupling between local vibrational modes that give rise to the observed normal modes.[12, 22] A 9 cm^{-1} shift of the amide-I band is observed for surfactin in Tris buffer over the concentration range studied. It is possible that the frequency shifts observed for the amide-I band are due to a change in the local environment surrounding the carbonyls of the peptide backbone. Hydrogen bonding between the peptide backbone and an aqueous solvent produces a 15-25 cm^{-1} red shift[23] which is approximately double the shift observed for this data. Strong coupling has been shown to induce frequency

shifts on the order of 10 cm^{-1} which contrasts with frequency shifts produced as a result of changes in the local environment of the peptide backbone.[12, 22] In combination with the amide-I band frequency shifts, a significant change in the amide-I band to amide-II band intensity ratios is also observed. The change in the intensity ratio indicates a change in the vibrational coupling along the peptide backbone providing a reporter on surfactin's conformation. Taken together, these data suggest that there are changes to the coupling between the carbonyls in the peptide backbone. As noted in Section 2.3.2, a change in the vibrational coupling between local modes will produce frequency shifts and intensity differences due to diagonalizing the vibrational Hamiltonian in the local mode basis.[9, 14]

A change in the vibrational coupling among the carbonyls in the peptide backbone provides strong evidence for a conformational transition in surfactin molecules. [9, 12, 14, 22] The origin of this conformational transition is obvious for surfactin in an aqueous buffer. Surfactin is a natural surfactant, and as such, micellization of surfactin in Tris buffer is expected across the concentration range investigated in this work. As the surfactin concentration is increased, surfactin micelles should form.[1, 24-27] In order to accommodate the formation of micelles, surfactin molecules are required to adopt a new conformation which allows for packing of the surfactin molecules into the micellar structure.[26-30] As the surfactin concentration is increased, it is expected that surfactin micelles will aggregate to form higher order structures. These higher order aggregates of surfactin micelles have previously been shown to possess ellipsoid or cylindrical shapes as well as amorphous structures.[24, 27, 29] Therefore, the amide-I vibrational frequency shift observed for the concentrations of surfactin ranging from 0.5 mM to 2.6 mM may indicate increasing micellization of surfactin while concentrations above 2.6 mM may indicate increasing higher order aggregate structures of surfactin. This is evidenced by the

inflection point seen in the plots of amide-I band frequency shifts as a function of surfactin concentration. Observing micellization in this concentration range is consistent with surfactin's critical micelle concentrations (CMC) previously reported in literature.[26-29] In both the micelles and higher order structures, the surfactin molecules should be in the same conformation.

Interestingly, in the presence of bicelles, surfactin's amide-I frequency experienced a 5 cm^{-1} in comparison to the 8 cm^{-1} shift for surfactin in Tris buffer over the same 0.5-4.5 mM concentration range. The data sets for surfactin in Tris buffer and bicelles exhibit the same behavior in their concentration-dependent amide-I band frequency shifts and the amide-I to amide-II band intensity ratios. The similarities observed for these trends indicate that the vibrational coupling that exists in the peptide backbone for surfactin in Tris buffer also exists for surfactin in the presence of bicelles.

The linear IR absorption spectra of the surfactin-bicelle samples with low surfactin concentrations are nearly identical to the linear IR absorption spectra of high surfactin concentrations in Tris buffer. For example, the amide-I band of 4.5 mM surfactin in Tris buffer is centered at 1641 cm^{-1} with a FWHM linewidth of 50 cm^{-1}. In comparison, the spectrum of 0.5 mM surfactin in the presence of bicelles shows an amide-I band centered at 1641 cm^{-1} with a FWHM linewidth of 52 cm^{-1}. As the concentration of surfactin is increased in the presence of bicelles, the center frequency of the amide-I band becomes centered at 1646 cm^{-1} which is a higher frequency than observed for any of the surfactin in Tris buffer samples. It appears that surfactin's interaction with the bicelles induces a conformational change. Due to the spectral similarities between surfactin at low concentrations in bicelles and high concentrations in Tris buffer, it may be noted that the bicelles could be inducing the same conformational change as micellization and the formation of higher order aggregates seen for surfactin in Tris buffer. The

onset of the conformational change is experienced at lower surfactin concentrations when bicelles are present. Moreover, as the surfactin concentration increases in bicelles, the FWHM linewidth narrows significantly to 32 cm^{-1}. Therefore, this data indicates that the bicelles lock surfactin into a narrower distribution of conformations possessing similar vibrational characteristics to those conformations present in surfactin micelles and higher order aggregates.

2.5 CONCLUDING REMARKS

PFTs are widely found in nature and many exhibit biological activities that could be useful in biomedical applications. To understand these activities, the mechanism of peptide and lipid interaction must be determined. The direct interaction between the bicelles used in this study and surfactin was verified through DLS measurements. Surfactin reduced the size of bicelles reaching a minimum plateau at a 2.0 mM concentration. At surfactin concentrations greater than this, the size distribution of the samples increased dramatically. This suggests surfactin acts with a detergent-like mechanism at these higher concentrations and exhibits a different mechanism at concentrations lower than 2.0 mM. This study demonstrated that IR spectroscopy can provide valuable structural and dynamic information regarding the surfactin-bicelle interaction. By monitoring shifts in the amide-I band location and changes in the amide-I to amide-II band intensity ratios, it was determined that surfactin undergoes a concentration-dependent conformational change. Surfactin adopts a different conformation from its monomer when packed into micelles and higher order aggregates. The data obtained for surfactin in bicelles indicates that surfactin may adopt the same conformation in bicelles as it does in micelles and higher order aggregates. The bicelles also narrow the conformational distribution of the surfactin.

2.6 REFERENCES

1. Li, Y.; Zou, A. H.; Ye, R. Q.; Mu, B. Z., Counterion-Induced Changes to the Micellization of Surfactin-C_{16} Aqueous Solution. *J. Phys. Chem. B* **2009,** *113* (46), 15272-15277.

2. Li, Y.; Ye, R. Q.; Mu, B. Z., Influence of Sodium Ions on Micelles of Surfactin-C^{16} in Solution. *J. Surfactants Deterg.* **2009,** *12* (1), 31-36.

3. Ottiger, M.; Bax, A., Characterization of Magnetically Oriented Phospholipid Micelles for Measurement of Dipolar Couplings in Macromolecules. *J. Biomol. NMR* **1998,** *12* (3), 361-372.

4. Glover, K. J.; Whiles, J. A.; Wu, G. H.; Yu, N. J.; Deems, R.; Struppe, J. O.; Stark, R. E.; Komives, E. A.; Vold, R. R., Structural Evaluation of Phospholipid Bicelles for Solution-State Studies of Membrane-Associated Biomolecules. *Biophys. J.* **2001,** *81* (4), 2163-2171.

5. Vold, R. R.; Prosser, R. S., Magnetically Oriented Phospholipid Bilayered Micelles for Structural Studies of Polypeptides. Does the Ideal Bicelle Exist? *J. Magn. Reson. Ser. B* **1996,** *113* (3), 267-271.

6. *Dynamic Light Scattering with Applications to Chemistry, Biology, and Physics*. Pecora, R., Ed. Dover Publications: New York, 2000.

7. Ford, N. C., Light Scattering Apparatus. In *Dynamic Light Scattering: Applications of Photon Correlation Spectroscopy*, Pecora, R., Ed. Springer: New York, 1985.

8. Skoog, D.; Holler, F.; Crouch, S., *Principles of Instrumental Analysis*. 6 ed.; Thomson Brooks/Cole: Belmont, California, 2007.

9. Hamm, P.; Zanni, M., *Concepts and Methods of 2D Infrared Spectroscopy*. Cambridge University Press: New York, 2011.

10. Henry, B. R., Local Modes in Description of Highly Vibrationally Excited Molecules. *Accounts Chem. Res.* **1977,** *10* (6), 207-213.

11. Wilson, E. B.; Decius, J. C.; Cross, P. C., *Molecular Vibrations: The Theory of Infrared and Raman Vibrational Spectra*. Dover Publications: New York, 1955.

12. Krimm, S.; Bandekar, J., Vibrational Spectroscopy and Conformation of Peptides, Polypeptides, and Proteins. *Advances in Protein Chemistry* **1986,** *38*, 181-364.

13. Torii, H.; Tasumi, M., Model Calculations on the Amide-I Infrared Bands of Globular-Proteins. *Computer Aided Innovation of New Materials Ii, Pts 1 and 2* **1993**, 1287-1290.

14. Barth, A., Infrared Spectroscopy. In *Methods in Protein Structure and Stability Analysis: Vibrational Spectroscopy*, Uversky, V. N.; Permyakov, E. A., Eds. Nova Science: New York, 2007.

15. Moran, A.; Mukamel, S., The Origin of Vibrational Mode Couplings in Various Secondary Structural Motifs of Polypeptides. *P. Natl. Acad. Sci. USA* **2004,** *101* (2), 506-510.

16. Schmidt, J. R.; Sundlass, N.; Skinner, J. L., Line Shapes and Photon Echoes Within a Generalized Kubo Model. *Chem. Phys. Lett.* **2003,** *378* (5-6), 559-566.

17. Deleu, M.; Bouffioux, O.; Razafindralambo, H.; Paquot, M.; Hbid, C.; Thonart, P.; Jacques, P.; Brasseur, R., Interaction of Surfactin with Membranes: A Computational Approach. *Langmuir* **2003,** *19* (8), 3377-3385.

18. Heerklotz, H.; Seelig, J., Leakage and Lysis of Lipid Membranes Induced by the Lipopeptide Surfactin. *Eur. Biophys. J. Biophy.* **2007,** *36* (4-5), 305-314.

19. Heerklotz, H.; Seelig, J., Detergent-Like Action of the Antibiotic Peptide Surfactin on Lipid Membranes. *Biophys. J.* **2001,** *81* (3), 1547-1554.

20. Heerklotz, H.; Wieprecht, T.; Seelig, J., Membrane Perturbation by the Lipopeptide Surfactin and Detergents as Studied by Deuterium NMR. *J. Phys. Chem. B* **2004,** *108* (15), 4909-4915.

21. Kragh-Hansen, U.; le Maire, M.; Moller, J. V., The Mechanism of Detergent Solubilization of Liposomes and Protein-Containing Membranes. *Biophys. J.* **1998,** *75* (6), 2932-2946.

22. Torii, H.; Tasumi, M., Model Calculations on the Amide-I Infrared Bands of Globular-Proteins. *J. Chem. Phys. B* **1992,** *96* (5), 3379-3387.

23. Torii, H.; Tatsumi, T.; Kanazawa, T.; Tasumi, M., Effects of Intermolecular Hydrogen Bonding Interactions on the Amide I Mode of N-methylacetamide: Matrix-Isolation Infrared Studies and ab Initio Molecular Orbital Calculations. *J. Phys. Chem. B* **1998,** *102* (1), 309-314.

24. Knoblich, A.; Matsumoto, M.; Ishiguro, R.; Murata, K.; Fujiyoshi, Y.; Ishigami, Y.; Osman, M., Electron Cryo-Microscopic Studies on Micellar Shape and Size of Surfactin, an Anionic Lipopeptide. *Colloid Surface B* **1995,** *5* (1-2), 43-48.

25. Dejugnat, C.; Diat, O.; Zemb, T., Surfactin Self-Assembles into Direct and Reverse Aggregates in Equilibrium and Performs Selective Metal Cation Extraction. *Chem. Phys. Chem.* **2011,** *12* (11), 2138-2144.

26. Shen, H. H.; Thomas, R. K.; Chen, C. Y.; Darton, R. C.; Baker, S. C.; Penfold, J., Aggregation of the Naturally Occurring Lipopeptide, Surfactin, at Interfaces and in Solution: An Unusual Type of Surfactant? *Langmuir* **2009,** *25* (7), 4211-4218.

27. Han, Y. C.; Huang, X.; Cao, M. W.; Wang, Y. L., Micellization of Surfactin and Its Effect on the Aggregate Conformation of Amyloid β(1-40). *J. Phys. Chem. B* **2008,** *112* (47), 15195-15201.

28. Zou, A. H.; Liu, J.; Garamus, V. M.; Yang, Y.; Willumeit, R.; Mu, B. Z., Micellization Activity of the Natural Lipopeptide [Glu_1, Asp_5] Surfactin-C15 in Aqueous Solution. *J. Phys. Chem. B* **2010,** *114* (8), 2712-2718.

29. Ishigami, Y.; Osman, M.; Nakahara, H.; Sano, Y.; Ishiguro, R.; Matsumoto, M., Significance of β-Sheet Formation for Micellization and Surface Adsorption of Surfactin. *Colloid Surface B* **1995,** *4* (6), 341-348.

30. Nicolas, J. P., Molecular Dynamics Simulation of Surfactin Molecules at the Water-Hexane Interface. *Biophys J* **2003,** *85* (3), 1377-1391.

3 ^{13}C-LABELING OF DMPC

The linear IR spectra for surfactin in the presence of bicelles presented in Chapter 2 illustrate a potential complication for data interpretation in future studies using multidimensional IR spectroscopy to study the surfactin-bicelle interaction. Surfactin's lactone ring and the carboxylic acid side chains of the Asp and Glu residues give rise to an IR signal centered at 1731 cm^{-1} which is overwhelmed by the signal arising from the ester carbonyls present on the phospholipids comprising the bicelles also centered at 1731 cm^{-1}. We would like to be to distinguish between these two signals in future studies allowing different aspects of the surfactin-bicelle interaction to be probed with multidimensional IR spectroscopy. In order to distinguish between the two signals, one of the signals must be shifted to a different frequency. Shifting IR spectral peaks is accomplished using selected isotope labeling of the molecule. Isotope labeling successfully shifts IR spectral peaks by altering the reduced mass of the oscillator thereby modifying its vibrational frequency. By labeling the phospholipid esters with ^{13}C, the bicelle signal would be red shifted approximately 30 cm^{-1} allowing it to be resolved from the surfactin signals. This chapter describes the progress that has been made toward synthesizing ^{13}C-labeled DMPC in a first step attempt to differentiate the surfactin and bicelle signals.

3.1 ^{13}C-LABELED DMPC SYNTHESIS

An esterification reaction described by Volkov *et al.*[1] was followed to synthesize DMPC with the sn-2 carbon labeled with ^{13}C. The reaction scheme is provided in Figure 3.1.

TBCR (0.3 mmol, 4-(4,6-dimethoxy-1,3,5-triazin-2-yl)-4-methylmorpholinium tetrafluoroborate; AK Scientific, Union City, CA) was added to a 10 mL round bottom flask and dissolved in 3 mL of acetonitrile (CH_3CN; Macron Chemicals, Charlotte, NC). MA (0.6 mmol,

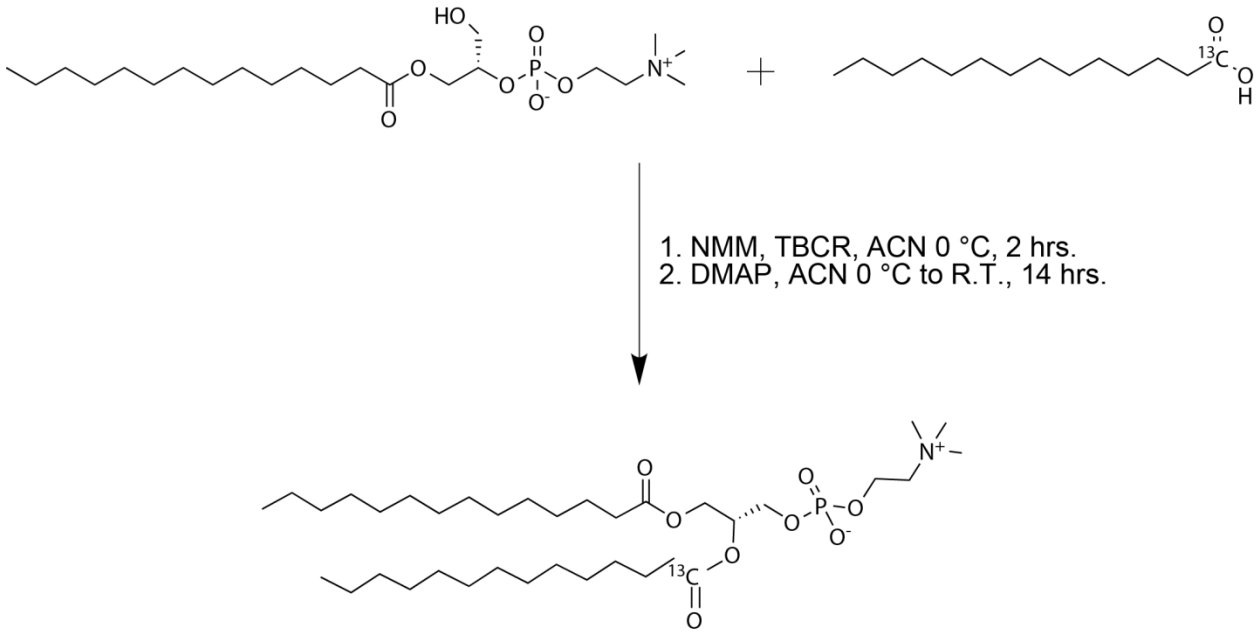

Figure 3.1: ^{13}C-labeled DMPC synthesis scheme. Esterification reaction between 1-myristyol-sn-glycero-3-phosphocholine and myristic acid-1-^{13}C to produce 1,2-dimyristoyl-sn-glycero-3-phosphocholine with the sn-2 location labeled with ^{13}C.

Myristic acid-1-^{13}C; Santa Cruz Biotechnology, Santa Cruz, CA) was added to the solution which was brought to 0°C and stirred. NMM (0.3 mmol, N-methylmorpholine; Sigma Aldrich, St. Louis, MO) was added to the stirred solution. The solution continued stirring at 0°C for two hours.

Concurrently, MPC (0.375 mmol, 1-myristoyl-sn-glycero-3-phosphocholine; Chem-Impex, Wood Dale, IL) and a catalytic amount (approximately 0.02 g) of DMAP (4-(dimethylamino)pyridine; Sigma Aldrich) were dissolved in 4.5 mL of acetonitrile in a 10 mL round bottom flask and stirred at room temperature. After the two hours of stirring was completed the MPC and DMAP solution was added to the TBCR, MA, and NMM solution. The new solution was stirred at 0°C for 30 minutes. The solution was then allowed to stir at room temperature for 14 hours.

The solvent was removed using a rotary evaporator. The residue was treated with chloroform (0.5 mL, $CHCl_3$; Mallinkrodt Chemicals, Phillipsburg, NJ) and filtered over Celite (Celite 545; Sigma Aldrich). The flask was rinsed with three 0.5 mL aliquots of chloroform to remove all traces of the product from the reaction flask and the rinsate was also filtered over Celite. The filtered product was dried and purified using flash column chromatography (FCC). For the milligram quantities of product synthesized, the column used for FCC purification was 20 mm wide. The column was packed with a cotton plug, a layer of sand (Fisher Scientific), silica gel (Sigma-Aldrich, 60 Å pore size, 200-400 mesh), and another layer of sand to protect the integrity of the column during sample loading and solvent addition. The layer of silica gel was 165 mm tall.

The column was run with a mobile phase solvent consisting of 65:25:4 by volume chloroform, methanol, and water, respectively. The ^{13}C-labeled DMPC had a retention

factor (R_f) of 0.2 using this solvent mixture as the mobile phase. Three fractions eluted from the column. The first fraction contains the DMAP catalyst, the second fraction is the desired ^{13}C-labeled DMPC product, and the third fraction consists of unreacted starting materials. The location of the fractions were determined by running thin layer chromatography (TLC) plates (Sigma-Aldrich, silica gel matrix on aluminum support, 60 Å pore size, normal phase), and their identity was predicted by running standards on the same plate. The TLC plates were placed into a jar containing a small amount of sand and iodine crystals (Fisher Scientific) then gently shaken to stain the spots. Fractions containing the ^{13}C-labeled DMPC were combined and dried. The identity of the product was confirmed with NMR and FTIR spectroscopies. The ^{13}C-labeled DMPC was used with non-labeled DHPC to make bicelles according to the procedure described in Section 2.1.2. The bicelles containing the ^{13}C-labeled DMPC were also used to prepare samples containing surfactin and bicelles according to the procedure outlined in Section 2.1.3.

3.2 RESULTS AND DISCUSSION

As demonstrated in the previous chapter, the IR signal that occurs at 1731 cm^{-1} from the phospholipid carbonyls overwhelms the signal from the carboxylic acid side chains from the Asp and Glu residues as well as the lactone ring of the surfactin molecules. We would like to be able to differentiate the two signals in future experiments. In order to separate the lipid and surfactin vibrational signals, the reduced mass of one of the oscillators must be altered to modify its vibrational frequency thereby shifting its spectral peak. This is accomplished through isotope labeling.[2] By labeling the phospholipid carbonyls with ^{13}C, the oscillator's spectral peak is red shifted approximately 30 cm^{-1}. If all phospholipid esters in the bicelle samples were labeled

with ^{13}C, the entire bicelle signal would be red shifted resolving it from surfactin's signal allowing different aspects of the surfactin-bicelle interaction to be probed.

The ^{13}C-labeled DMPC product was identified using NMR. The NMR spectrum for the ^{13}C-labeled DMPC is provided in Figure 3.2, and the list of the chemical shifts for each peak and the identity of the responsible protons are provided in Table 3.1. Figure 3.3 shows a diagram of ^{13}C-labeled DMPC with the protons labeled according to the location of their respective NMR peaks. A closer examination of the NMR spectrum reveals that a contaminant is present in the purified product. Results of comparing the peaks not associated with the ^{13}C-labeled DMPC to NMR spectra for the starting materials (Figures 3.4 through 3.8) and running comparative TLC plates indicate that the contaminant is most likely DMAP. The NMR spectrum for the ^{13}C-labeled DMPC is also missing some peaks that should be present. The missing peaks correspond to the unlabeled protons on the DMPC molecule provided in Figure 3.3. The multiplicities of some peaks were also not clearly resolved. Both of these issues arise from the fact that the DMPC product was too dilute to produce strong enough NMR signals.

The linear IR spectra for regular bicelles and bicelles containing ^{13}C-labeled DMPC and regular DHPC are provided in Figure 3.9a and b, respectively. The calculated linear IR spectrum for the ^{13}C-labeled DMPC/DHPC bicelles exhibits a small peak centered at 1702 cm^{-1} which was identified as the ^{13}C-labeled DMPC carbonyl. Only one ester on the DMPC head group is labeled with ^{13}C. The other DMPC ester and both DHPC esters were not isotope-labeled so they still vibrate with the natural frequency for a $^{12}C=^{16}O$ carbonyl. The contribution of the unlabeled ester carbonyls to the linear IR spectrum still present a dominant peak centered at 1731 cm^{-1}. The NMR spectrum and the presence of the 1702 cm^{-1} peak in the linear IR spectrum confirms the success of the isotope-labeling procedure. For future studies, both DMPC esters

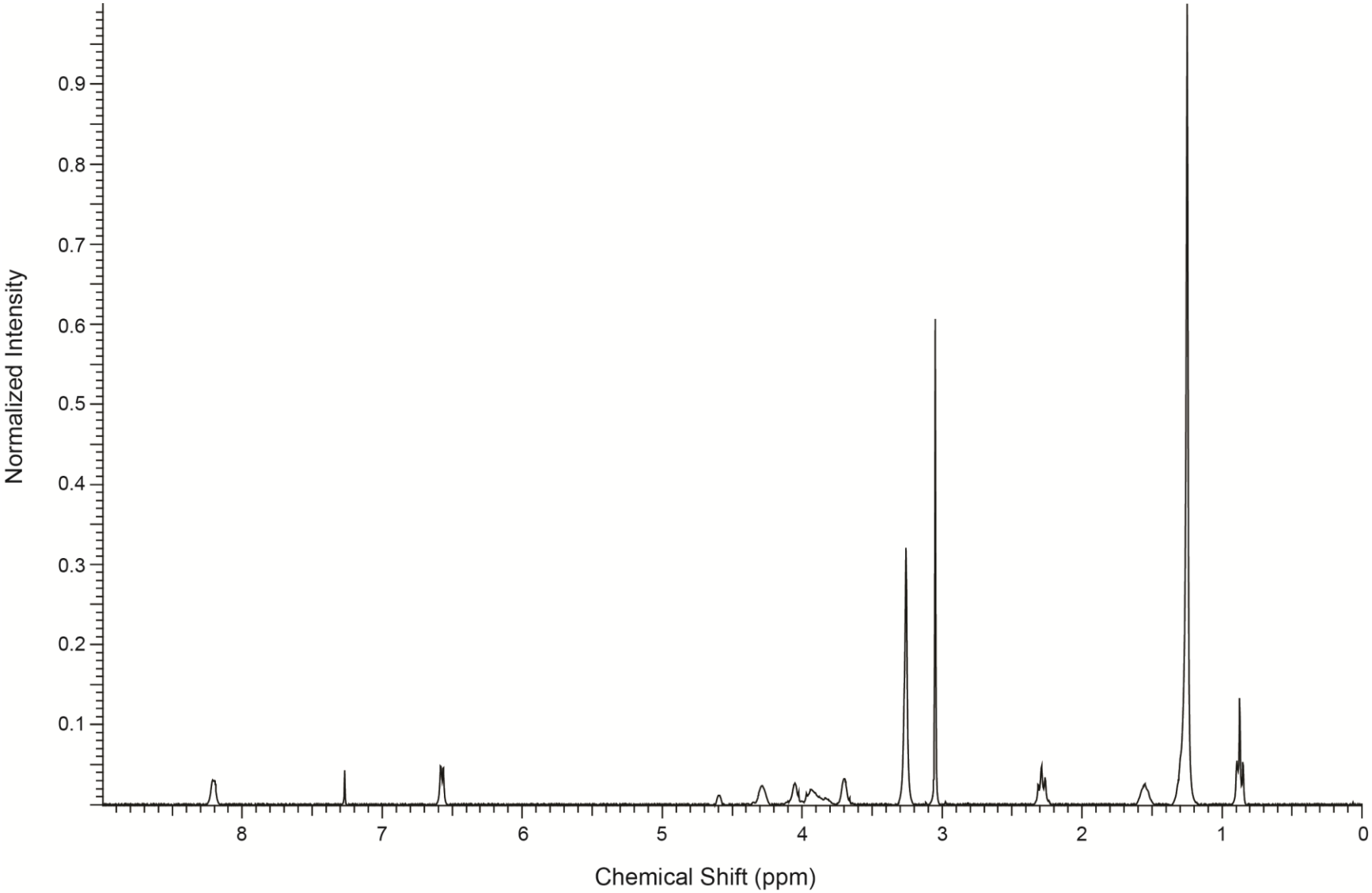

Figure 3.2: NMR spectrum of ^{13}C-labeled DMPC

Table 3.1: Summary of NMR data collected for ^{13}C-labeled DMPC.

Number	Shift (ppm)	Type	DMPC Proton
1	0.87	t	2 x CH_3
2	1.25	s	2 x $(CH_2)_{10}$
3	1.55	m	2 x $COCH_2CH_2$
4	2.29	t	2 x $COCH_2CH_2$
5	3.05	s	DMAP
6	3.27	br. s	$N(CH_3)_3$
7	3.7	m	OCH_2CH_2N
8	4.05	m	OCH_2CH_2N
9	4.29	m	$CHCH_2OP$
10	6.57	d	DMAP
11	7.27	s	$CDCl_3$ reference
12	8.2	d	DMAP

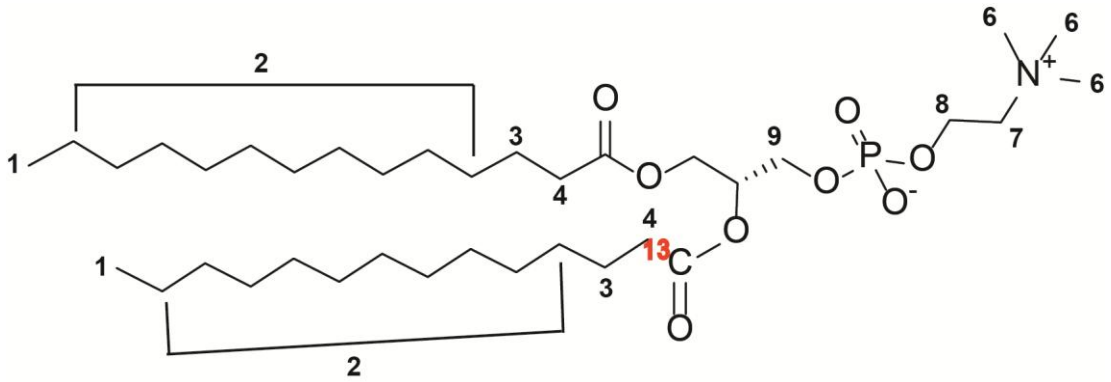

Figure 3.3: ^{13}C-labeled DMPC with protons numbered according to their NMR chemical shifts.

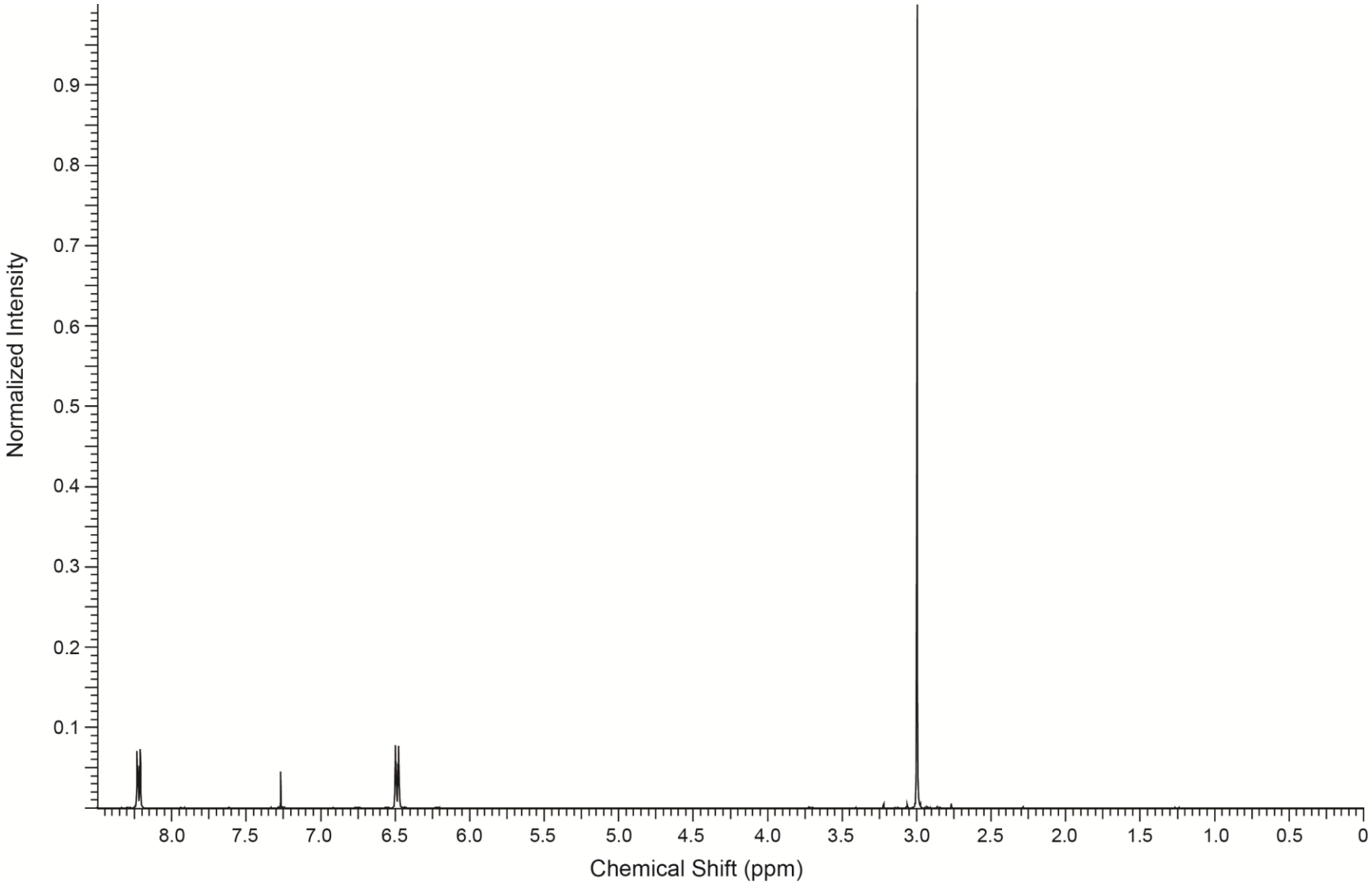

Figure 3.4: NMR spectrum of DMAP.

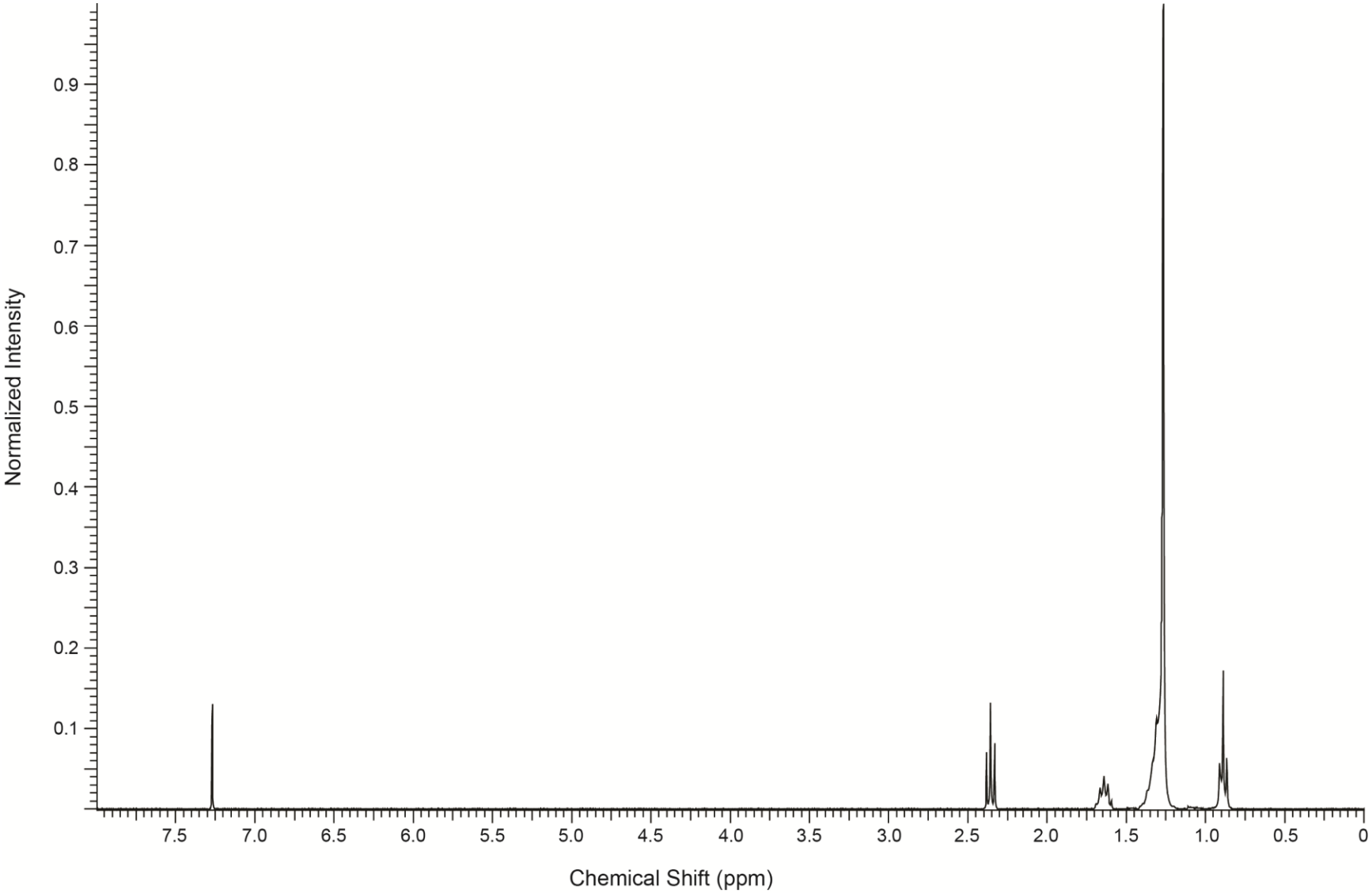

Figure 3.5: NMR spectrum of MA.

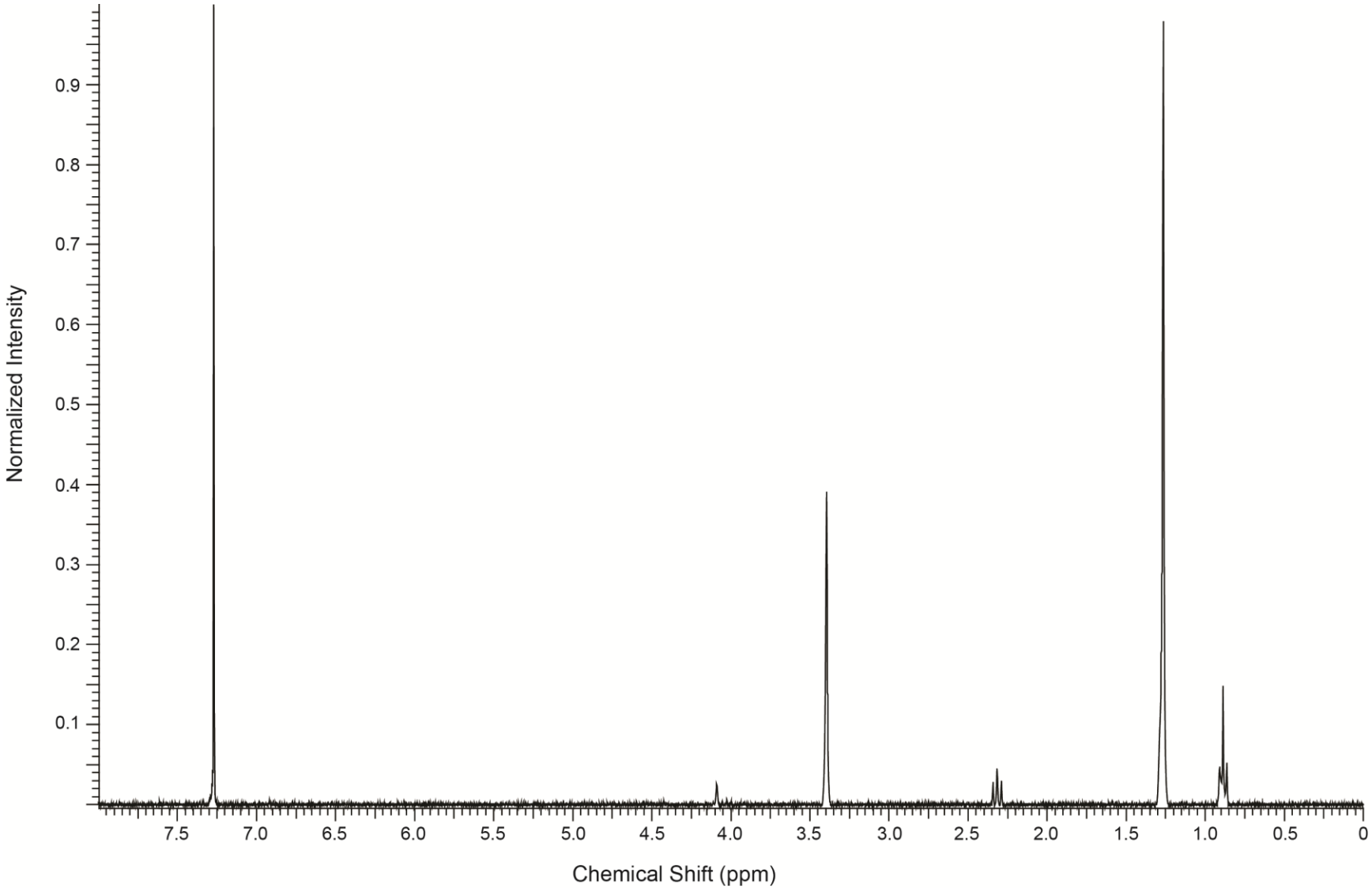

Figure 3.6: NMR spectrum of MPC.

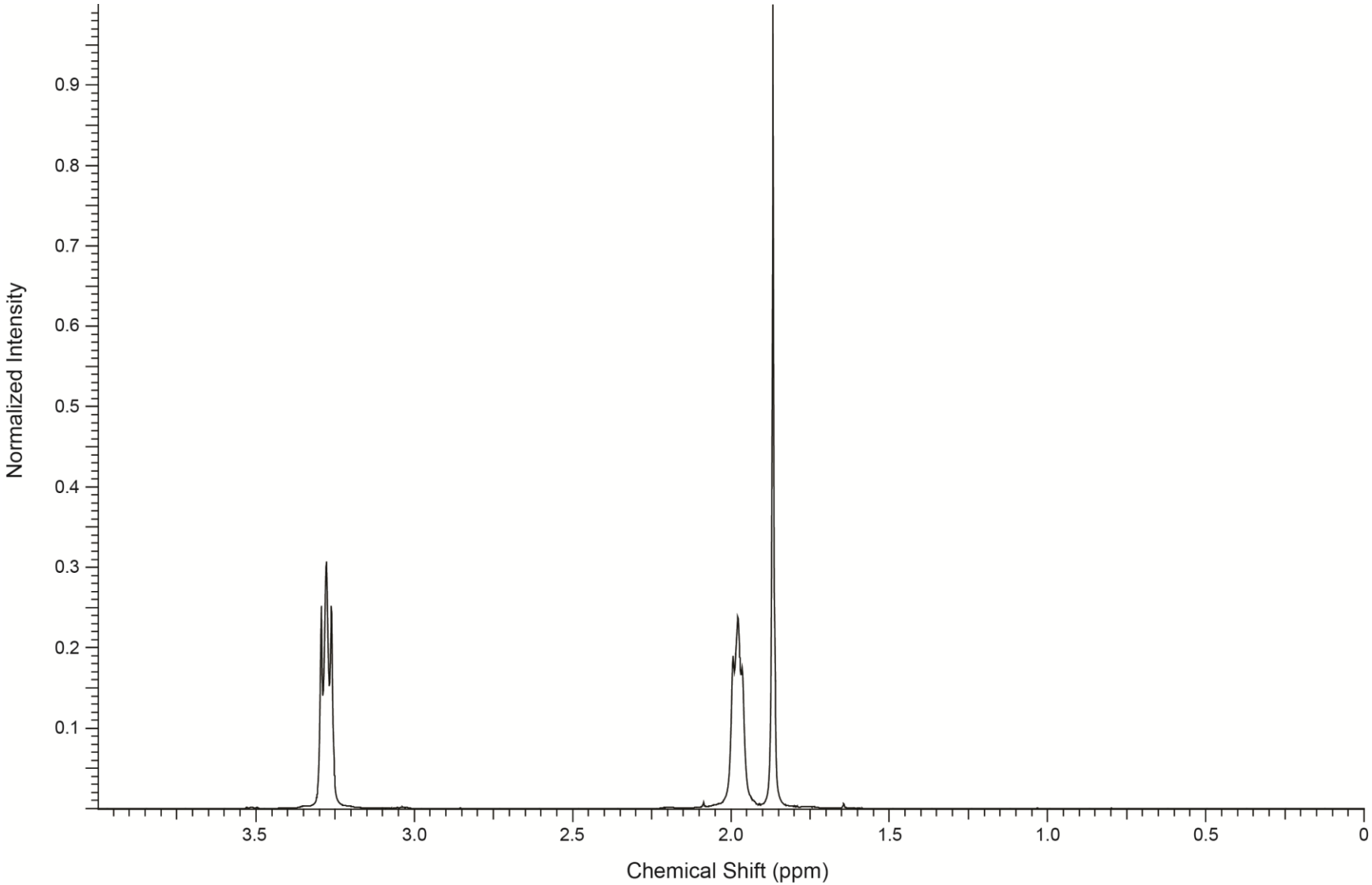

Figure 3.7: NMR spectrum of NMM.

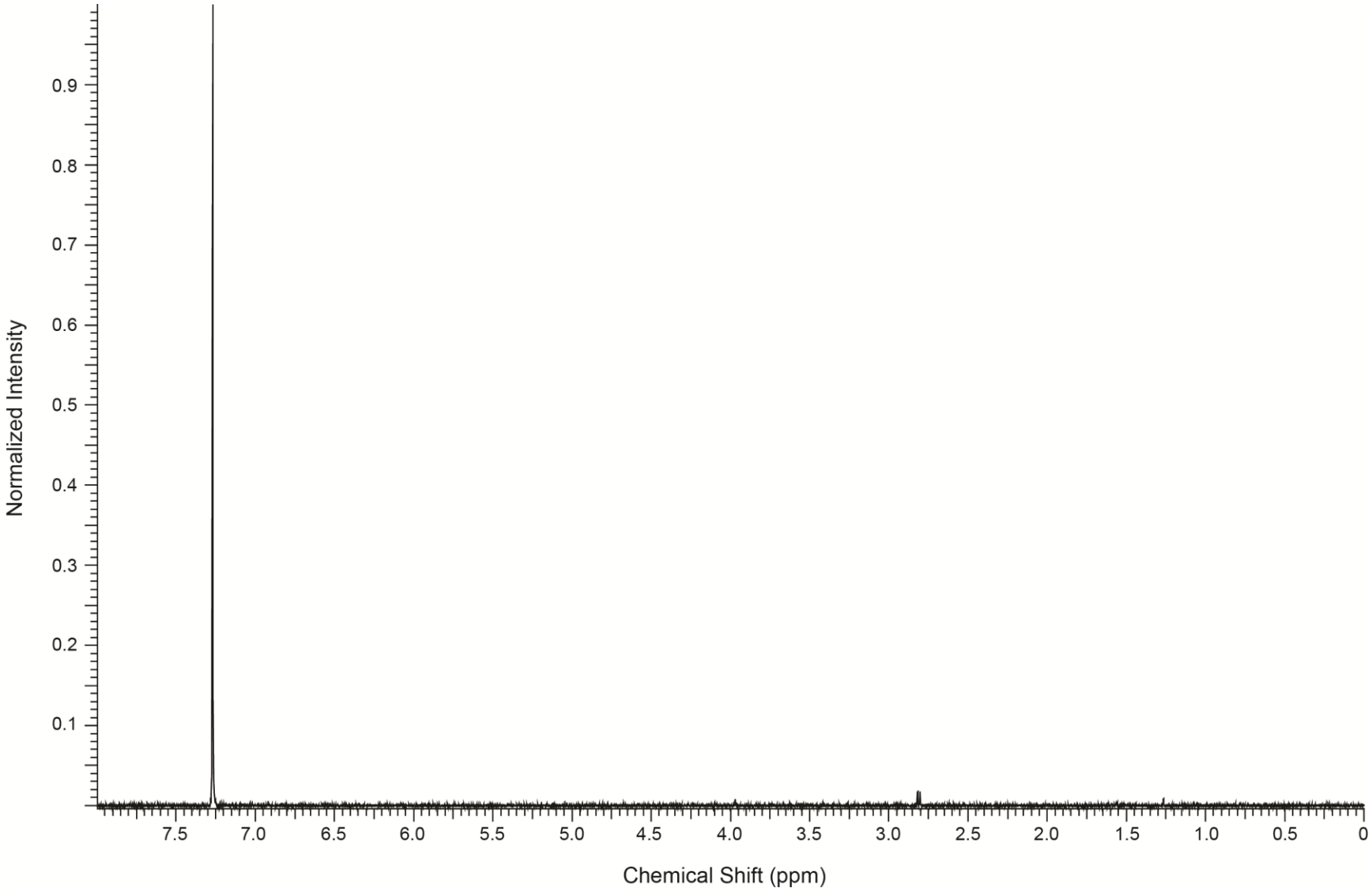

Figure 3.8: NMR spectrum of TBCR.

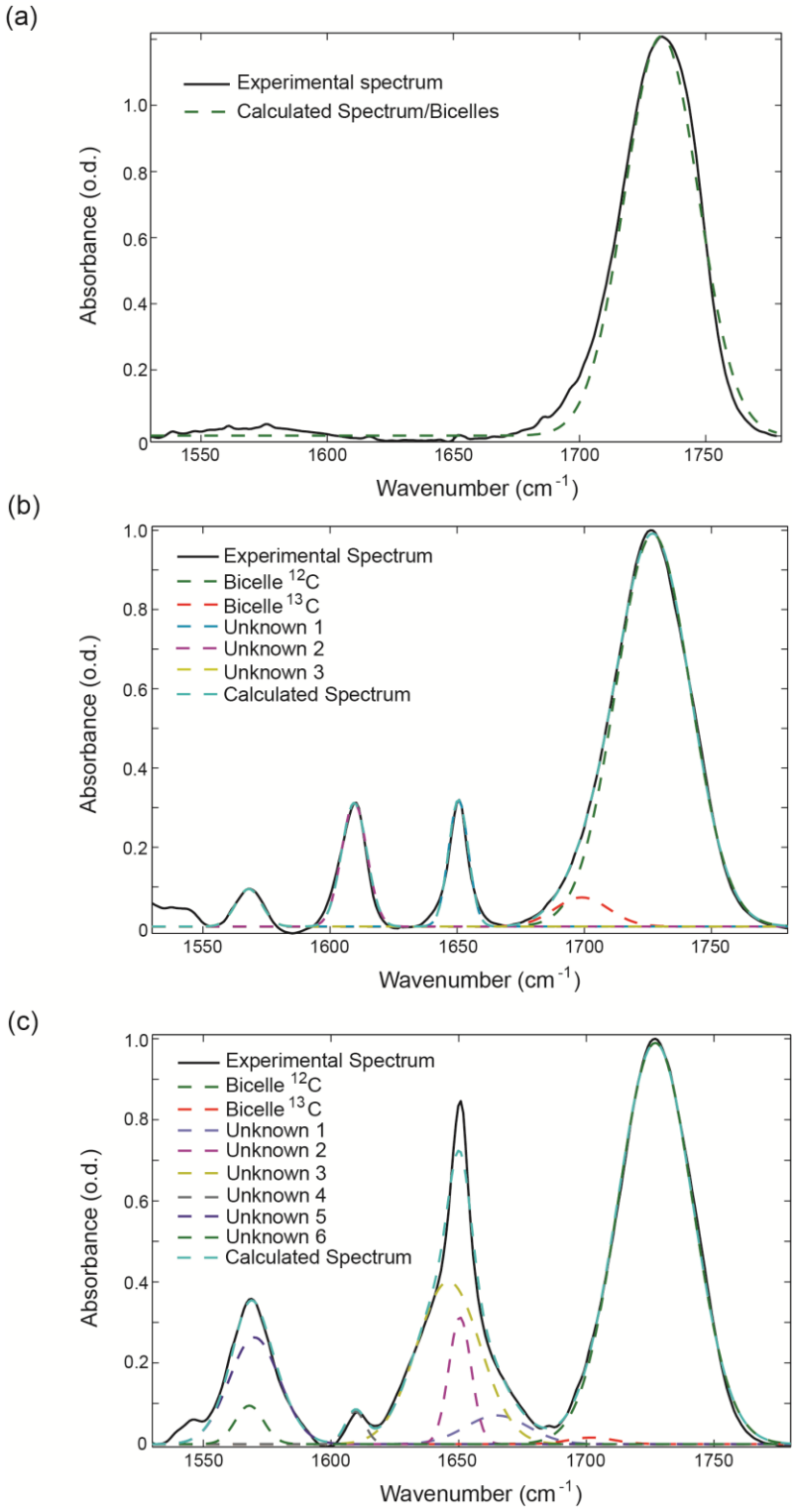

Figure 3.9: FTIR spectra for ^{13}C-labeled DMPC bicelles (a) Non-labeled DMPC/DHPC bicelles. (b) ^{13}C-labeled DMPC/DHPC bicelles with a contaminant present. (c) 4.5mM surfactin in ^{13}C-labeled DMPC/DHPC bicelles.

should be ^{13}C-labeled as well as the DHPC esters. By labeling all lipid carbonyls with ^{13}C, the entire lipid signal should be shifted to a center frequency of 1702 cm^{-1} allowing it to be resolved from the surfactin signal.

It should also be noted that the linear IR spectrum of the ^{13}C-labeled bicelles presents three peaks that are not the result of the phospholipids. As mentioned previously, NMR and TLC experimentation has indicated a potential source of the ^{13}C-DMPC contamination could be the DMAP catalyst that was not completely removed from the sample during purification. Figure 3.4c demonstrates the problem that arises from the presence of these peaks. The linear IR spectrum provided in Figure 3.9c shows 4.5 mM surfactin in the presence of the ^{13}C-labeled DMPC/DHPC bicelles. It is clearly observed that the contaminant peaks occur at frequencies that interfere with surfactin's amide-I and amide-II bands. The surfactin peaks cannot be resolved from the contaminant peaks complicating data analysis.

To remove the interfering contaminant peaks from the FTIR spectrum, different background subtraction algorithms could be developed; however, there is a greater chance of introducing error into the data. In addition, spectra of surfactin in the ^{13}C-labeled bicelles over various concentrations appear to have inconsistent contaminant peak intensities. This could be solely due to the overlapping signals or it could be due to inconsistencies in the sample. It is also unclear if the contaminant interacts with constituents of the sample to alter the surfactin-bicelle interaction. The best route to remove the interfering contaminant peaks is to employ a better purification protocol. The ^{13}C-labeled DMPC is purified by FCC, so an attempt to achieve better product purification was made by using a wider column. Using a wider column spreads the product over a wider surface area increasing the number of theoretical plates to enhance separation[2]; however, this ended up diluting the ^{13}C-labeled DMPC product to the point where it

was undetectable and unrecoverable. Experimenting with varying DMAP concentrations in buffer indicate that DMAP must be present in concentrations less than 10 mM to be undetectable in a linear IR spectrum. It was also found that reducing the DMAP content during synthesis resulted in no product formation. Additional methods to purify the product must be developed to reduce the final DMAP concentration below this threshold. Developing a better purification protocol can begin by identifying a different and more effective mobile phase solvent to use to in the flash column or employing high performance liquid chromatography (HPLC) instruments which would allow for more control over the separation parameters such as mobile phase composition, solvent speed, and column characteristics.

3.3 CONCLUDING REMARKS

Isotope-labeling all of the phospholipid carbonyls would allow the surfactin and bicelle IR signals to be differentiated. The ability to distinguish the bicelle and surfactin IR signals will prove beneficial in future works utilizing multidimensional IR spectroscopy to study the surfactin-bicelle interaction. Progress has been made to label the phospholipid carbonyls with ^{13}C in order to modify its vibrational frequency resulting in a red shift of the IR spectral peak. However, the product exhibits contamination from starting materials that were not completely removed during the purification process. The contamination significantly impairs interpretation of the linear IR data when surfactin is present. A better purification protocol must be developed to remove the contamination. A more pure product may be achieved by identifying a more effective mobile phase solvent to use in the FCC purification or utilizing HPLC to control the parameters involved in purification such as the identity of the mobile phase, the solvent flow rate, and column characteristics.

3.4 REFERENCES

1. Volkov, V. V.; Nuti, F.; Takaoka, Y.; Chelli, R.; Papini, A. M.; Righini, R., Hydration and Hydrogen Bonding of Carbonyls in Dimyristoylphosphatidylcholine Bilayer. *J. Am. Chem. Soc*. **2006,** 128 (29), 9466-9471.

2. Skoog, D.; Holler, F.; Crouch, S., *Principles of Instrumental Analysis*. 6 ed.; Thomson Brooks/Cole: Belmont, California, 2007.

4 FUTURE DIRECTIONS

4.1 TWO-DIMENSIONAL INFRARED SPECTROSCOPY (2D IR)

Understanding the physical principles and mechanisms that define the function of biological molecules is a key goal in biomedical research that aims to use proteins and peptides as therapeutic agents. The structural and dynamic features of protein/peptide functions must be understood to safely utilize them in biomedical applications.[1-3] Vibrational spectroscopy is able to characterize intra- and intermolecular interactions on a picosecond time scale. On the picosecond time scale, large structural dynamics like the changes in peptide backbone conformation appear static. Faster events such as changes in the hydrogen bonding and/or solvent environments would appear dynamic.[4-7] This means that the lineshapes of vibrational spectroscopy are sensitive to structural distributions that are typically averaged out in techniques with a slower time resolution so they can be used to monitor events such as protein folding.

As discussed in previous sections, the absorption spectrum of a peptide's amide-I band reports on the secondary structure of the peptide backbone because it is determined by the angular and distance dependence of the transition dipole interactions. Linear IR spectra can indicate the type of secondary structure present in a peptide, but the spectra do not contain separate peaks for all of the amide-I local modes that together constitute the amide-I normal mode. Homogeneous and inhomogeneous broadening contributions widen the spectral peaks producing broad bands thereby limiting the information available from linear IR measurements.[8] With the development of new spectroscopic techniques, information can be gleaned from the spectra to enhance interpretation of structural parameters. A way to provide better structural and dynamic information is to increase the number of observables produced by the technique.[9]

Two-dimensional IR (2D IR) provides bond-specific structural resolution at any time scale down to the femtosecond regime. 2D IR provides more observables than linear IR allowing for additional data to be extracted and fit with coupling models to elucidate protein structure and vibrational dynamics. The structural sensitivity stems from coupling between vibrational modes which produces characteristic IR bands and cross-peaks.[10] Vibrational transitions observed in linear IR lie along the diagonal of the 2D IR spectrum while the presence of coupling produces cross-peaks that depend on the secondary and tertiary structures of peptides.[11] The spectra also reveal dynamic information in their lineshapes. The anti-diagonal linewidths provide a measure of the homogeneous contribution while the diagonal linewidth contains both homogeneous and inhomogeneous contributions.[3, 10, 12-13]

Collected spectra can be quantitatively computed from molecular dynamics simulations to directly compare to all-atom models in determining molecular structure. Using the features of the cross-peaks present in the spectrum and understanding the angular and distance dependence of molecular coupling can provide information regarding the distance and orientation of coupled molecules or coupled portions of the same molecule. Monitoring the lineshapes provides dynamic information.[3, 10, 12-13]

By collecting 2D IR spectra for a protein or peptide, spectral features like peak locations, intensities, existence of cross-peaks, the polarization dependence of the cross-peaks, and linewidths provide data that can be fit with models and computer simulated to calculate structural and dynamic parameters from the system. 2D IR spectroscopy provides more observables to structure and dynamics than linear IR spectroscopy proving it to be a valuable tool to study protein-lipid interactions. The tools developed and described in this work are valuable in conducting future 2D IR studies.

A tunable bicelle system allows different parameters of the surfactin-bicelle interaction to be probed by controlling peak locations. Isotope-labeling in the bicelles isolates the bicelle and surfactin carbonyl signals allowing for cross-peaks to emerge if coupling is present. Surfactin could also have selected residues isotope-labeled to control peak locations and extract information regarding the coupling between different residues along the peptide backbone. Selective isotope-labeling allows different information to be extracted from the spectra providing detailed structural and dynamic information necessary to understand the function of surfactin in a lipid membrane. Applying 2D IR spectroscopy to the surfactin-bicelle system brings science closer to understanding the mechanism behind its biological activities enabling a safer and controlled use of the peptide in biomedical applications.

4.2 REFERENCES

1. Chung, J. K.; Thielges, M. C.; Fayer, M. D., Dynamics of the Folded and Unfolded Villin Headpiece (HP35) Measured with Ultrafast 2D IR Vibrational Echo Spectroscopy. *P. Natl. Acad. Sci. USA* **2011,** *108* (9), 3578-3583.

2. Dill, K. A.; Shortle, D., Denatured States of Proteins. *Annu. Rev. Biochem.* **1991,** *60*, 795-825.

3. Hunt, N. T., 2D-IR Spectroscopy: Ultrafast Insights into Biomolecule Structure and Function. *Chem. Soc. Rev.* **2009,** *38* (7), 1837-1848.

4. Mukherjee, P.; Kass, I.; Arkin, I.; Zanni, M. T., Picosecond Dynamics of a Membrane Protein Revealed by 2D IR. *P. Natl. Acad. Sci. USA* **2006,** *103* (10), 3528-3533.

5. Hamm, P.; Hochstrasser, R. M., *Ultrafast Infrared and Raman Spectroscopy*. Dekker: New York, 2001.

6. Hamm, P.; Lim, M.; Hochstrasser, R. M., Non-Markovian Dynamics of the Vibrations of Ions in Water from Femtosecond Infrared Three-Pulse Photon Echoes. *Phys. Rev. Lett.* **1998,** *81* (24), 5326-5329.

7. Zimdars, D.; Tokmakoff, A.; Chen, S.; Greenfield, S. R.; Fayer, M. D.; Smith, T. I.; Schwettman, H. A., Picosecond Infrared Vibrational Photon Echoes in a Liquid and Glass Using a Free-Electron Laser. *Phys. Rev. Lett.* **1993,** *70* (18), 2718-2721.

8. Hamm, P.; Lim, M. H.; Hochstrasser, R. M., Structure of the Amide I Band of Peptides Measured by Femtosecond Nonlinear-Infrared Spectroscopy. *J. Phys. Chem. B* **1998,** *102* (31), 6123-6138.

9. Hochstrasser, R. M., Two-Dimensional Spectroscopy at Infrared and Optical Frequencies. *P. Natl. Acad. Sci. USA* **2007,** *104* (36), 14190-14196.

10. Hamm, P.; Zanni, M., *Concepts and Methods of 2D Infrared Spectroscopy*. Cambridge University Press: New York, 2011.

11. Zanni, M. T.; Hochstrasser, R. M., Two-Dimensional Infrared Spectroscopy: A Promising new Method for the Time Resolution of Structures. *Curr. Opin. Struc. Biol.* **2001,** *11* (5), 516-522.

12. Mukamel, S., Multidimensional Femtosecond Correlation Spectroscopies of Electronic and Vibrational Excitations. *Annu. Rev. Phys. Chem.* **2000,** *51*, 691-729.

13. Golonzka, O.; Khalil, M.; Demirdoven, N.; Tokmakoff, A., Vibrational Anharmonicities Revealed by Coherent Two-Dimensional Infrared Spectroscopy. *Phys. Rev. Lett.* **2001,** *86* (10), 2154-2157.

APPENDIX A

BIOCHEMISTRY BASICS

Proteins and peptides are essential macromolecules produced by every living organism. The twenty standard amino acids act as building blocks for protein synthesis, and the specific combination of amino acids define the various proteins and peptides. All amino acids have the same general structure consisting of a central α carbon to which an amine group, a carboxylic acid group, a hydrogen atom, and a unique R group side chain are attached. The general structure of an amino acid is provided in Figure A1.

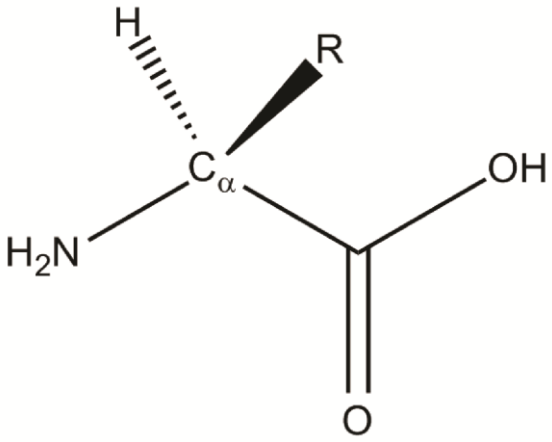

Figure A1: The general structure of an amino acid. R represents the unique side chain.

Amino acids are linked through amide bonds to form peptides. The beginning of the peptide chain is called the N terminal because it contains a free amine group. The C terminal ends the chain with a free carboxylic acid group. The carbonyl and amide groups within the peptide chain provide the opportunity for hydrogen bonding. Hydrogen bonding is also possible with the functional groups of the amino acid side chains.

The sequence of amino acids causes proteins and peptides to spontaneously fold into three dimensional structures which are crucial to their function. Protein function also depends on the chemical functional groups present in the side chain of each amino acid residue. The three

dimensional structure of a protein comes from the amino acid sequence, secondary structure, tertiary structure, and quaternary structure. There are three main types of secondary structures: α-helix, β-sheets, and β-turns which are illustrated in Figure A2. Tertiary structures involve the specific arrangement of secondary structures to ultimately define the three dimensional geometry of the protein. The quaternary structure describes how folded protein subunits assemble to form larger complexes.

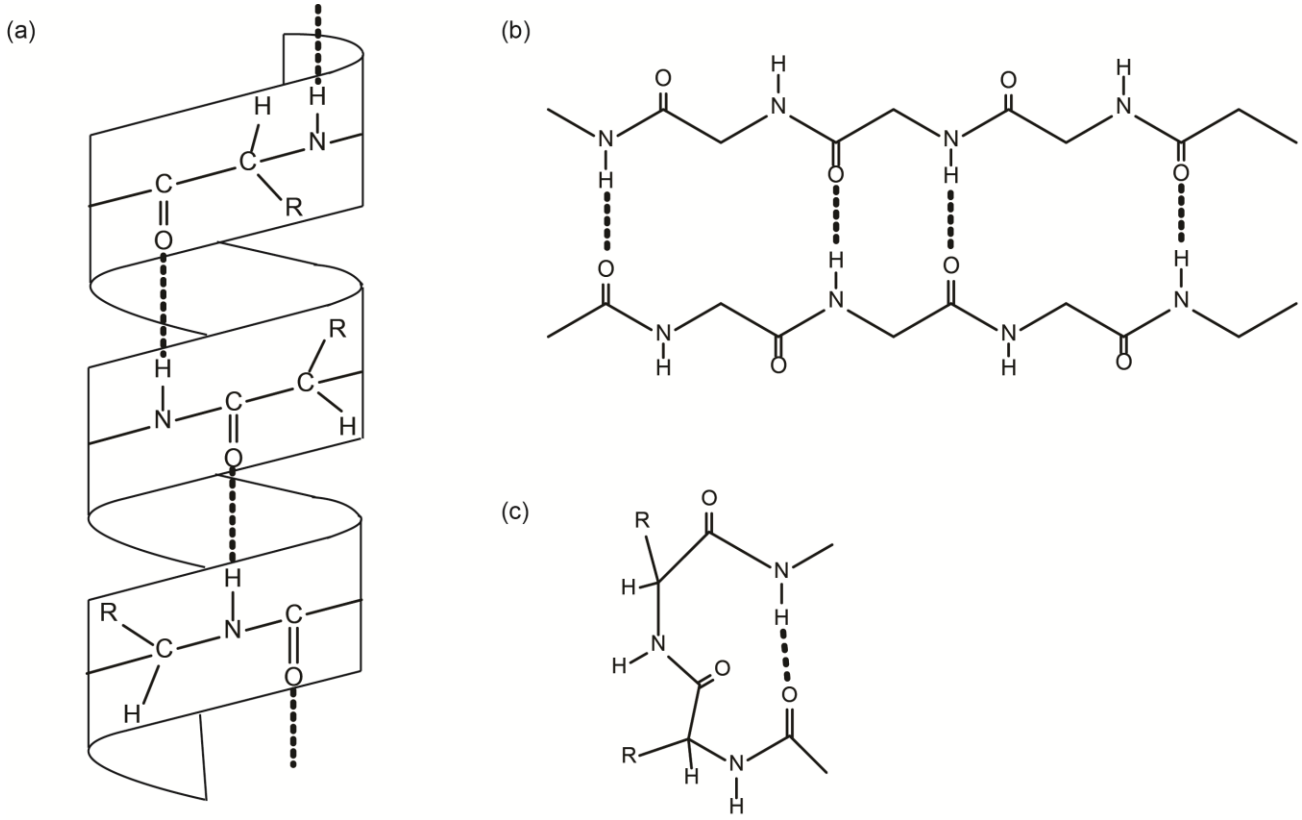

Figure A2: Secondary protein structures. (a) an α-helix, (b) a β-sheet, and (c) a β-turn. The dotted lines represent hydrogen bonds.

Biochemistry 6th Edition. Berg, J.M; Tymoczko, J.L.; and Stryer, L. Eds. W.H. Freeman and Company: New York, 2007.

APPENDIX B

^{13}C-LABELED DMPC SYNTHESIS MECHANISM

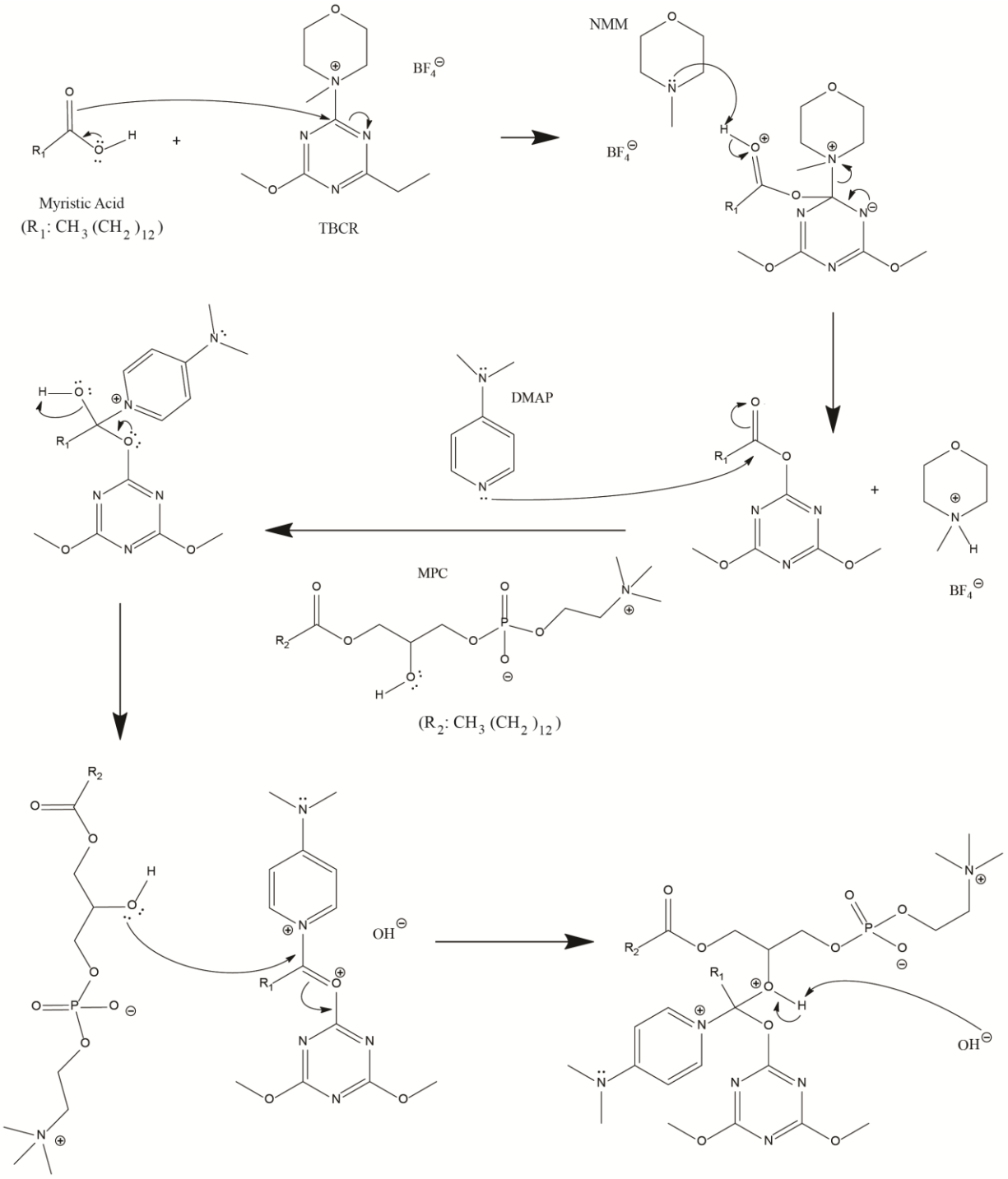

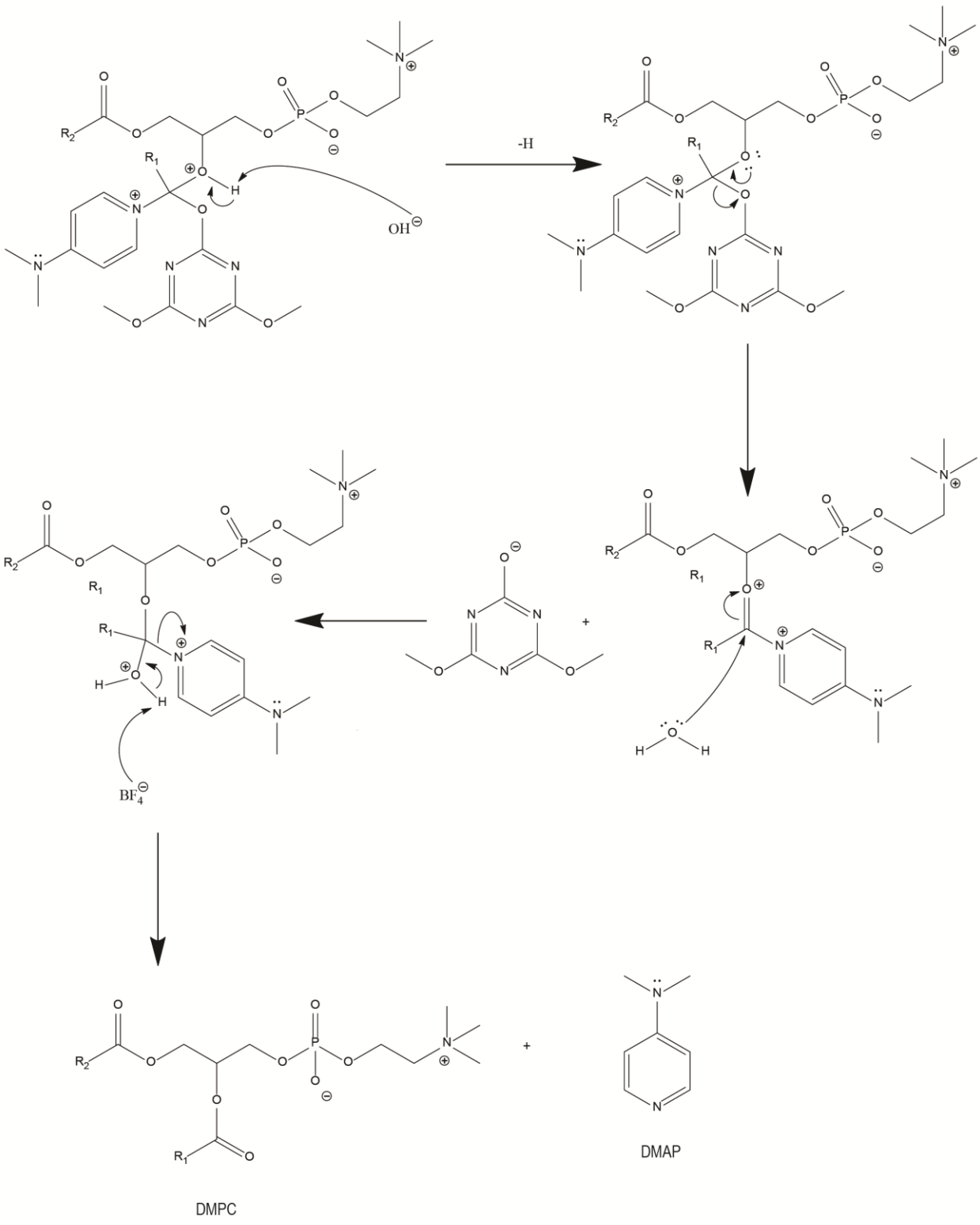

Figure B1: Mechanism for ^{13}C-labeled DMPC synthesis